NATIONAL COOPERATIVE HIGHWAY RESEARCH PROGRAM
REPORT 181

SUBCRITICAL CRACK GROWTH AND FRACTURE OF BRIDGE STEELS

TRANSPORTATION RESEARCH BOARD
NATIONAL RESEARCH COUNCIL

NATIONAL COOPERATIVE HIGHWAY RESEARCH PROGRAM
REPORT 181

SUBCRITICAL CRACK GROWTH AND FRACTURE OF BRIDGE STEELS

J. M. BARSOM AND S. R. NOVAK
UNITED STATES STEEL CORPORATION
MONROEVILLE, PENNSYLVANIA

RESEARCH SPONSORED BY THE AMERICAN ASSOCIATION OF STATE HIGHWAY AND TRANSPORTATION OFFICIALS IN COOPERATION WITH THE FEDERAL HIGHWAY ADMINISTRATION

AREAS OF INTEREST:
BRIDGE DESIGN
GENERAL MATERIALS
GENERAL MAINTENANCE
RAIL TRANSPORT

TRANSPORTATION RESEARCH BOARD
NATIONAL RESEARCH COUNCIL
WASHINGTON, D.C. 1977

NATIONAL COOPERATIVE HIGHWAY RESEARCH PROGRAM

Systematic, well-designed research provides the most effective approach to the solution of many problems facing highway administrators and engineers. Often, highway problems are of local interest and can best be studied by highway departments individually or in cooperation with their state universities and others. However, the accelerating growth of highway transportation develops increasingly complex problems of wide interest to highway authorities. These problems are best studied through a coordinated program of cooperative research.

In recognition of these needs, the highway administrators of the American Association of State Highway and Transportation Officials initiated in 1962 an objective national highway research program employing modern scientific techniques. This program is supported on a continuing basis by funds from participating member states of the Association and it receives the full cooperation and support of the Federal Highway Administration, United States Department of Transportation.

The Transportation Research Board of the National Research Council was requested by the Association to administer the research program because of the Board's recognized objectivity and understanding of modern research practices. The Board is uniquely suited for this purpose as: it maintains an extensive committee structure from which authorities on any highway transportation subject may be drawn; it possesses avenues of communications and cooperation with federal, state, and local governmental agencies, universities, and industry; its relationship to its parent organization, the National Academy of Sciences, a private, nonprofit institution, is an insurance of objectivity; it maintains a full-time research correlation staff of specialists in highway transportation matters to bring the findings of research directly to those who are in a position to use them.

The program is developed on the basis of research needs identified by chief administrators of the highway and transportation departments and by committees of AASHTO. Each year, specific areas of research needs to be included in the program are proposed to the Academy and the Board by the American Association of State Highway and Transportation Officials. Research projects to fulfill these needs are defined by the Board, and qualified research agencies are selected from those that have submitted proposals. Administration and surveillance of research contracts are responsibilities of the Academy and its Transportation Research Board.

The needs for highway research are many, and the National Cooperative Highway Research Program can make significant contributions to the solution of highway transportation problems of mutual concern to many responsible groups. The program, however, is intended to complement rather than to substitute for or duplicate other highway research programs.

NCHRP Report 181

Project 12-14 FY '73
ISBN 0-309-02755-1
L. C. Catalog Card No. 77-95287

Price: $5.60

Notice

The project that is the subject of this report was a part of the National Cooperative Highway Research Program conducted by the Transportation Research Board with the approval of the Governing Board of the National Research Council, acting in behalf of the National Academy of Sciences. Such approval reflects the Governing Board's judgment that the program concerned is of national importance and appropriate with respect to both the purposes and resources of the National Research Council.

The members of the technical committee selected to monitor this project and to review this report were chosen for recognized scholarly competence and with due consideration for the balance of disciplines appropriate to the project. The opinions and conclusions expressed or implied are those of the research agency that performed the research, and, while they have been accepted as appropriate by the technical committee, they are not necessarily those of the Transportation Research Board, the National Research Council, the National Academy of Sciences, or the program sponsors.

Each report is reviewed and processed according to procedures established and monitored by the Report Review Committee of the National Academy of Sciences. Distribution of the report is approved by the President of the Academy upon satisfactory completion of the review process.

The National Research Council is the principal operating agency of the National Academy of Sciences and the National Academy of Engineering, serving government and other organizations. The Transportation Research Board evolved from the 54-year-old Highway Research Board. The TRB incorporates all former HRB activities but also performs additional functions under a broader scope involving all modes of transportation and the interactions of transportation with society.

Published reports of the

NATIONAL COOPERATIVE HIGHWAY RESEARCH PROGRAM

are available from:

Transportation Research Board
National Academy of Sciences
2101 Constitution Avenue, N.W.
Washington, D.C. 20418

Printed in the United States of America.

FOREWORD

By Staff
Transportation
Research Board

This report contains the findings of an experimental study with the objective of developing information that will lead to prevention of unstable crack growth in welded steel bridge members. The results describe the fatigue crack growth behavior, corrosion fatigue crack propagation, stress-corrosion cracking, and fracture behavior of five grades of steel commonly used in bridges, under loadings such as occur in highway bridges. The findings from this research should be of value to structural engineers and others involved in the design, construction, and maintenance of steel bridges.

Highway bridges are subjected to a variety of forces ranging from constant dead load plus slowly changing forces due to temperature differentials and material creep to an infinite variety of superimposed live loads caused by moving vehicles.

The life of a welded steel bridge member is determined by (1) the number of loading cycles necessary to initiate a crack in the member; (2) the size of the largest actively growing crack in the member that was not detected by inspection or was considered acceptable at the time of fabrication; (3) the effect of geometry of the welded details on the rate of stable fatigue or corrosion-fatigue crack growth; (4) the increase of fatigue crack growth rate due to an aggressive environment; (5) the stress-corrosion-cracking behavior of the steel under static loading conditions; and (6) the crack size that can initiate a rapid crack extension when the combined residual and applied stresses, crack size, and fracture toughness provide a critical condition. Some steel bridges have failed prematurely during the last 35 years because one or more of these factors were not considered properly in design or taken into account during maintenance inspections.

This study was intended to provide information relative to stress-corrosion cracking, fatigue and corrosion-fatigue crack growth rate behavior for bridge steels under constant- and variable-amplitude loadings such as occur in highway bridges. Also, the fracture-toughness behavior of these steels was investigated using standard Charpy V-notch specimens, dynamic tear specimens, and fracture-mechanics type specimens. Fracture toughness of bridge steels and fatigue of welded details have been and are being studied by a number of research agencies. However, little has been published on the effects of aggressive environment on the rate of fatigue crack growth for bridge steels. In addition, at the time of initiation of this project, no requirements had been established for fracture toughness levels for bridge steels, nor had fracture mechanics been applied to welded bridge details.

The long-range objective of this project was to develop information that can

be used to define material requirements and design specifications to avoid brittle fracture in steel bridges. The purpose of this research was:

1. To develop corrosion-fatigue data on bridge steels in distilled water and 3 percent sodium chloride solution under stress fluctuations such as occur in actual bridges.
2. To develop an analytical method for predicting the cyclic life of bridge components in distilled water and 3 percent sodium chloride solution under stress fluctuations such as occur in actual bridges.
3. To develop methods of utilizing the results for design and specifications purposes.

The steels studied were A36, A588 grades A and B, and A514 grades E and F. The longitudinal and transverse tensile properties at room temperature were established for each grade of steel. Fatigue tests, stress corrosion cracking tests, and corrosion-fatigue tests were all conducted in this study. Moreover, energy absorption, lateral expansion, and percent shear were determined in the temperature range between $-100°$ F and room temperature by using standard impact Charpy V-notch specimens. Additional studies of the type already described were also conducted and included in the study to provide statistical behavior for five different heats of A588 steel that would provide insight into the influence of heat-to-heat variations on structural performance.

CONTENTS

ACKNOWLEDGMENTS

The research reported herein was performed under NCHRP Project 12-14 by U. S. Steel Research, a division of United States Steel Corporation, Monroeville, Pa. J. M. Barsom, Associate Research Consultant, and S. R. Novak, Research Engineer, were both co-principal investigators for the project and the authors of the report.

Gratefully acknowledged is the invaluable assistance given the authors by their colleagues, E. J. Imhoff, Jr., and J. F. Sovak, in developing the experimental procedures, conducting the experimental work, and calculating the test data.

SUBCRITICAL CRACK GROWTH AND FRACTURE OF BRIDGE STEELS

SUMMARY

Well-conceived procedures used to study the safety and reliability of structures recognize that the performance of a structure, or a structural component, is governed not only by material properties, but also by the design, fabrication, inspection, erection, and use of the structure. These parameters govern the initiation of subcritical cracks and their propagation to critical dimensions and, therefore, determine the useful cyclic life of structural components subjected to load fluctuations.

The research described herein provides information on the fatigue crack growth behavior and the corrosion fatigue, crack propagation behavior of various bridge steels (A36, A588 Grade A, A588 Grade B, A514 Grade E, and A514 Grade F) under constant amplitude stress spectra and variable amplitude, random sequence stress spectra such as occur in actual bridges. Also included in the discussion are details concerning the chemical composition, tensile properties, fracture toughness, and stress-corrosion-cracking behavior of the steels investigated.

The data obtained for these steels showed that the average rate of fatigue crack growth, da/dN, under variable amplitude, random sequence load fluctuation and under constant amplitude load fluctuation agreed closely when da/dN is plotted as a function of the root mean square of the stress intensity factor range, ΔK_{rms}. Thus, within the limits of this investigation, the average rate of fatigue crack growth of various bridge steels subjected to variable amplitude, random sequence load fluctuations and to constant amplitude load fluctuations can be represented by the equation

$$da/dN = A\ (\Delta K_{rms})^n$$

where ΔK_{rms} is the root mean square of the stress intensity factor fluctuation and A, n are material constants.

The corrosion fatigue data obtained for these steels at 60 cycles per minute (cpm) indicated that the rate of crack propagation was essentially the same for exposures in distilled water and in 3-percent solution of sodium chloride in distilled water, for stress ratios of 0.1 and 0.5 for sine-wave and square-wave cyclic stress forms, and for different heats of a given steel.

Corrosion fatigue, crack propagation rates for these steels at 12 cpm were equal to or slightly greater than the fatigue crack propagation rates in a room-temperature air environment. The corrosion fatigue, crack propagation threshold, ΔK_{th} (the value of the stress intensity factor fluctuation below which corrosion fatigue cracks do not propagate), of bridge steels subjected to a stress ratio of 0.1 and at 12 cpm was greater in the 3-percent solution of sodium chloride in distilled water than it was in a room-temperature air environment.

Corrosion fatigue, crack propagation rates were retarded significantly by alternate wet and dry environmental conditions. The corrosion fatigue, crack propagation life of bridge-steel components under actual operating (wet and dry) conditions in the aqueous environments investigated was equal to or greater than their fatigue life in a room-temperature air environment.

Specifications for bridge details are currently based on fatigue data in air. The aqueous solutions used in these studies—distilled water and 3-percent solution of sodium chloride in distilled water—represent environmental conditions that are potentially more aggressive than that of air. However, no major effects of these aqueous environments were observed in this investigation to be related to the rate of propagation of fatigue crack. Additional research is needed to determine how actual bridge environments affect the rate of fatigue crack propagation.

CHAPTER ONE

INTRODUCTION AND RESEARCH APPROACH

DESCRIPTION OF THE PROBLEM

Most engineering structures in existence perform safely and reliably because of the improvements made in connection with the weak links that were observed during the life of each component in the system. The majority of the specifications on material, design, and fabrication are based on correlations with service experience. The comparatively few service failures in steel bridges indicate that steel properties, design, and fabrication procedures of present-day bridges are generally satisfactory. However, the service failures that have occurred suggest that some modifications in present-day practices are desirable. Identification of the specific modifications needed calls for a thorough study of material properties, design, fabrication, inspection, erection, and service conditions.

In certain instances, the useful life of a welded steel bridge member may be determined by the initiation and the propagation of a subcritical crack to critical dimensions. Crack initiation and subcritical crack propagation may be caused by cyclic stresses in the absence of an aggressive environment (fatigue), by an aggressive environment under sustained load (stress-corrosion cracking), or by the combined effects of cyclic stresses and an aggressive environment (corrosion fatigue).

Fracture toughness of bridge steels and fatigue crack growth in welded details have been and are being studied by a number of research agencies. References (*1*), (*2*), and (*24*) deal with fatigue and crack growth in welded details in a benign environment. However, little has been published on the effects of an aggressive environment on the rate of fatigue crack growth in bridge steels.

Understanding of the corrosion fatigue behavior of bridge steels is very important, because the cyclic life of a structural component *may be decreased significantly* when the component is subjected simultaneously to cyclic loading and an aggressive environment. In general, such environmental effects cause an acceleration in the rate of fatigue crack growth, and the magnitude of this acceleration increases with increased material yield strength (σ_y) (that is to say, the cyclic life for high-strength steels ($\sigma_y > 130$ ksi) is more susceptible to environmental effects than that for low-yield-strength steels).

In order to obtain maximum information within a cost effective and timely framework, the environments were restricted in this investigation to air, distilled water, and 3-percent solution of sodium chloride in distilled water. The cyclic test frequencies of 60 cpm and 12 cpm were selected to simulate typical behavior encountered in high-speed arteries and slow-moving vehicular traffic, respectively. Background information and a review of previous work that is pertinent to this investigation are given in Appendix A.

OBJECTIVES AND SCOPE

The long-range objective of this research was to develop information that would lead to the prevention of unstable crack growth in welded steel bridge members. This objective was to be achieved through several phases of work that included both the definition of material requirements and the development of design requirements to avoid brittle fracture.

The principal objectives of the project can be stated, as follows:

1. To develop corrosion fatigue data on bridge steels in distilled water and in 3-percent sodium chloride solution in distilled water under stress fluctuations such as occur in actual bridges.
2. To develop an analytical method for predicting the cyclic life of bridge components in distilled water and in 3-percent sodium chloride solution under stress fluctuations such as occur in actual bridges.
3. To develop methods of utilizing the results for design and specification purposes.

To accomplish these objectives, five steels were investigated: A36, A588 grades A and B, and A514 grades E and F. The test specimens were made from 1-in.-thick (25.4-mm) plates. Additionally, the investigation included determinations of the chemical composition, the tensile properties, and the fracture toughness of the five steels; the behavior of these steels (fatigue crack growth; stress-corrosion cracking; and corrosion fatigue crack growth) was also studied. The test conditions employed in the tests conducted on each steel are summarized in Table 1. The analysis of the test data was based on concepts of fracture mechanics.

FRACTURE MECHANICS METHODOLOGY

The application of fracture mechanics concepts offers considerable promise in solving the problem of designing to prevent subcritical crack propagation and unstable crack propagation in bridges. Linear elastic fracture mechanics (LEFM) is based on an analytical procedure that relates the stress field in the vicinity of a crack tip to the nominal stress applied to the structure, to the size and shape of the crack or cracklike discontinuity, and to the material properties. The equations in Figure 1 describe the elastic stress field in the vicinity of a crack tip in a body subjected to tensile stresses normal to the plane of the crack (Mode I deformation) (*3*). The stress field equations show that the distribution of the elastic stress field in the vicinity of the crack tip is invariant in all structural components subjected to Mode I deformation. They also show that the magnitude of the elastic stress field can be described by a single-term parameter, K_I, designated the stress intensity factor. Con-

TABLE 1

SUMMARY OF RESEARCH WORK FOR EACH STEEL INVESTIGATED

Item No.	Type of Test	Specimen	Number of Tests	Test Temperature, F	Stress Ratio, R	Wave Form	Wave Amplitude	Frequency, cpm	Environment
1	Chemical composition	Check analysis	1		-	-	-	-	-
2	Tensile properties	0.505(L)*	3	RT+	-	-	-	-	-
		0.505(T)**	3	RT	-	-	-	-	-
3	Dynamic fracture toughness	CVN(L)	20	-100 to RT	-	-	-	-	-
		CVN(T)	20	-100 to RT	-	-	-	-	-
4	Dynamic fracture toughness	5/8" DT(L)	15	-100 to RT	-	-	-	-	-
		5/8" DT(T)	15	-100 to RT	-	-	-	-	-
5	Static fracture toughness	1-T WOL(L)	2	RT	-	-	-	-	Air
6	Fatigue	1-T WOL(L)	2	RT	0.1	Sine	Constant	300	Air
7	Fatigue	1-T WOL(L)	2	RT	0.1	Sine	Random	300	Air
8	Stress corrosion	Cantilever beam	8	RT	-	-	Static load	-	3% NaCl
9	Corrosion fatigue	1-T WOL(L)	2	RT	0.1	Sine	Random	60	Distilled water
		1-T WOL(L)	2	RT	0.1	Sine	Random	60	3% NaCl
10	Corrosion fatigue	1-T WOL(L)	2	RT	0.5	Sine	Random	60	3% NaCl
11	Corrosion fatigue	1-T WOL(L)	1	RT	0.1	Sine	Constant	60	3% NaCl
12	Corrosion fatigue	1-T WOL(L)	2	RT	0.1	Sine	Constant	12	3% NaCl
13++	Corrosion fatigue	1-T WOL(L)	5	RT	0.1	Sine	Constant	60	3% NaCl
14	Corrosion fatigue	1-T WOL(L)	1	RT	0.1	Square	Constant	60	More severe

* L = longitudinal.
** T = transverse.

+RT = room temperature.
++This test was conducted on one of the five steels only. The five specimens were obtained from various sources.

Conversion Factors:

1 inch = 25.4 mm
C = 5/9(F - 32)

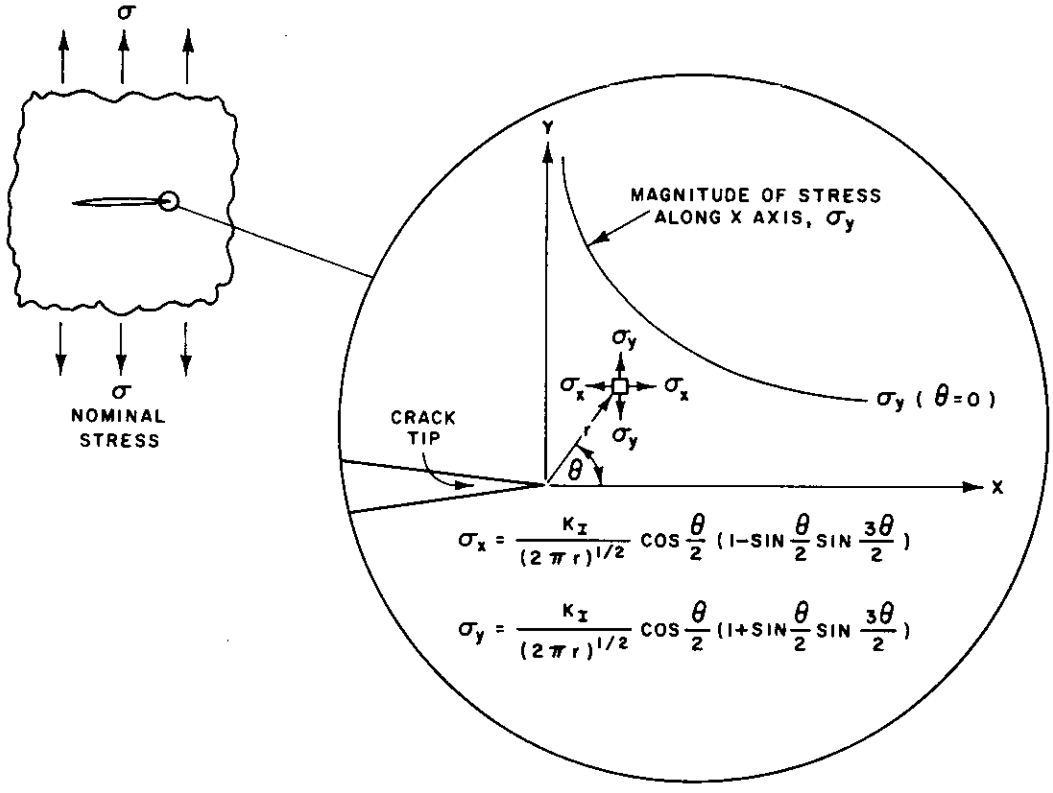

Figure 1. Schematic of the elastic stress field distribution near the tip of a fatigue crack (Mode 1 deformation).

sequently, the applied stress, the shape and size of the crack, and the structural configuration associated with structural components subjected to Mode I deformation affect the value of the stress intensity factor, but they do not alter the stress field distribution. Relationships between the stress intensity factor, crack sizes and shapes of various body configurations, and loading conditions have been published in Refs. (*4*) and (*5*).

One of the underlying principles of fracture mechanics is that unstable fracture occurs when the stress intensity factor at the crack tip reaches a critical value, K_c. For Mode I deformation and for small crack-tip plastic deformation (plane-strain conditions), the critical stress intensity factor for fracture instability is designated K_{Ic}. The term K_{Ic} represents the inherent ability of a material to withstand a given stress field intensity at the tip of a crack and to resist progressive tensile crack extension. Thus, K_{Ic} represents the fracture toughness of the material.

The critical stress intensity factor, K_{Ic} (or K_c), represents the terminal condition in the life of a structural component. The total useful life of the component is determined by the time necessary to initiate a crack and to propagate the crack from subcritical dimensions to the critical size, a_c. The primary causes of crack initiation and subcritical crack propagation may be attributed to cyclic stresses in the absence of an aggressive environment, to an aggressive environment under sustained load, or to the combined effects of cyclic stresses and an aggressive environment. Because these modes of subcritical crack propagation are localized phenomena that depend on the boundary conditions at the crack tip, it is logical to expect the subcritical crack propagation rate to depend on the stress intensity factor, K_I, which provides a single-term parameter representative of the stress conditions in the vicinity of the crack tip. Sufficient data are available in support of this observation (*6-11*). Recent studies in which fracture mechanics parameters have also been used show the effect of stress concentration on the initiation of fatigue crack (*12, 13*).

The life of a component can be prolonged by extending crack-initiation life and subcritical-crack propagation life. The latter may be accomplished by decelerating the rate of subcritical crack propagation and/or extending the size of the critical crack. Consequently, crack initiation, subcritical crack propagation, and fracture characteristics of steels are primary considerations in the formulation of fracture-control guidelines for steel structures.

The rate of fatigue crack growth has been investigated in many materials and has been found to depend on the magnitude of the stress range, $\Delta\sigma$, the crack length, a, and the material properties. The stress range and crack length can be incorporated in a single-term parameter, ΔK_I, which represents the fluctuation of the stress intensity in the vicinity of the crack tip. Consequently, the rate of fatigue crack growth, da/dN, is related to ΔK_I by the empirical relationship

$$da/dN = A(\Delta K_I)^n \qquad (1)$$

where a is the crack length, N is the number of cycles, ΔK_I is the fluctuation of the stress intensity factor, and A, n are constants that reflect effects of material properties and environments. Sufficient data obtained under constant amplitude, cyclic load fluctuations are available in support of this observation (*6-10, 14-16*). Furthermore, Eq. 1 can be used to characterize the general behavior of certain classes of materials under specific test conditions. In particular, values of A and n in Eq. 1 for upper bound (conservative) fatigue behavior in air are given by Eqs. A-5 and A-6, respectively, in Appendix A for martensitic steels and ferrite-pearlite steels. The ability to formulate such general relationships for fatigue behavior in air stems from the fact that the corresponding crack growth rate, da/dn, in air is independent of the frequency of cyclic load application. As discussed in detail in Appendix A, this is generally *not* the case for corrosion fatigue behavior.

Fracture mechanics concepts also provide a means to study the stress-corrosion-cracking behavior of various materials (*17-21*). Tests can be conducted in a specific environment to determine a threshold stress intensity factor, K_{Iscc}, value below which subcritical crack growth does not occur for a material loaded statically in the aggressive environment.

MATERIALS

Five types of steels were investigated in this project: A36, A588 grades A and B, and A514 grades E and F. Each steel was obtained in the form of a 1-in.-thick plate. The chemical composition and mechanical properties of the steels are given in Tables 2 and 3, respectively.

In addition to the aforementioned five steels, three other heats of A588 Grade A steel were tested to determine possible variations in the corrosion fatigue behavior of a given steel. The chemical composition and the mechanical properties of these three steels are given in Tables 4 and 5, respectively.

SPECIMEN PREPARATION AND EXPERIMENTAL PROCEDURE

Fracture Toughness Tests

Fracture toughness tests were conducted by using Charpy V-notch (CVN) specimens, dynamic tear (DT) specimens, cantilever beam specimens, and wedge-opening-loading (WOL) specimens.

The CVN specimens (Type A of ASTM Standard E23-72) are shown in Figure 2 (*22*). The specimens were machined from the midthickness plane of the 1-in.-thick plates. The tests were conducted in temperatures ranging from −180 F (−118 C) to room temperature. This temperature range was extended in some cases to obtain the upper energy shelf or the lower energy values. Sets of 20 longitudinal and 20 transverse specimens were used for each of the five steels investigated. The energy absorption, lateral expansion, and fibrous fracture behavior characteristics of each steel were recorded.

The DT specimens, shown in Figure 3, were prepared and tested in accordance with a method developed by the Naval Research Laboratory (*23*). The specimens were

TABLE 2
CHEMICAL COMPOSITION OF STEELS TESTED, PERCENT (CHECK ANALYSIS)

Steel	Heat No.	Plate No.	C	Mn	P	S	Si	Cu	Ni	Cr	Mo	V	Ti	Sol Al	Insol Al	Total Al	N*	O**	B
A36	74C515	195264	0.26	1.14	0.009	0.023	0.038	0.031	0.042	0.05	0.016	<0.005	<0.005	0.001	0.001	0.002	0.004	90	ND+
A588-A	67C611	193804	0.13	1.14	0.011	0.026	0.22	0.31	0.022	0.57	0.020	0.033	0.005	0.040	0.001	0.040	0.006	15	ND
A588-B	662J487	551528	0.11	1.16	0.011	0.018	0.27	0.26	0.35	0.63	0.016	0.052	<0.005	0.021	0.001	0.022	0.009	27	ND
A514-E	50343	P70074	0.16	0.61	0.008	0.018	0.28	0.21	ND	1.84	0.53	ND	0.063	0.033	0.001	0.034	0.010	41	0.0020
A514-F	70C125	79873A1	0.17	0.60	0.014	0.013	0.22	0.28	0.78	0.56	0.45	0.050	0.005	0.024	0.001	0.025	0.005	26	0.0041

* Kjeldahl determination.

** Parts per million.

\+ Not determined.

TABLE 3

MECHANICAL PROPERTIES * OF STEELS TESTED

Steel	Heat No.	Plate No.	Yield Strength (0.2% Offset), ksi	Tensile Strength, ksi	Elongation in 2 Inches, %	Reduction of Area, %	Charpy V-Notch Energy Absorption at 72 F, ft-lb
				Longitudinal			
A36	74C515	195264	43.6	78.2	28.2	62.4	28
A588-A	67C611	193804	54.9	81.7	28.2	68.3	69
A588-B	662J487	551528	55.6	82.1	27.8	76.2	66
A514-E	50343	P70074	107.9	122.6	19.0	65.1	68
A514-F	70C125	79873A1	126.0	134.0	18.3	57.8	45
				Transverse			
A36	74C515	195264	43.9	78.6	25.3	57.4	26
A588-A	67C611	193804	54.6	81.3	24.2	54.0	31
A588-B	662J487	551528	55.8	82.7	24.2	60.5	29
A514-E	50343	P70074	106.1	123.1	17.3	55.5	43
A514-F	70C125	79873A1	126.0	134.0	18.3	58.0	32

* Tension and impact specimens were taken in the longitudinal orientation from the midthickness point of the plates, which were all 1 inch thick. Tension-test results are the average of three 0.505-inch-diameter tension specimens, and impact results are the average of two Charpy V-notch specimens.

Conversion Factors:

1 inch = 25.4 mm
1 ksi = 6.895 MN/m^2
1 ft-lb = 1.36 J
C = 5/9(F - 32)

machined from the midthickness plane of the 1-in.-thick plates. The tests were conducted in temperature ranges similar to the Charpy V-notch test temperatures. In total, 15 longitudinal and 15 transverse specimens of each of the five steels investigated were tested, and the energy absorption and fibrous fracture behavior characteristics of each steel were recorded.

Two longitudinal orientation, cantilever beam specimens (see Fig. 4) and two longitudinal orientation, WOL specimens (see Fig. 5) were tested to fracture under a slow rate of loading to assess the fracture behavior of the five steels under "static" loading conditions. The nominal dimensions of these specimens are shown in Figures 4 and 5. Additional information relating to the preparation of these specimens and to the experimental procedure is given in Appendix B.

Fatigue and Corrosion Fatigue Tests

All fatigue and corrosion fatigue, crack growth data were obtained by using 1-in.-thick (1T), WOL specimens (Fig. 5). Details of the specimen preparation and experimental procedure are reported in Appendix B.

Crack propagation tests were conducted at room temperature in air, in continuously aerated distilled water, and in 3-percent solution of sodium chloride in distilled water. The tests were conducted in 100- and 50-kip (444.8- and 222.4-kN) Materials Testing Systems (MTS) machines. The fatigue crack growth data in air were obtained at cyclic stress frequencies of 300 cpm. The corrosion fatigue, crack growth data were obtained at 60 and 12 cpm, as outlined in Table 1. The specimens were tested under constant amplitude, sinusoidal or square-wave loading and under variable amplitude, random sequence loading (such as occurs in actual bridges) (*24*). In each test, the fatigue crack was initiated and propagated in tension-to-tension loading at a constant minimum load and at a constant amplitude or variable amplitude maximum load, under conditions which were controlled within ±1.0 percent. The crack was initiated and propagated from the notch root so that, at the time crack-length measurements were begun, the total crack length, a, was equal to about 1 in.

The fatigue crack growth rates were measured optically with a Type M-101 Gaertner microscope mounted in a micrometer slide. To improve the accuracy of measuring the rate of crack extension, a series of hardness indentations was made on the specimen surface along a line parallel to the plane of the initial crack and in the direction of expected crack extension, as described in Appendix B.

The rate of corrosion fatigue crack growth was measured by using the same procedure as that used for fatigue crack growth except for the fact that the specimens were fully immersed in the environment (see Appendix B).

Stress spectra typical of bridge loadings can be defined in terms of a minimum stress, σ_{min}, and parameters that define the frequency of occurrence of stress ranges, $\Delta\sigma$, at various magnitudes, as shown in Figure 6. The first step in determining the frequency of occurrence of $\Delta\sigma$ is to select a particular type of distribution curve. In this investigation, a Rayleigh (skewed) distribution curve was used to represent bridge loadings (*24*). The exact shape of the Rayleigh curve can be varied by changing the standard deviation, σ_{rd},

and the curves can be shifted to higher or lower values of $\Delta\sigma$ by changing the modal (peak) value of the distribution, σ_{rm}. In Figure 6, distributions corresponding to three different values of σ_{rd}/σ_{rm} (0, 0.5, and 1.0) are shown for a single value of σ_{rm}. In Figure 7, distributions corresponding to two different values of σ_{rm} are shown for a single value of σ_{rd}/σ_{rm}. The same value of $\sigma_{\min}$ is used for all distributions in both figures. A value of σ_{rd}/σ_{rm} equal to zero corresponds to constant amplitude loadings.

In the crack growth tests, all variable amplitude loadings followed a Rayleigh distribution curve, with the ratio of the load-range deviation to the modal (peak) load, P_{rd}/P_{rm}, equal to either 0 or 1.0. A block of 500 individual (usually different) loads satisfying one of these distribution curves was repeated throughout each test. Within the block, the loads were arranged in random sequence.

Although the cyclic loading spectrum was not changed during a test, the stress intensity factor range, ΔK, for successive blocks increases as the crack length increases. Thus, a single test gives crack growth rates for a range of ΔK values. The value of ΔK corresponding to a given crack length and loading was calculated from an available theoretical analysis (*25*).

Stress-Corrosion-Cracking Tests

The stress-corrosion-cracking tests were conducted on eight longitudinal orientation, cantilever beam specimens (see Fig. 4) for each of the five steels of interest. The specimens were about 1 in. thick and 2.5 in. (63.5 mm) wide. The notch was extended about 0.25 in. (6.35 mm) by fatigue cracking in air.

All specimens were tested in cantilever bending under dead-weight loading conditions by using the procedures described in Ref. (*21*). Two specimens of each steel were initially tested to fracture in air to establish the "static" fracture toughness value, K_{Ix}, of the steels. (These fracture toughness values are designated K_{Ix} rather than K_{Ic}, because the fracture of the 1-in.-thick specimens did not occur under plane-strain conditions.) The remaining specimens were dead-weight loaded to initial stress intensity levels, K_{Ii}, ranging from the plane-strain measurement capacity value of the specimens to greater than 90 percent of the K_{Ix} value. The specimens were fatigue cracked, then immersed in a 3-percent solution of sodium chloride in distilled water, and finally loaded to the desired K_{Ii} value. The test solution was maintained at room temperature throughout the course of the tests (it was initially saturated with laboratory air and continuously aerated thereafter to maintain saturation to test completion). The test solution for all tests was changed periodically.

The nominal test time for all stress-corrosion-cracking tests was 5000 h (30 weeks). Specimens that did not fracture during this test period (run-out tests) were cooled to −320 F (−196 C) in liquid nitrogen and then fractured to delineate any crack extension due to stress-corrosion cracking. The threshold stress intensity factor, K_{Iscc}, value at which no crack extension occurred in the environment was based on observation of the specimen fracture surfaces.

Additional details of specimen design, analysis, and experimental procedure are given in Appendix B.

TABLE 4

CHEMICAL COMPOSITION OF THREE A588 GRADE A STEELS TESTED IN CORROSION FATIGUE, PERCENT (CHECK ANALYSIS)

Code No.	Heat No.	Plate No.	C	Mn	P	S	Si	Cu	Ni	Cr	Mo	V	Ti	Sol Al	Insol Al	Total Al	N*	O**	B
14F	622976	4-2***	0.19	1.01	0.018	0.024	0.16	0.30	0.012	0.50	0.005	0.038	ND+	ND	ND	0.010	0.006	ND+	ND
14G	M31992	97007	0.15	1.03	0.009	0.017	0.25	0.29	0.020	0.56	0.007	0.036	0.005	0.035	>0.001	0.035	0.005	ND	ND
14H	685283	97001	0.15	1.07	0.009	0.018	0.25	0.33	0.031	0.55	0.017	0.036	0.005	0.039	0.001	0.040	0.006	ND	ND

* Kjeldahl determination.

** Parts per million.

*** Slab number.

\+ Not determined.

TABLE 5

MECHANICAL PROPERTIES * OF THREE A588 GRADE A STEELS TESTED

Code No.	Heat No.	Plate No.	Yield Strength (0.2% Offset), ksi	Tensile Strength, ksi	Elongation in 2 Inches, %	Reduction of Area, %	Charpy V-Notch Energy Absorption, at 72 F, ft-lb
				Longitudinal			
14F	622976	4-2**	55.9	81.9	28.0	71.2	58
14G	M31992	97007	54.4	80.1	29.0	74.0	89
14H	68E283	97001	53.7	83.0	27.2	69.2	45
				Transverse			
14F	622976	4-2	55.9	82.1	24.0	53.6	32
14G	M31992	97007	50.8	75.9	26.5	60.4	33
14H	68E283	97001	53.5	83.0	22.8	54.9	27

* Tension-test results are the average of three 0.505-inch-diameter tension specimens, and impact results are the average of three Charpy V-notch specimens. All plates were 1 inch thick.

** Slab number.

Conversion Factors:

1 inch = 25.4 mm
1 ksi = 6.895 MN/m^2
1 ft-lb = 1.36 J
C = 5/9(F - 32)

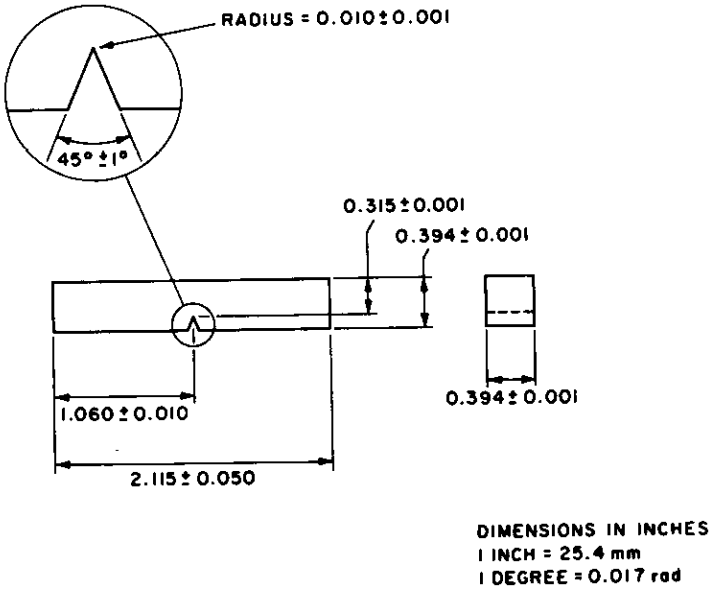

Figure 2. Charpy V-notch test specimen.

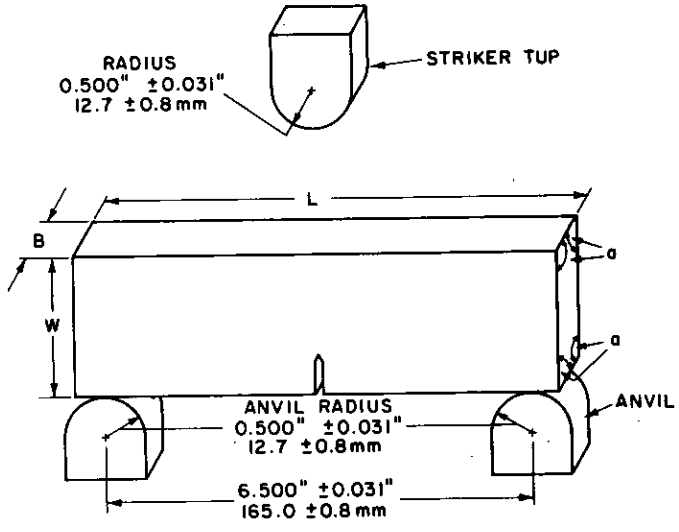

DIMENSIONS AND TOLERANCE FOR SPECIMEN BLANK

PARAMETER	UNITS	DIMENSION	TOLERANCE
LENGTH, L	IN.	7.125	±0.125
	MM	181.0	±3.2
WIDTH, W	IN.	1.60	±0.10
	MM	38.0	±2.5
THICKNESS, B	IN.	0.625	±0.033
	MM	15.8	±0.8
ANGULARITY, a	DEGREES	90	±2
	RAD	π/2	±0.034

Figure 3. Dynamic tear test specimen, anvil supports, and striker.

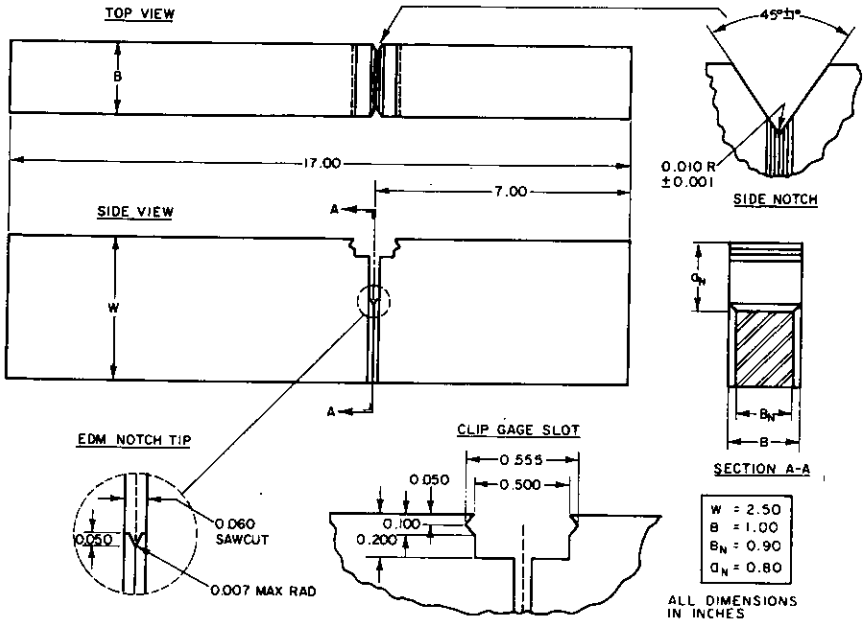

Figure 4. Fatigue-cracked cantilever-beam test specimen.

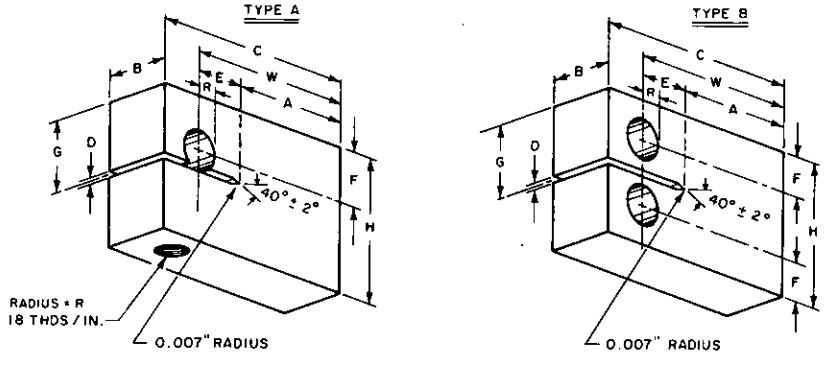

SPEC	B	W	C	A	E	H	G	D	R	F
1T-A	1.000	2.550	3.200	1.783	0.767	2.480	1.240	0.094	0.350	1.000
1T-B	1.000	2.550	3.200	1.783	0.767	2.480	1.240	0.094	0.250	0.650

1 inch = 25.4 mm
1 degree = 0.017 rad

Figure 5. Two types of 1T and 2T WOL specimens.

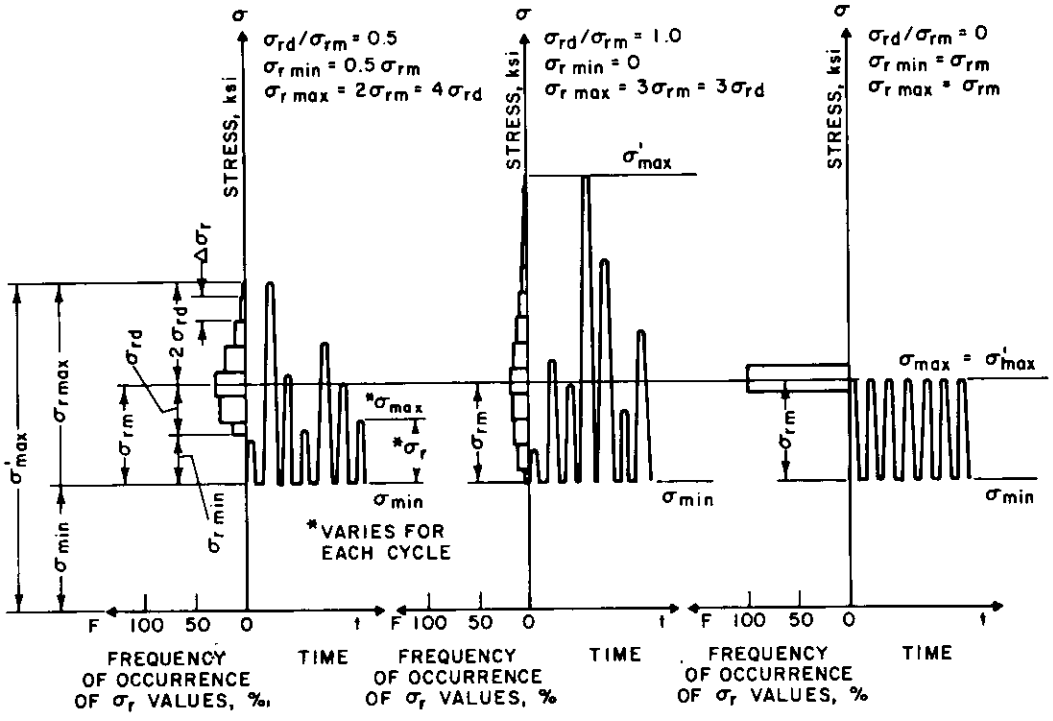

Figure 6. Stress spectra—constant σ_{rm}.

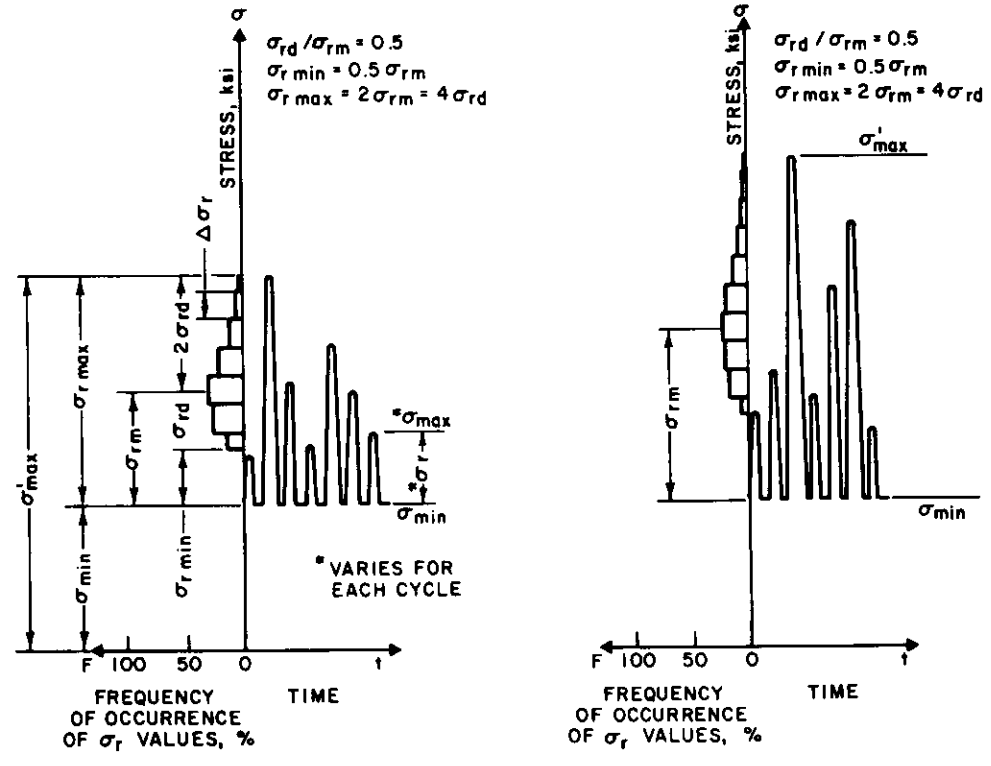

Figure 7. Stress spectra—different σ_{rm}.

CHAPTER TWO

FINDINGS

FRACTURE TOUGHNESS BEHAVIOR

The fracture toughness tests of the A36, A588 grades A and B, and A514 grades E and F steels were included in this study for background information and for possible future use. The fracture toughness characterization of these steels was done by conducting Charpy V-notch (CVN) tests, dynamic tear (DT) tests, and K_{Ic}-type tests. Detailed documentation of the results obtained by testing CVN and DT specimens is given in Apepndix C (Figs. C-1 through C-25).

The fracture toughness behavior obtained by testing 1-in.-thick WOL specimens and precracked cantilever beam specimens at room temperature resulted in extensive plastic deformation of the specimens prior to crack extension. This behavior represents high fracture resistance of the steels tested to crack extension under slow rates of loading. Details of the test results are given in Appendix D and are summarized in Table 6.

FATIGUE CRACK GROWTH BEHAVIOR

Most tests of fatigue crack growth are conducted by subjecting a fatigue-cracked specimen to constant amplitude, cyclic load fluctuations. Incremental increase of crack length is measured and the corresponding number of elapsed load cycles is recorded. The data are plotted in terms of crack length, a, versus total number of elapsed load cycles, N. Figures 8 and 9 show the effects on crack growth of specimens subjected to constant amplitude, cyclic load fluctuations. As shown in Figure 8, an increase in the magnitude of cyclic load fluctuation results in a decrease of fatigue life of specimens having identical geometry. Figure 9 shows that the fatigue life of specimens subjected to a fixed, constant amplitude, cyclic load fluctuation decreases as the length of the initial crack is increased. Consequently, various a-versus-N curves can be generated by varying the magnitude of the cyclic load fluctuation and/or the size of the initial crack. These curves reduce to a single curve when the data are represented in terms of crack growth rate per cycle of loading, da/dN, and the fluctuation of the stress intensity factor, ΔK_I, because ΔK_I is a single-term parameter that incorporates the effect of changing crack length and cyclic load magnitude.

Incremental increase of crack length and the corresponding number of elapsed load cycles can be measured under variable amplitude, random sequence load spectra. However, unlike constant amplitude, cyclic load data, the magnitude of ΔK_I changes for each cycle. Reduction of data in terms of fracture mechanics concepts therefore requires establishing a correlation parameter that incorporates the effects of crack length, cyclic load amplitude, and cyclic load sequence.

It is desirable to determine the magnitude of constant amplitude, cyclic load fluctuation that results in the same a-versus-N curve obtained under variable amplitude, cyclic load fluctuation when both spectra are applied to identical specimens (including initial crack length). In other words, the objective is to find a single stress intensity parameter—such as mean, modal, or root mean square—that can be used to define the crack growth rate under both constant amplitude and variable amplitude loadings. The a-versus-N curve obtained under constant amplitude, cyclic load fluctuation equal to the maximum cyclic load fluctuation of a variable amplitude load spectrum results in shorter fatigue life than that experienced under the variable amplitude spectrum. Similarly, a curve based on the minimum cyclic load fluctuation results in a longer life than that obtained under the variable amplitude load spectrum. The magnitude of the correlating parameter is bounded by these extremes. Moreover, the selected parameter *must* characterize the distribution curve.

Fatigue crack propagation behavior under variable amplitude, random sequence stress spectra such as occur in actual bridges has been investigated as part of NCHRP Project 12-12 (*24, 26*). The tests were conducted on A514 Grade B steel under variable amplitude, random sequence load spectra having P_{rd}/P_{rm} values of 0.5 and 1.0; a typical portion of the 500-cycle loading block for each is shown in Figure 10. It is apparent from Figure 11 that the average rate of fatigue crack propagation under variable amplitude, random sequence and ordered sequence load fluctuations is approximately equal to the rate of fatigue crack propagation under constant amplitude, cyclic load fluctuation equal to the root-mean-square value of the variable amplitude function. The root mean square is the square root of the mean of the squares of the individual load cycles in a spectrum; it is related to the modal value of the spectrum, as shown in Figure 12. The average rate of fatigue crack propagation, da/dN, under variable amplitude, random load fluctuation and ordered load fluctuation and under constant amplitude load fluctuation was found to agree closely when da/dN was plotted as a function of the root mean square of the stress intensity factor range, ΔK_{rms} (see Fig. 13). Thus, within the limits of the available experimental data, the average rate of fatigue crack growth per cycle, da/dN, under variable amplitude stress spectra typical of spectra occurring in actual bridges can be represented by the equation

TABLE 6

SUMMARY OF FRACTURE BEHAVIOR FOR STEELS INVESTIGATED

	1-T WOL Specimen Results					1-T Cantilever-Beam Specimen Results					Predicted Behaviors		
Steel	$K_{I,Lub}$, ksi $\sqrt{inch}$*	K_Q, ksi $\sqrt{inch}$**	K_{Ix}, ksi $\sqrt{inch}$***	$(\frac{K_Q}{K_{I,Gub}})^+$	$(\frac{\sigma_{N,max}}{\sigma_{ys}})^{++}$	$K_{I,Lub}$, ksi $\sqrt{inch}$*	K_Q, ksi $\sqrt{inch}$**	K_{Ix}, ksi $\sqrt{inch}$***	$(\frac{K_Q}{K_{I,Gub}})^+$	$(\frac{\sigma_{N,max}}{\sigma_{ys}})^{++}$	Estimated Range of K_{Ic}, # ksi $\sqrt{inch}$	B_{min} for Throughthickness Cracks, inches##	B_{min} for Partial-Thickness Cracks (PTC), inches###
A36	27.6	37	95	0.85	2.34	26.0	41	90	1.00	2.60	> 82	> 8.9	>17.8
A588-A	34.1	40	108	0.74	2.13	32.2	57	100	1.12	2.26	>120	>12.0	>24.0
A588-B	33.8	42	122	0.79	2.41	32.4	54	104	1.05	2.37	>120	>11.7	>23.4
A514-E++	67.8	107	166	1.00	1.63	66.4	110	146	1.05	1.68	150-200	4.85	9.70
A514-F++	81.5	93	132	0.72	1.08	78.3	96.5	104	0.78	1.04	125-160	2.45	4.90

* $K_{I,Lub} = \sigma_{ys} (\frac{B}{2.50})^{1/2}$, where $K_{I,Lub}$ = least-upper-bound for plane-strain fracture under LEFM conditions.

** K_Q = 5 percent secant intercept value from P versus V fracture test record.

*** K_{Ix} = stress-intensity value at maximum load (P_{max}) calculated on the basis of LEFM using the appropriate K_I equation (WOL or cantilever-beam specimens subjected to pure bending).

\+ $K_{I,Gub} = \sigma_{ys} (\frac{B}{1.00})^{1/2}$, where $K_{I,Gub}$ = greatest-upper-bound for plane-strain fracture under LEFM conditions, and the interrelationship $K_{I,Gub} = 1.58\ K_{I,Lub}$ applies.

++ $\sigma_{N,max}$ = value of the nominal net-section stress at maximum load (P_{max}) calculated using the following beam-theory equations:

$$\sigma_N = \frac{Mc}{I} + \frac{P}{A} = \frac{P}{B(W - a)^2} [4W + 2a] \text{ for the WOL specimen}$$

and $$\sigma_N = \frac{Mc}{I} = \frac{6PL}{B_N(W - a)^2} \text{ for the cantilever-beam specimen.}$$

Estimates of K_{Ic} based on concepts of the K_I-Suppression Effect based on the following criteria:

No suppression - $K_Q \leq K_{I,Lub}$, or $(\frac{K_Q}{K_{I,Gub}}) \leq 0.63$

Moderate suppression - $K_{I,Lub} < K_Q < K_{I,Gub}$, or $0.63 < (\frac{K_Q}{K_{I,Gub}}) < 1.00$

Severe suppression - $K_Q \geq K_{I,Gub}$, or $(\frac{K_Q}{K_{I,Gub}}) \geq 1.00$

B_{min} = minimum value of plate thickness and throughthickness crack size (a_{min}) required for valid plane-strain (K_{Ic}) fracture calculated on the basis of the minimum estimated value of K_{Ic} (preceding column) and actual yield strength, σ_{ys} (Table 3) as follows:

$$B_{min} = 2.50 \left(\frac{K_{Ic}}{\sigma_{ys}}\right)^2 = a_{min}$$

B_{min} = minimum value of plate thickness and partial-thickness crack (PTC) depth (a_{min}) required for valid plane-strain (K_{Ic}) fracture calculated on the basis of the minimum estimated value of K_{Ic} (a preceding column) and actual yield strength, σ_{ys} (Table 3) as follows:

$$B_{min} = 5.00 \left(\frac{K_{Ic}}{\sigma_{ys}}\right)^2 = \frac{a_{min}}{2}$$

⊕ K_Q values for WOL specimens are low (less than corresponding K_Q values obtained from cantilever-beam specimens) as a result of premature plastic bending of the WOL specimen arms.

⊖ Supplementary estimated K_{Ic} values calculated using the Charpy V-notch shelf correlation equation for K_{Ic} of high-strength martensitic steels, $\left(\frac{K_{Ic}}{\sigma_{ys}}\right)^2 = \frac{5}{\sigma_{ys}}\left(CVN - \frac{\sigma_{ys}}{20}\right)$, and the appropriate mechanical properties (σ_{ys} and CVN, Table 3), are as follows:

A514-E steel - $K_{Ic} = 184$ ksi $\sqrt{inch}$ (202 $MNm^{-3/2}$), with $B_{min} = 7.25$ inches for throughthickness cracks and $B_{min} = 14.5$ inches for partial-thickness cracks (PTC).

A514-F steel - $K_{Ic} = 156$ ksi $\sqrt{inch}$ (172 $MNm^{-3/2}$), with $B_{min} = 3.85$ inches for throughthickness cracks and $B_{min} = 7.70$ inches for partial-thickness cracks (PTC).

Conversion Factors:

1 ksi $\sqrt{inch}$ = 1.099 $MNm^{-3/2}$

1 inch = 2.54 cm

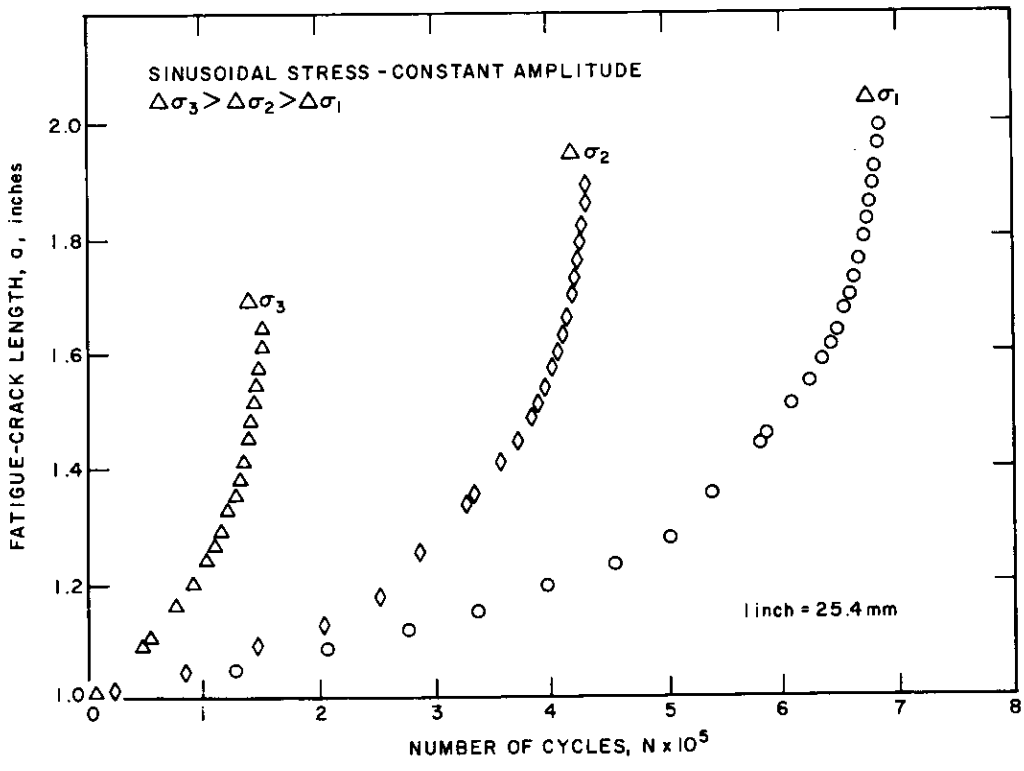

Figure 8. Effect of cyclic stress range on crack growth.

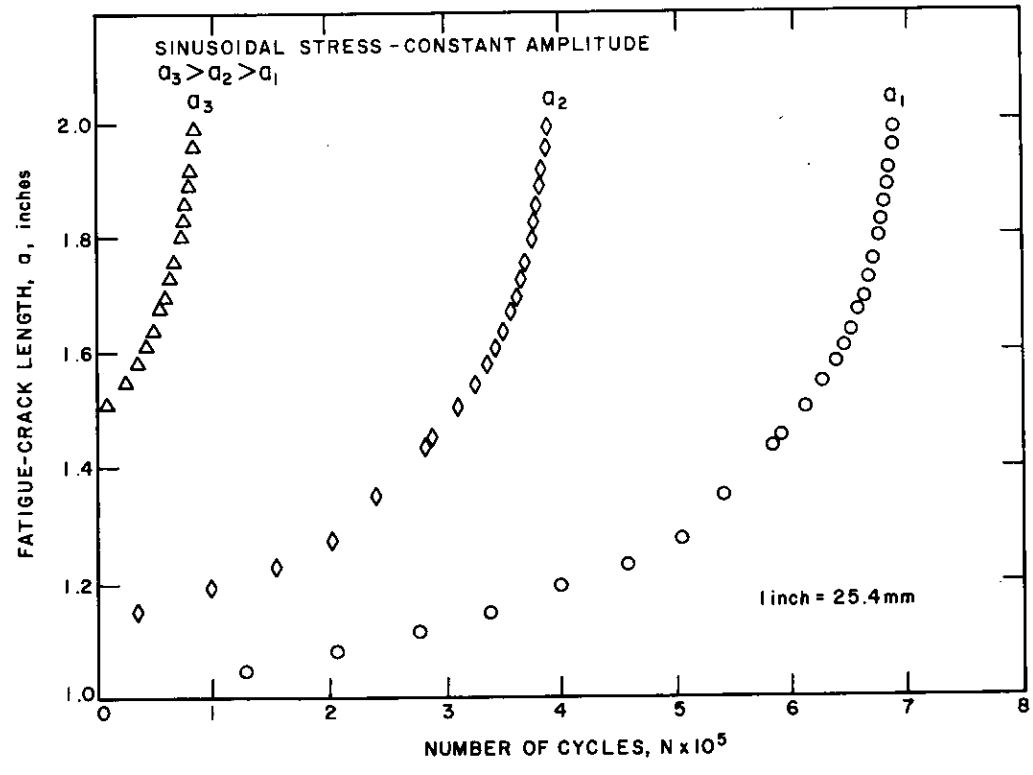

Figure 9. Effect of initial crack length on crack growth.

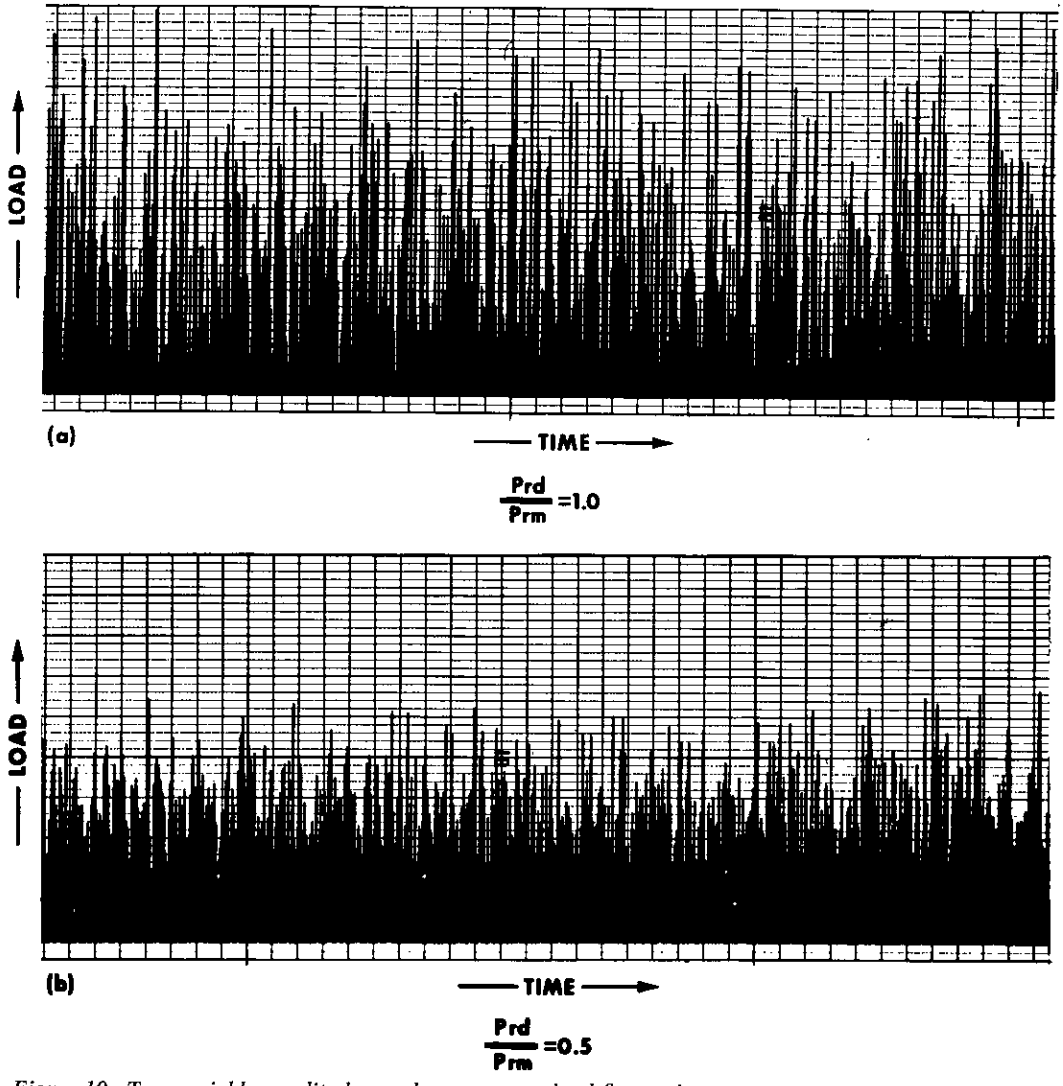

Figure 10. Two variable amplitude, random sequence load fluctuations.

$$da/dN = A(\Delta K_{rms})^n \qquad (2)$$

where A and n are material constants.

The root-mean-square value of the stress intensity factor under constant amplitude, cyclic load fluctuation is equal to the stress intensity factor fluctuation. Consequently, the average rate of fatigue crack growth for variable amplitude loadings can be predicted from constant amplitude data by using Eq. 2.

FATIGUE CRACK GROWTH IN VARIOUS BRIDGE STEELS

The preceding results (Fig. 13) were obtained by testing A514 Grade B steel. Because several investigators (*27-31*) have noted that changes in cyclic load magnitude can lead to either accelerated or retarded rates of fatigue crack growth, the applicability of the RMS (root-mean-square) model for correlating crack growth rates under random loading must be established for bridge steels of various yield strengths. Consequently, the fatigue crack growth rates under constant amplitude load fluctuations and under variable amplitude, random sequence load fluctuations were investigated in A36, A588 grades A and B, and A514 grades E and F steels. All loadings followed a Rayleigh distribution curve, with the ratio of the load-range deviation to the modal (peak) load, P_{rd}/P_{rm}, equal to either 0 or 1.0. Data on crack length and the corresponding number of elapsed load cycles obtained by subjecting identical specimens of each steel to constant amplitude load spectra and to variable amplitude, random sequence load spectra are given in Appendix E (Figs. E-1 through E-7). The load range, ΔP, for every cycle in the constant amplitude tests was equal to ΔP_{rm}. The results show that the fatigue life under constant amplitude, cyclic load fluctuations was longer than the fatigue life obtained under random sequence load spectra having the same value of ΔP_{rm}. The data are plotted in Figures 14 through 18 in terms of crack growth rate, da/dN, and the root mean square of the stress intensity factor range, ΔK_{rms}.

Figures 14 through 18 show that, within the limits of this experimental work, the average rate of fatigue crack

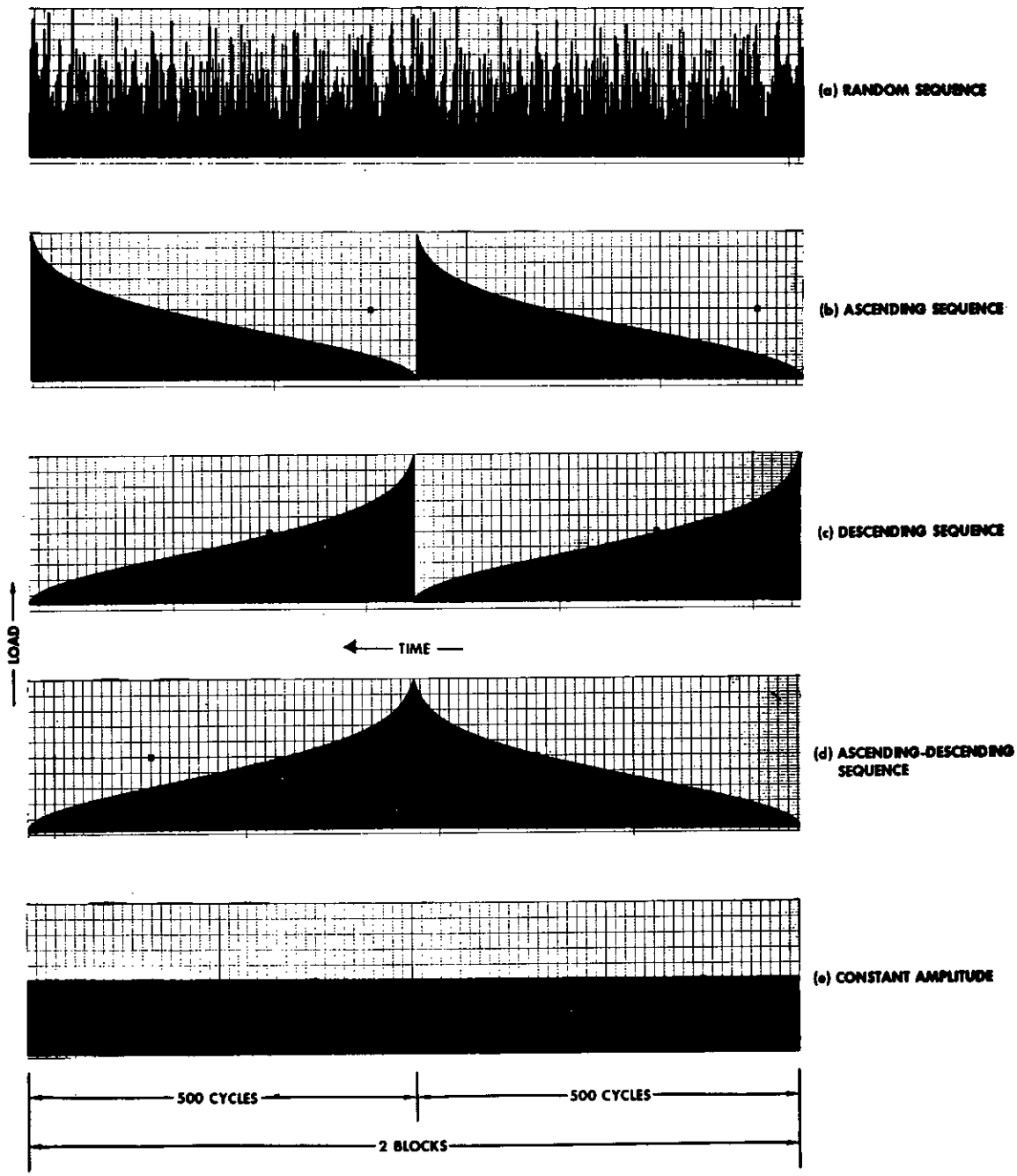

Figure 11. Various random sequence and ordered sequence load fluctuations.

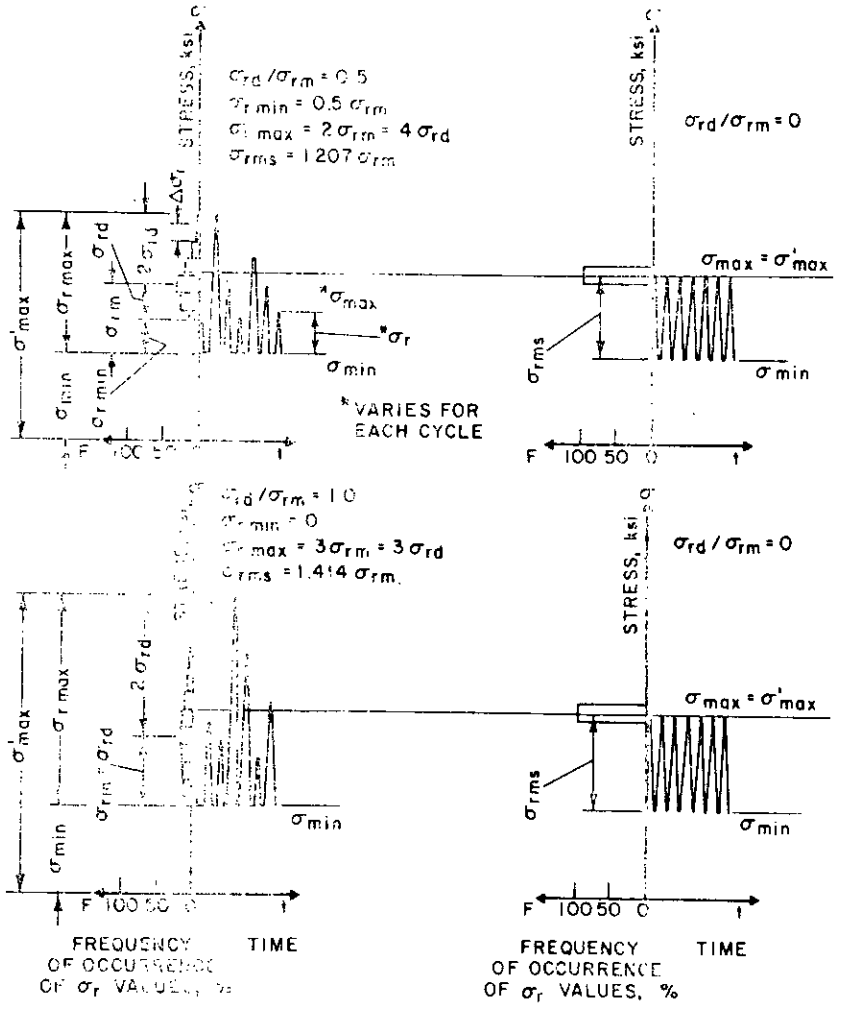

Figure 12. Stress spectra—constant σ_{rms}.

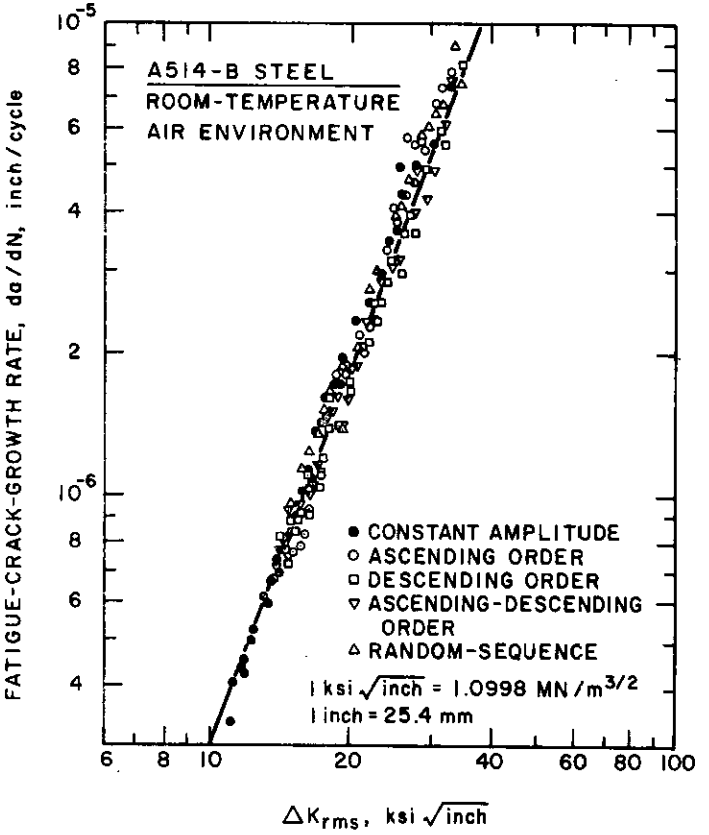

Figure 13. Summary of crack growth rate data under random sequence and ordered sequence load fluctuations.

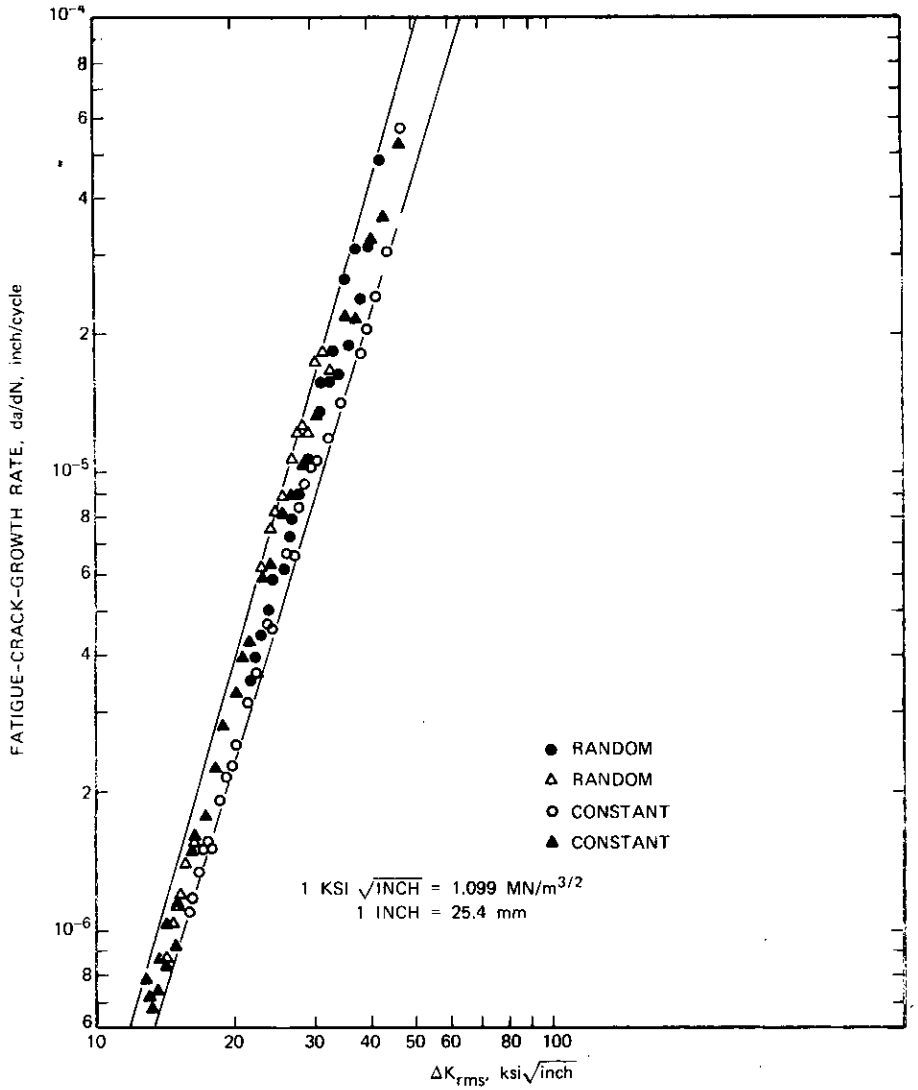

Figure 14. Crack growth rate as a function of the root mean square of the stress intensity factor for A36 steel.

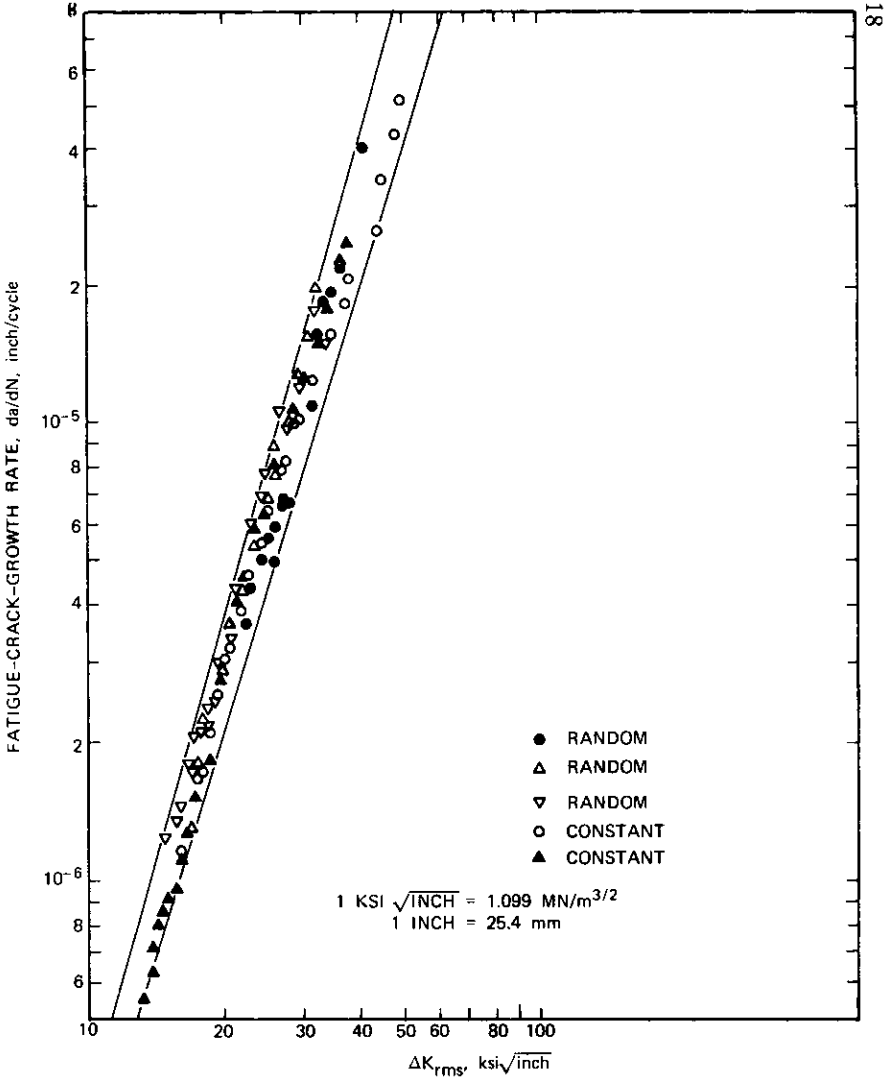

Figure 15. Crack growth rate as a function of the root mean square of the stress intensity factor for A588 Grade A steel.

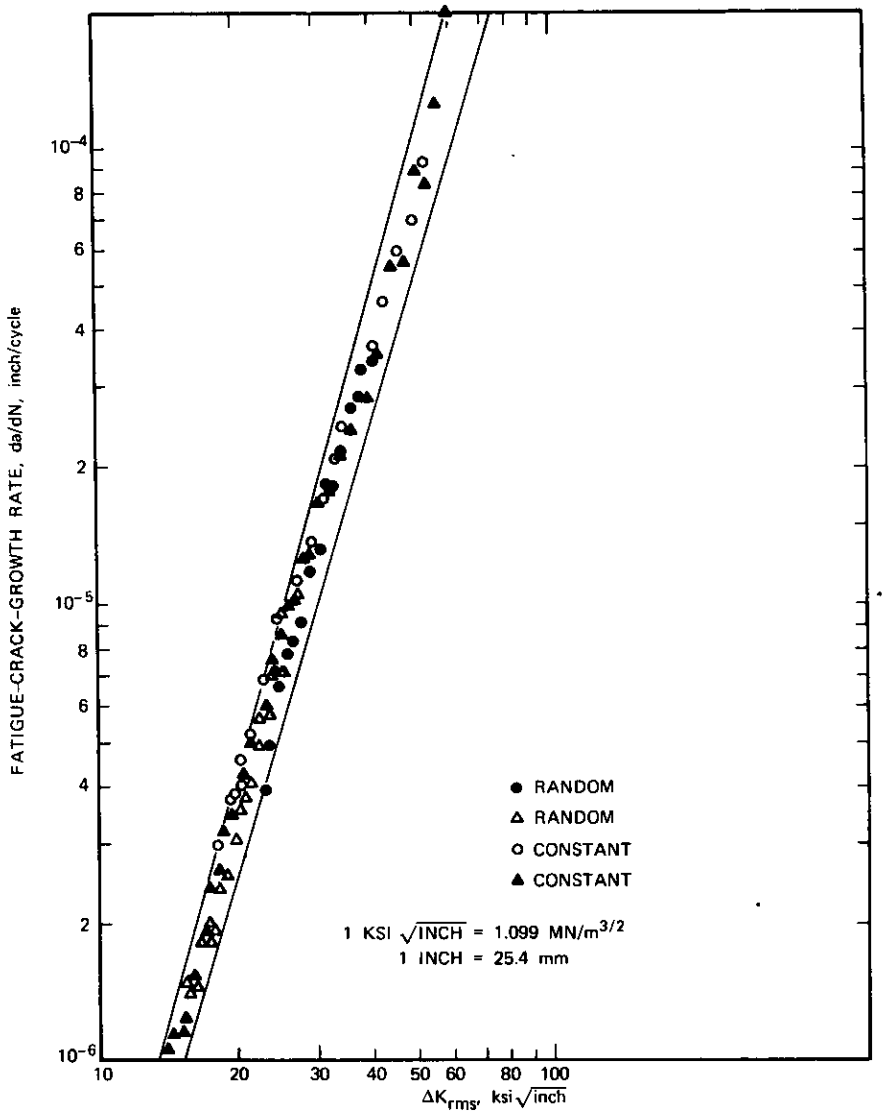

Figure 16. Crack growth rate as a function of the root mean square of the stress intensity factor for A588 Grade B steel.

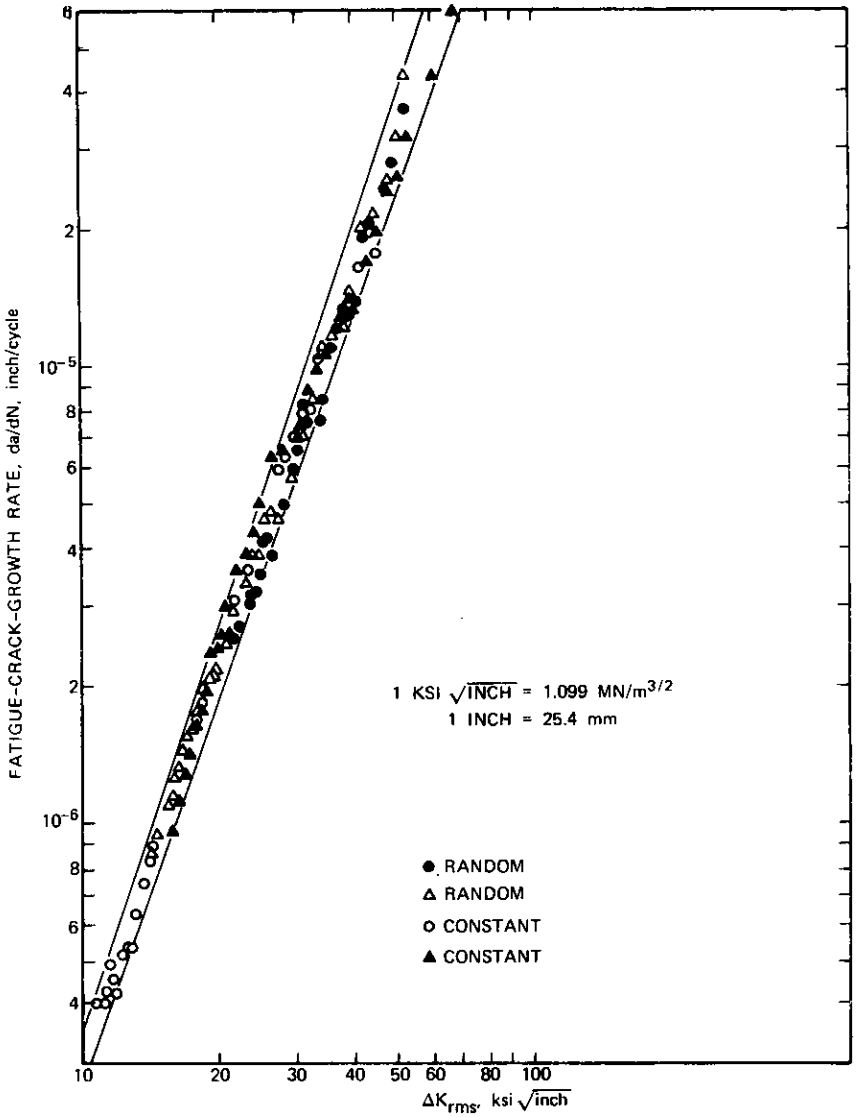

Figure 17. Crack growth rate as a function of the root mean square of the stress intensity factor for A514 Grade E steel.

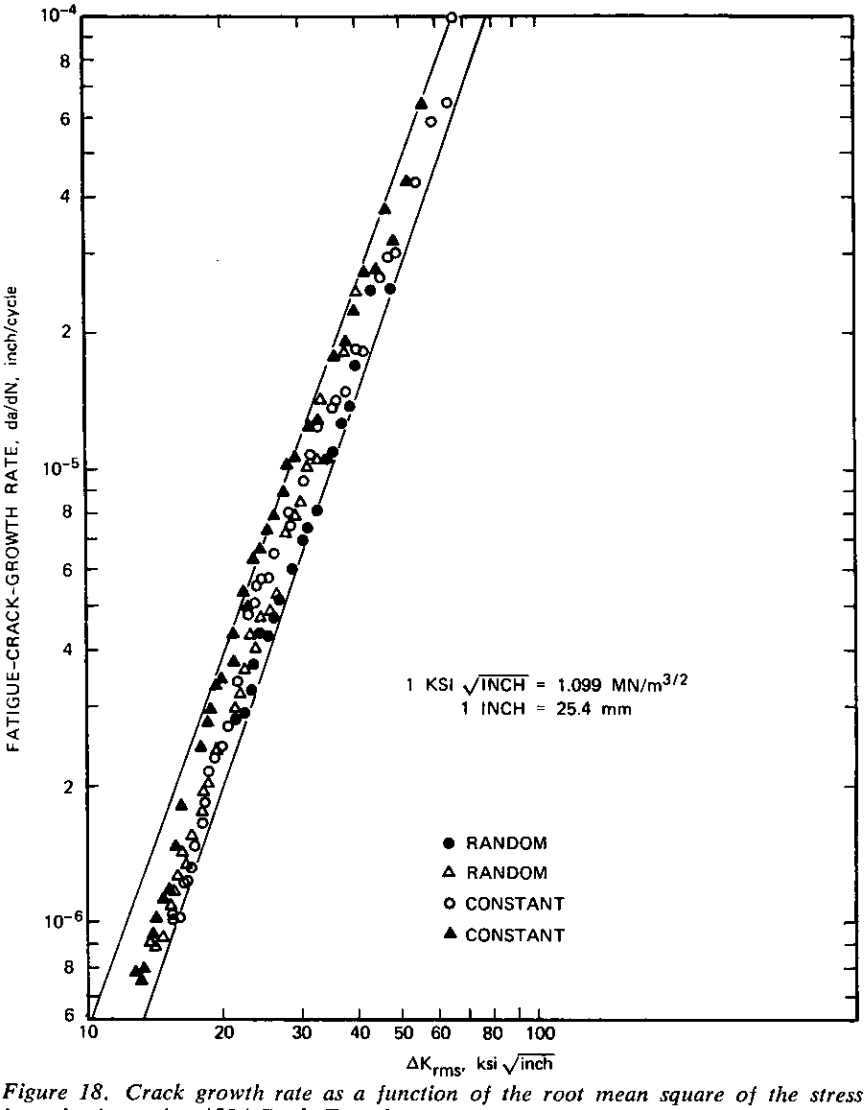

Figure 18. Crack growth rate as a function of the root mean square of the stress intensity factor for A514 Grade F steel.

growth, da/dN, in various bridge steels subjected to variable amplitude load spectra (such as occur in actual bridges) can be represented by Eq. 2. The root-mean-square value of the stress intensity factor range under constant amplitude, cyclic load fluctuation is equal to the stress intensity factor range. Consequently, the average rate of fatigue crack growth under variable amplitude load spectra can be predicted from constant amplitude data by using Eq. 2.

STRESS-CORROSION-CRACKING BEHAVIOR

A detailed discussion of the stress-corrosion-cracking tests for each of the five steels investigated is covered in Appendix F. Figures 19 through 23 and Table 7 summarize the test results for each steel. The figures are plots of the value of the initial stress intensity factors, K_{Ii}, to which a specimen was loaded in the environment and the time to specimen failure. The results in Figures 19 through 23 show apparent K_{Iscc} values that ranged from 80 to 106 ksi $\sqrt{\text{in.}}$ (88 to 117 MNm$^{-3/2}$). These results are designated apparent K_{Iscc} values because they are beyond the limits of analysis by LEFM methods.

CORROSION FATIGUE, CRACK GROWTH BEHAVIOR

A survey of the published literature indicated that the data obtained in this study represent the first systematic investigation of the corrosion fatigue, crack growth behavior of bridge steels in aqueous environments under constant amplitude and variable amplitude loading conditions. The effects of cyclic frequency and waveform on the corrosion fatigue and crack growth rate in high-yield-strength steels, as discussed in Appendix A, show that the 60 cpm and 12 cpm used in this investigation represent the equivalent transient-loading times in the neighborhood of a given bridge detail that result from the passage of a single vehicle (*8*). The correspondence between the frequency of loading used in this study and the transient-loading times at a given location in a bridge depends on the span length,

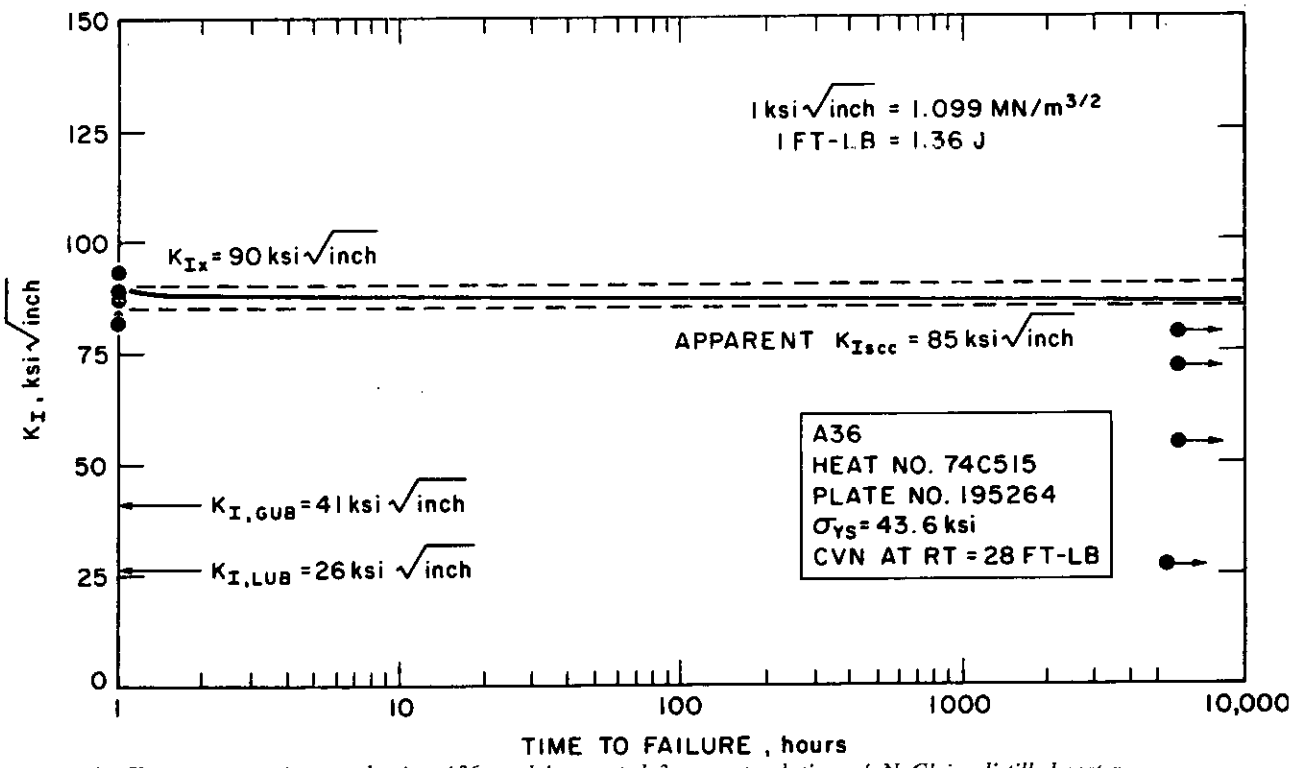

Figure 19. K_I-stress corrosion results for A36 steel in aerated 3-percent solution of NaCl in distilled water.

the bridge design, and the speed of the vehicle. However, for a given bridge, the change from 60 to 12 cpm represents a corresponding change in vehicle speed.

Corrosion Fatigue Behavior at 60 CPM

The corrosion fatigue data obtained by testing A36, A588 grades A and B, and A514 grades E and F steels in distilled water and in 3-percent solution of sodium chloride in distilled water are discussed in Appendix G in terms of crack length, a, and the corresponding number of elapsed cycles, N. The data obtained by testing these steels at 60 cpm under constant amplitude loading and under variable amplitude, random sequence loading are shown in Figures 24 through 28 in terms of crack growth rate per cycle, da/dN, and the root mean square of the stress intensity factor fluctuation, ΔK_{rms}. The curves plotted in each of these figures were obtained by testing duplicate specimens in distilled water under variable amplitude, random sequence loading; duplicate specimens in 3-percent solution of sodium chloride in distilled water under variable amplitude, random sequence loading; a single specimen in the 3-perecnt sodium chloride solution under constant amplitude sinusoidal loading; and a single specimen in the 3-percent sodium chloride solution under constant amplitude, square-wave loading. Superimposed on these figures are the upper and lower bounds of data scatter obtained by testing these steels under constant amplitude loading and under variable amplitude, random sequence loading in a room-temperature air environment.

The results (Figs. 24 through 28) indicate that the addition of 3-percent (by weight) sodium chloride to distilled water had no effect on the corrosion fatigue behavior of the bridge steels tested at 60 cpm under both constant amplitude loading and variable amplitude, random sequence loading. The data also show that the corrosion fatigue crack growth rate behavior at 60 cpm under sinusoidal loading and under square-wave loading is essentially identical. The scatter in the test results obtained in a single specimen under corrosion fatigue conditions was equal to or greater than that obtained under fatigue conditions. The increase in scatter, which decreased the accuracy in determining the exact location of the cracktip, was caused by the general corrosion of the specimen surfaces. On the basis of the scatter caused by the corrosion of the specimen surfaces and the inherent scatter observed in fatigue crack growth data, it was apparent that, at 60 cpm, the distilled water and the 3-percent solution of sodium chloride in distilled water had negligible effect on the rate of growth of fatigue cracks in the bridge steels investigated. This conclusion is supported further by the fact that the rate of growth of corrosion fatigue crack under sinusoidal loading and the rate under square-wave loading were identical.

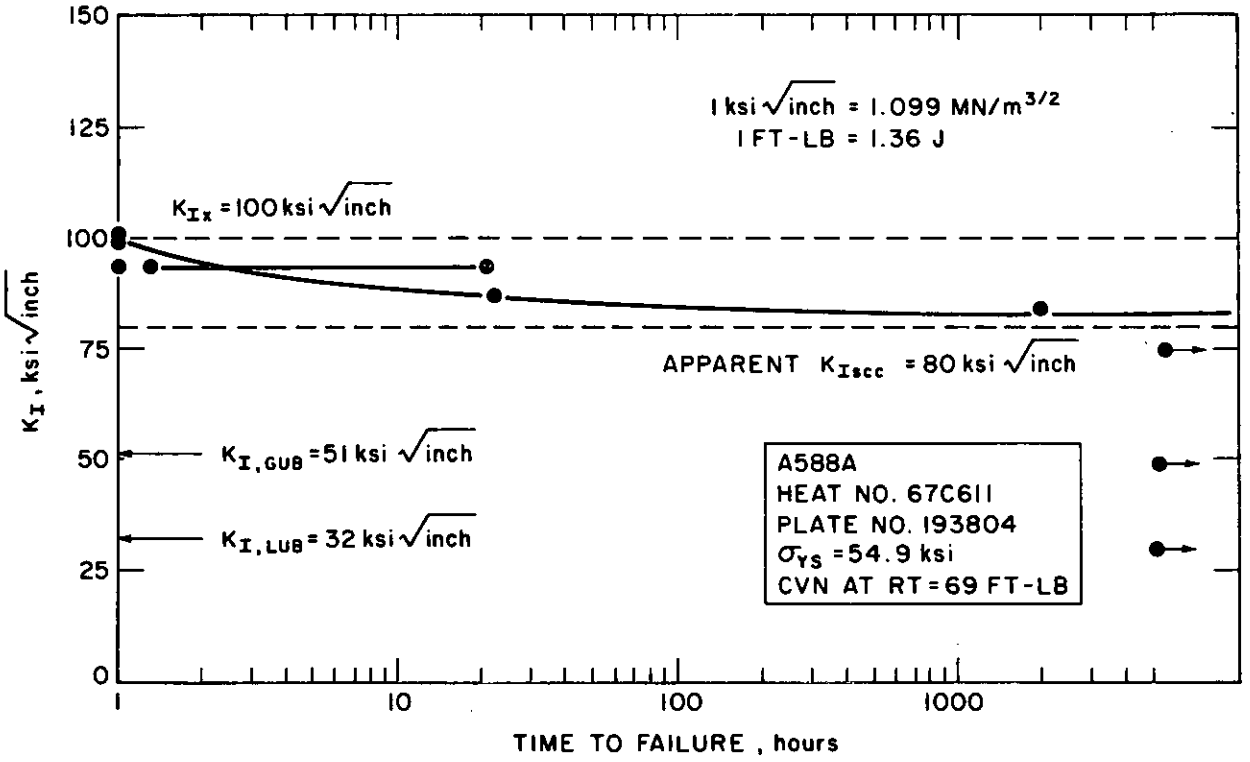

Figure 20. K_I-stress corrosion results for A588 Grade A steel in aerated 3-percent solution of NaCl in distilled water.

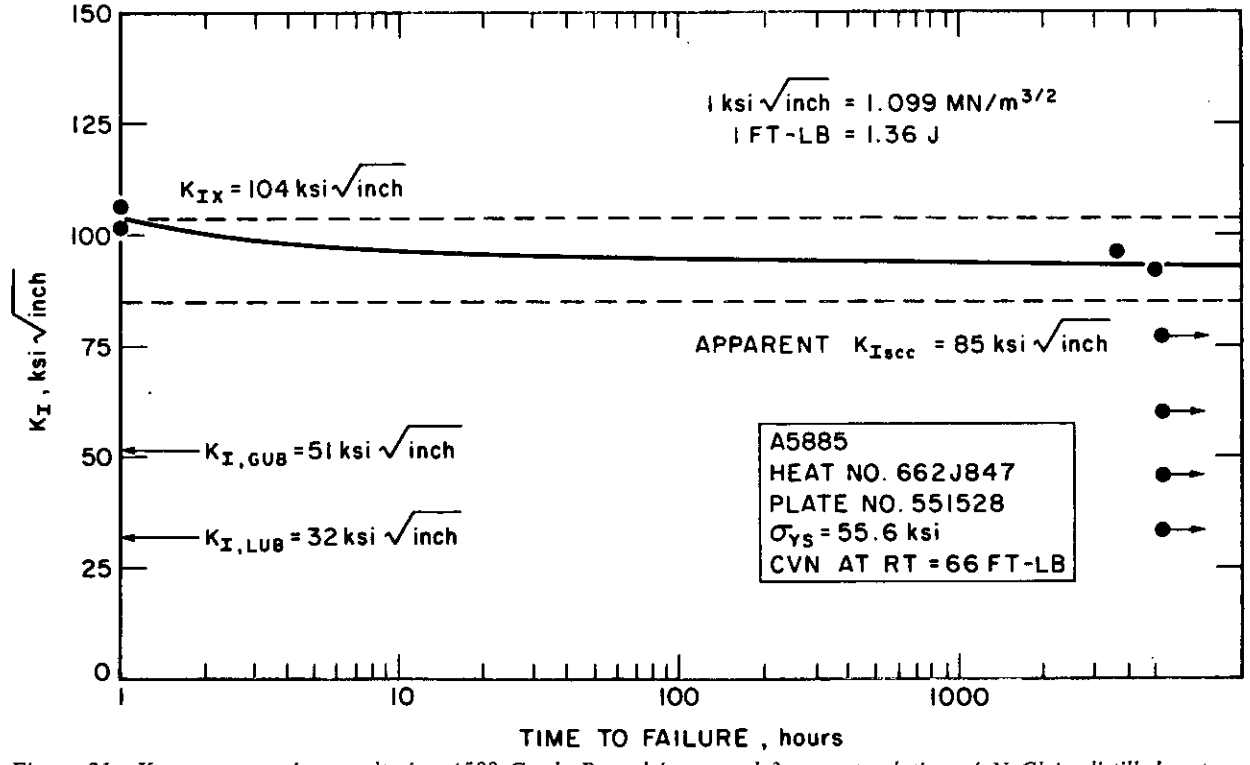

Figure 21. K_I-stress corrosion results for A588 Grade B steel in aerated 3-percent solution of NaCl in distilled water.

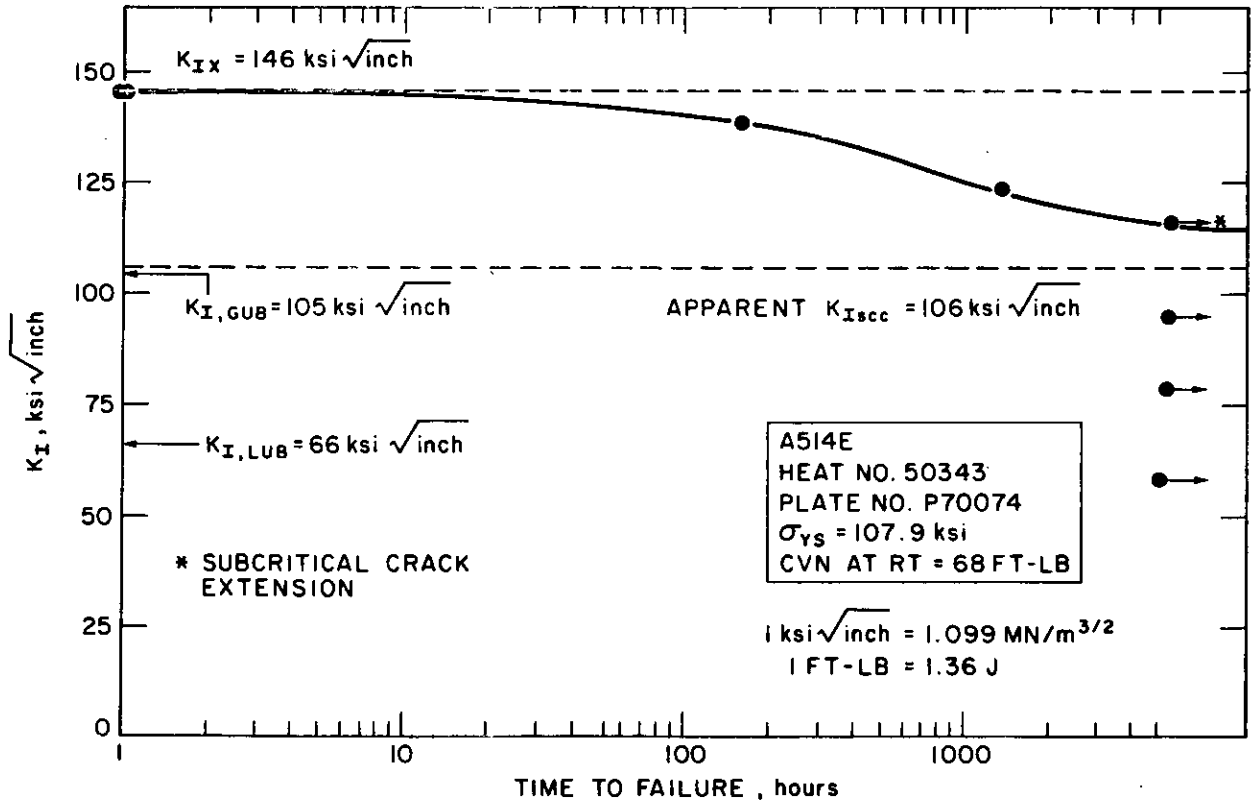

Figure 22. K_I-stress corrosion results for A514 Grade E steel in aerated 3-percent solution of NaCl in distilled water.

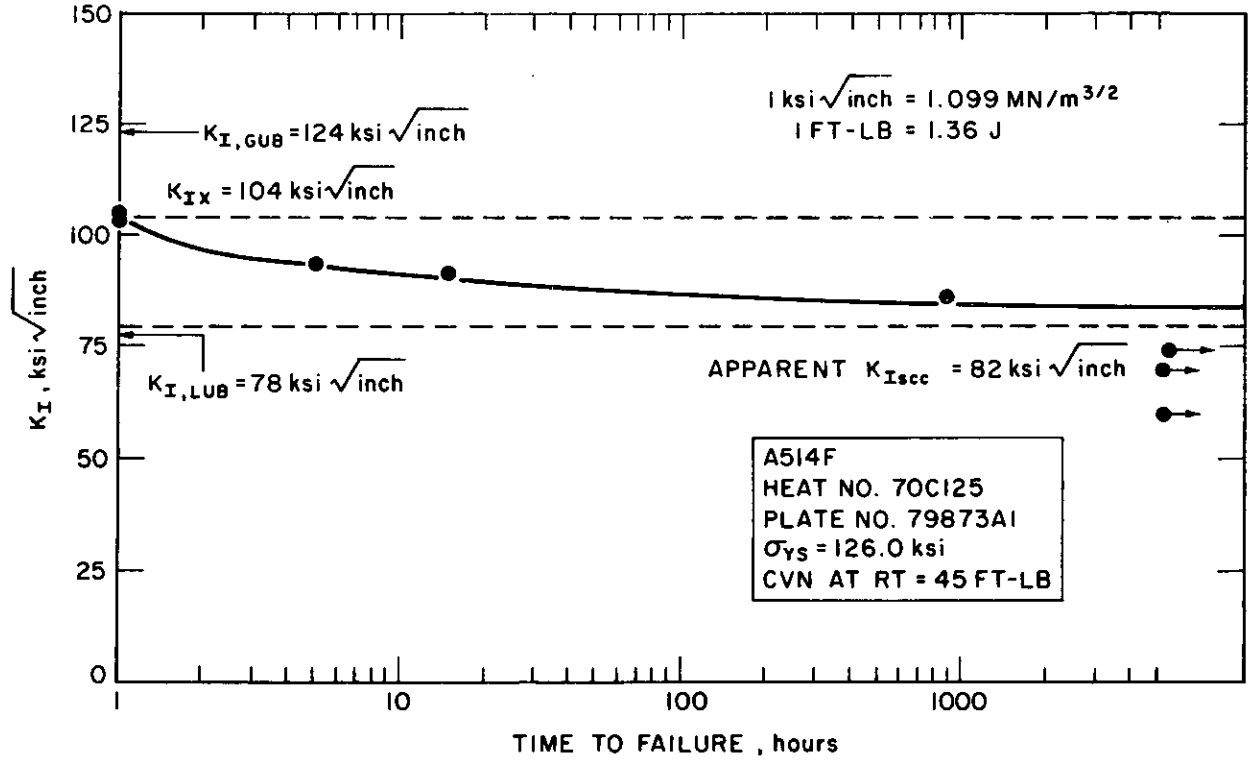

Figure 23. K_I-stress corrosion results for A514 Grade F steel in aerated 3-percent solution of NaCl in distilled water.

TABLE 7

SUMMARY OF STRESS-CORROSION-CRACKING (SCC) BEHAVIOR OF STEELS INVESTIGATED *

Item No.	Steel Type	Basic Mechanical Properties* σ_{ys}, ksi	Basic Mechanical Properties* CVN at 72 F, ft-lb	Plane-Strain Limits** $K_{I,Lub}$, ksi $\sqrt{inch}$	Plane-Strain Limits** $K_{I,Gub}$, ksi $\sqrt{inch}$	K_{-x}, ksi $\sqrt{inch}$***	Apparent K_{Iscc}, ksi $\sqrt{inch}$#	σ_{Nscc}, ksi##	Apparent K_{Iscc} / K_{Ix}	Type of Environmental Behavior###	Extent of Suppression on Apparent K_{Iscc}###
1	A36	43.6	28	26	41	90	85	106	0.95	III	Severe
2	A588-A	54.9	69	32	51	100	80	101	0.80	III	Severe
3	A588-B	55.6	66	32	51	104	85	108	0.82	III	Severe
4	A514-E	107.9	68	66	105	146	106	132	0.73	II	Severe to Moderate
5	A514-F	126.0	45	78	124	104	82	103	0.79	II	Moderate

* See summary of specimen preparation and test conditions employed, Appendix Table F-1. NOTE: All specimens, including both precracked cantilever-beam specimens and mechanical-property specimens, were taken in the longitudinal (RT designation for notched specimens) orientation.

** $K_{I,Lub} = \sigma_{ys}\left[\frac{(B \cdot B_N)^{1/2}}{2.50}\right]^{1/2}$ $K_{I,Gub} = \sigma_{ys}\left[\frac{(B \cdot B_N)^{1/2}}{1.00}\right]^{1/2}$ and $K_{I,Gub} = 1.58\ K_{I,Lub}$.

*** K_{Ix} = stress-intensity value at maximum load (P_{max}) in a fracture test, calculated on the basis of the initial fatigue-crack length (a_i) and LEFM concepts.

\# Apparent K_{Iscc} = value calculated on the basis of LEFM concepts (regardless of applicability) for threshold behavior observed under dead-weight-loading conditions (P = constant) and exposure to a continuously aerated solution of 3 percent NaCl (by weight) in distilled water at room temperature (72 F) for a nominal test period of 5000 hours. See Table F-1 for summary of specimen preparation and test conditions employed.

\#\# $\sigma_{Nscc} = \frac{6M}{(B \cdot B_N)^{1/2}(W - a)^2}$, calculated on the basis of apparent K_{Iscc} and average specimen dimensions for each steel.

\#\#* Type of environmental behavior and extent of K_I-suppression effects reflected for each classification are as follows:

Type I behavior - No suppression - for apparent $K_{Iscc} \geq K_{I,Lub}$.

Type II behavior - Moderate suppression - for $K_{I,Lub}$ < apparent K_{Iscc} < $K_{I,Gub}$.

Type III behavior - Severe suppression - for apparent $K_{Iscc} \leq K_{I,Gub}$.

NOTE: Calculations of critical-flaw-size values, a_{cr}, for Type III behavior are not admissible due to gross underestimates of intrinsic a_{cr}.

Conversion Factors:

1 ksi = 6.895 MN/m^2 = 6.895 N/mm^2

1 ft-lb = 1.36 J

1 ksi $\sqrt{inch}$ = 1.099 $MNm^{-3/2}$

C = 5/9(F - 32)

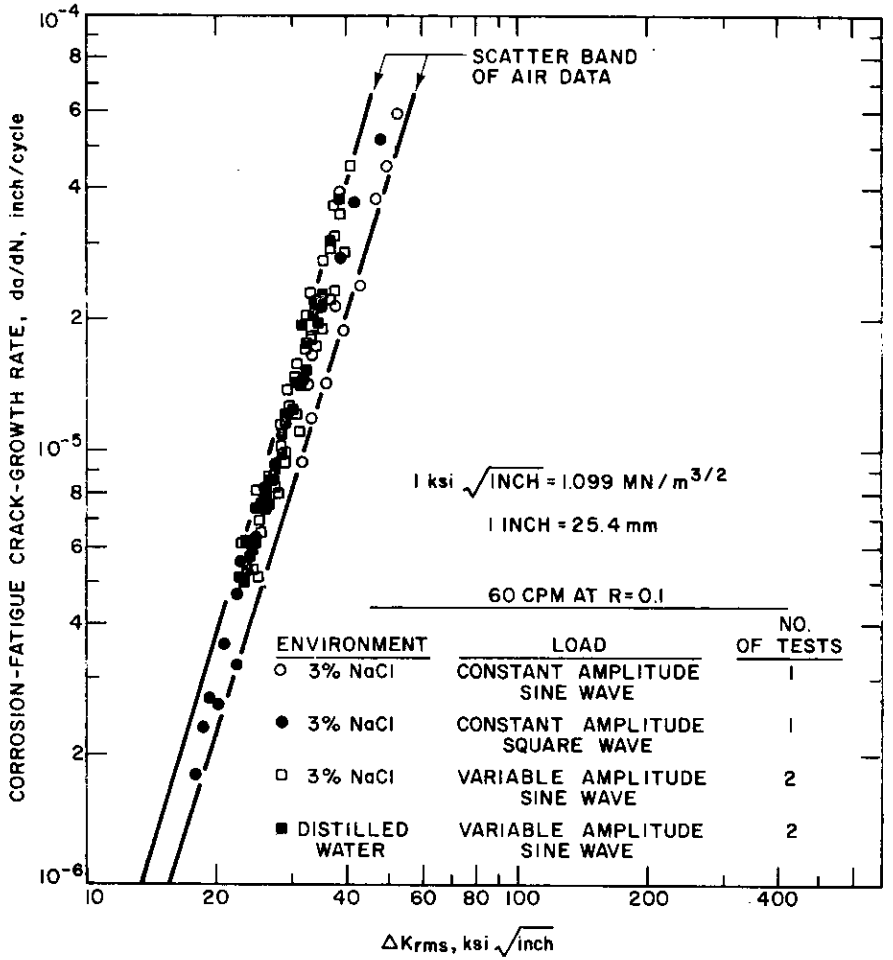

Figure 24. Corrosion fatigue, crack growth rate as a function of the root mean square of the stress intensity factor for A36 steel.

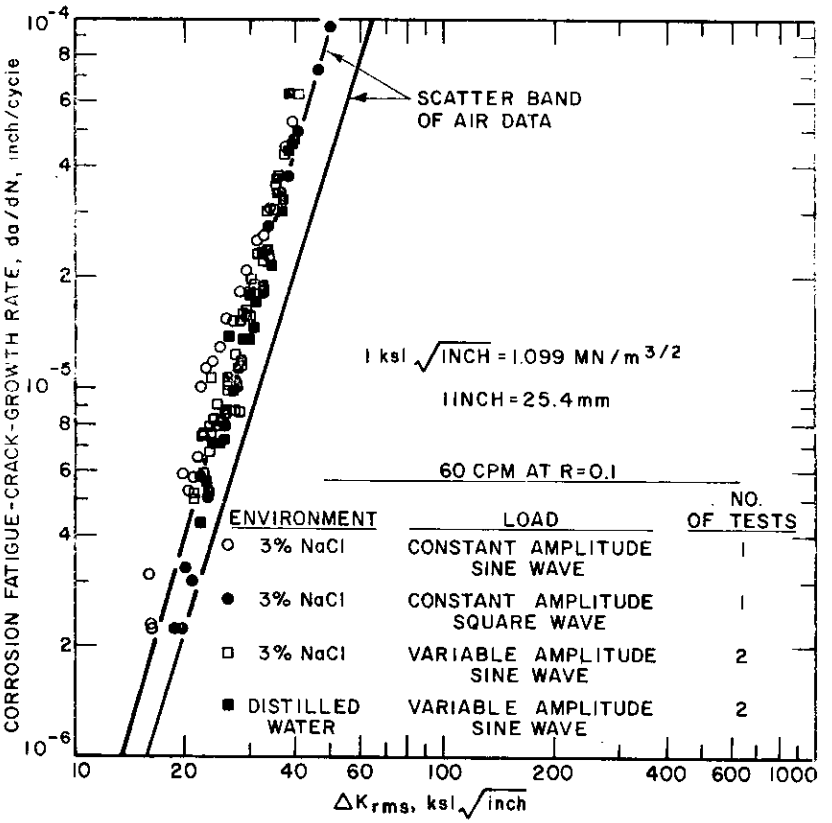

Figure 25. Corrosion fatigue, crack growth rate as a function of the root mean square of the stress intensity factor for A588 Grade A steel.

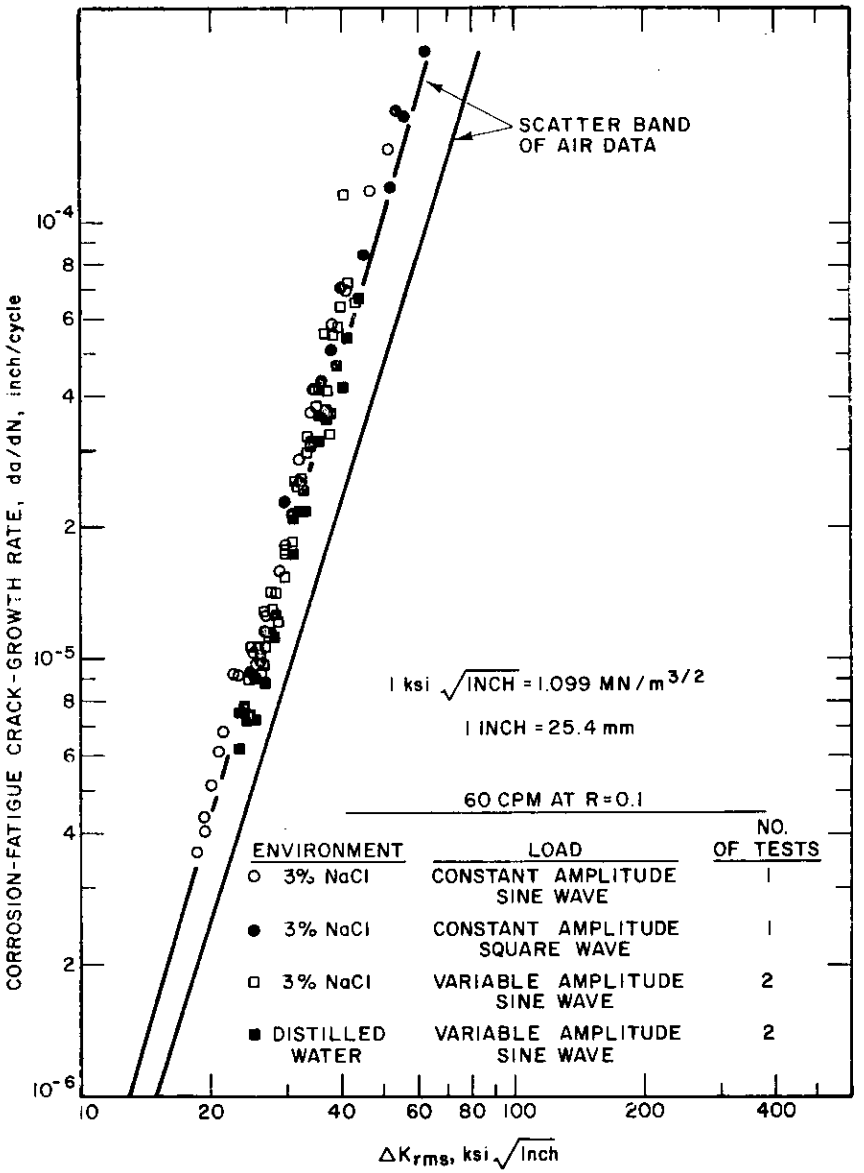

Figure 26. Corrosion fatigue, crack growth rate as a function of the root mean square of the stress intensity factor for A588 Grade B steel.

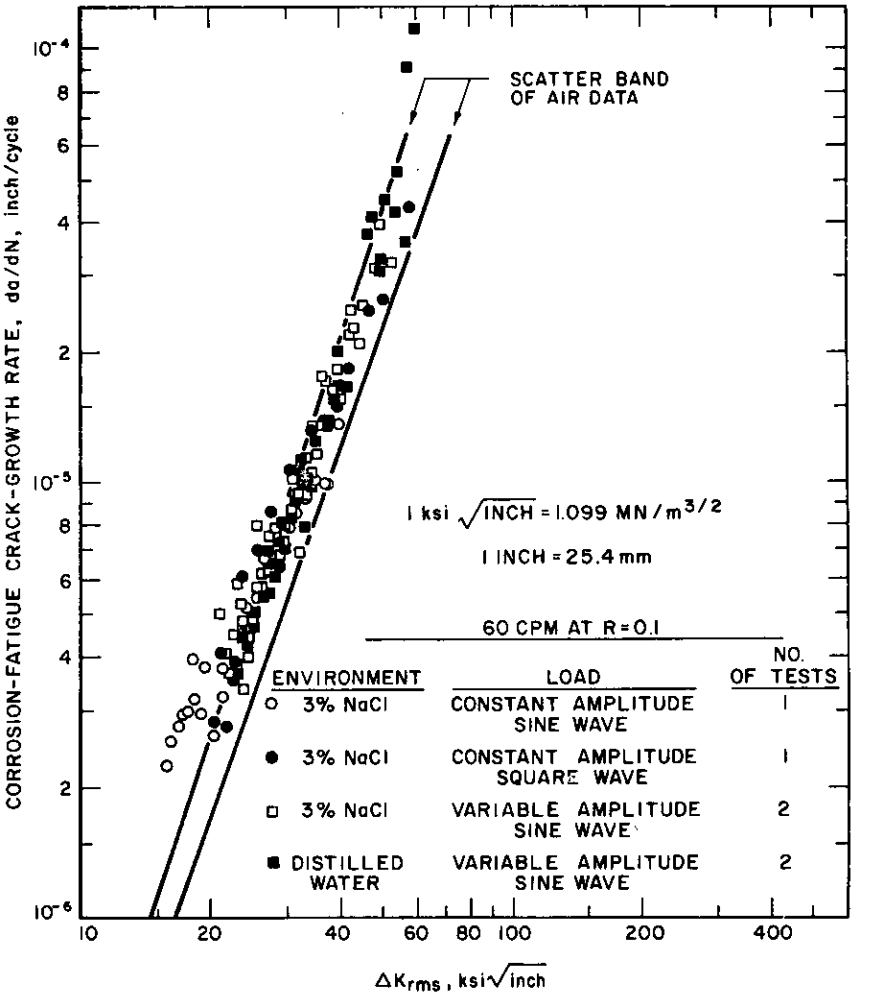

Figure 27. Corrosion fatigue, crack growth rate as a function of the root mean square of the stress intensity factor for A514 Grade E steel.

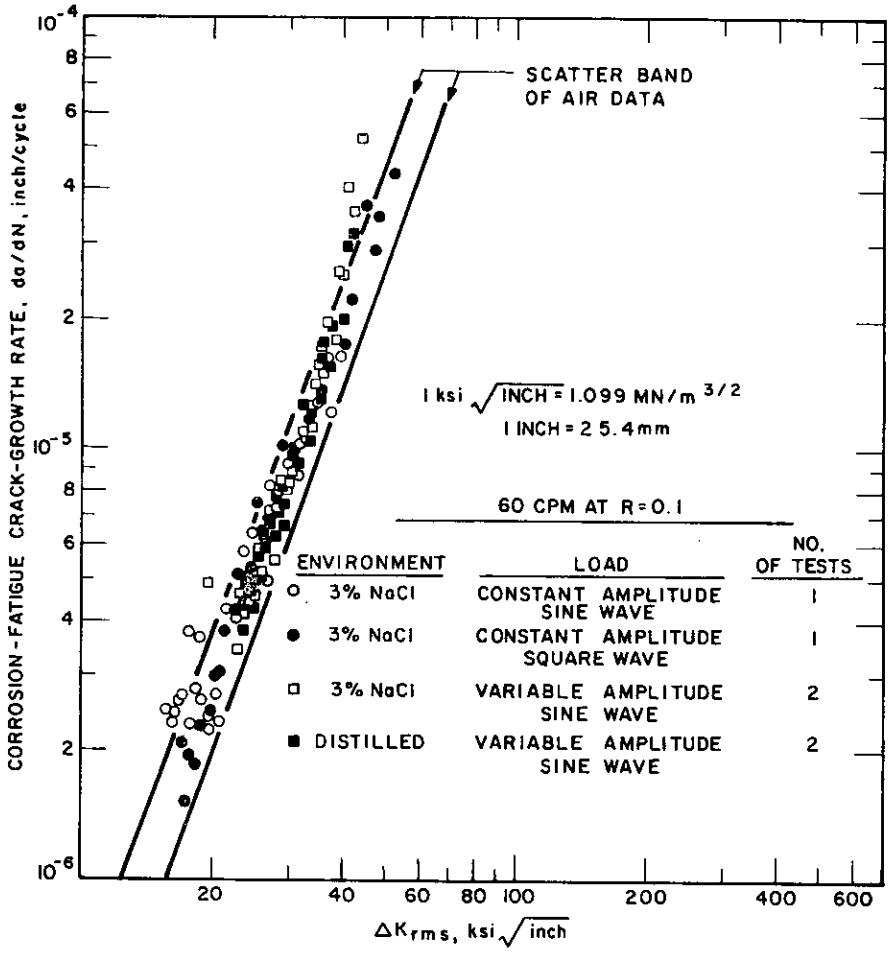

Figure 28. Corrosion fatigue, crack growth rate as a function of the root mean square of the stress intensity factor for A514 Grade F steel.

Corrosion Fatigue Behavior at 12 CPM

Details of the corrosion fatigue data obtained by testing A36, A588 grades A and B, and A514 grades E and F steels in 3-percent solution of sodium chloride in distilled water are given in Appendix G (Figs. G-1 through G-13) in terms of crack length, a, and the corresponding number of elapsed cycles, N. Figures 29 through 33 show the data obtained by testing duplicate specimens of these steels at 12 cpm under constant amplitude sinusoidal loading. Superimposed on these figures is the upper bound of data scatter obtained by testing these steels at 60 cpm under constant amplitude loading and under variable amplitude, random sequence loading in distilled water and in 3-percent solution of sodium chloride. The time required to initiate and propagate a corrosion fatigue crack in some of the specimens tested at 12 cpm was 850 h. Consequently, the general corrosion of the surfaces of these specimens was more extensive than that observed on similar specimens tested at 60 cpm. This extensive surface corrosion resulted in greater data scatter than the scatter obtained in tests at 60 cpm. The corrosion fatigue data in Figures 29 through 33 show that the rate of crack growth for bridge steels tested at 12 cpm and at stress intensity factor fluctuations greater than about 15 ksi $\sqrt{\text{in.}}$ (16.5 $\text{MNm}^{-3/2}$) was equal to or slightly greater than the rate observed at 60 cpm.

Corrosion Fatigue Behavior at Low ΔK_I *Values*

The corrosion fatigue, crack growth data for A36 steel tested at 12 cpm indicated that the rate of crack growth decreased significantly at ΔK_I values less than 20 ksi $\sqrt{\text{in.}}$ (22.0 $\text{MNm}^{-3/2}$) (see Fig. 34). Similar behavior was observed in the other steels tested. To verify this observation, one specimen of A514 Grade E steel and one specimen of A514 Grade F steel were tested at 12 cpm in 3-percent sodium chloride solution under cyclic load fluctuations corresponding to ΔK_I of about 11 ksi $\sqrt{\text{in.}}$ (12.1 $\text{MNm}^{-3/2}$). The test results, shown in Figures 35 and 36, point out that a corrosion fatigue, crack gowth rate threshold, ΔK_{th}, does exist in A514 steels at a value of about 11 ksi $\sqrt{\text{in.}}$ This ΔK_{th} represents the value of the stress intensity factor fluctuation below which corrosion fatigue cracks do not propagate at 12 cpm in the environment-steel system tested. The value of ΔK_{th} in A514 steels tested at 12 cpm in 3-percent sodium chloride solution was twice as large as the value of 5.5 ksi $\sqrt{\text{in.}}$ (6.0 $\text{MNm}^{-3/2}$) for room-temperature air (*32*).

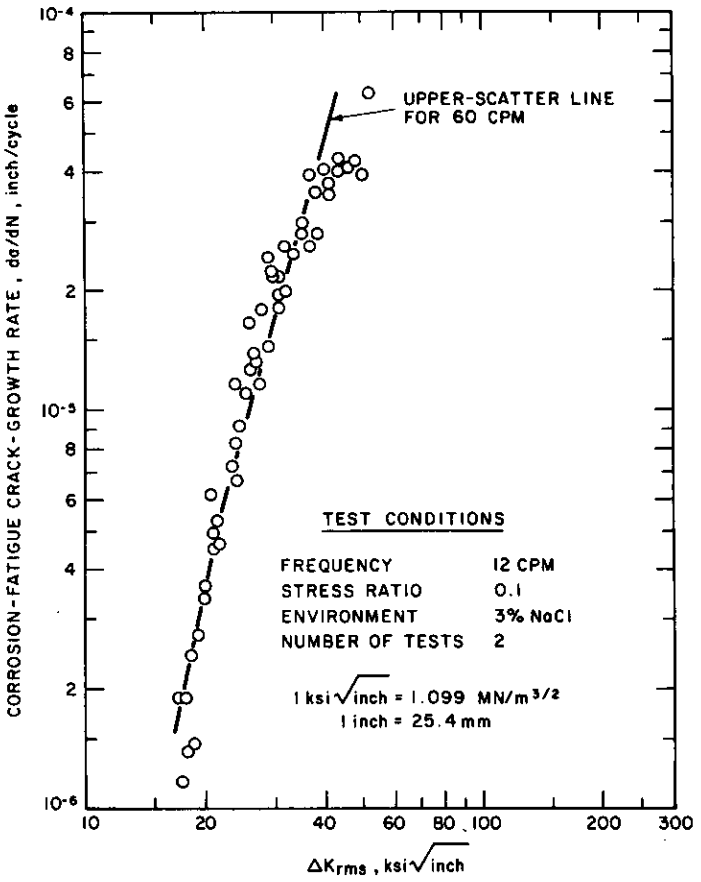

Figure 29. Corrosion fatigue, crack growth rate as a function of the root mean square of the stress intensity factor for A36 steel.

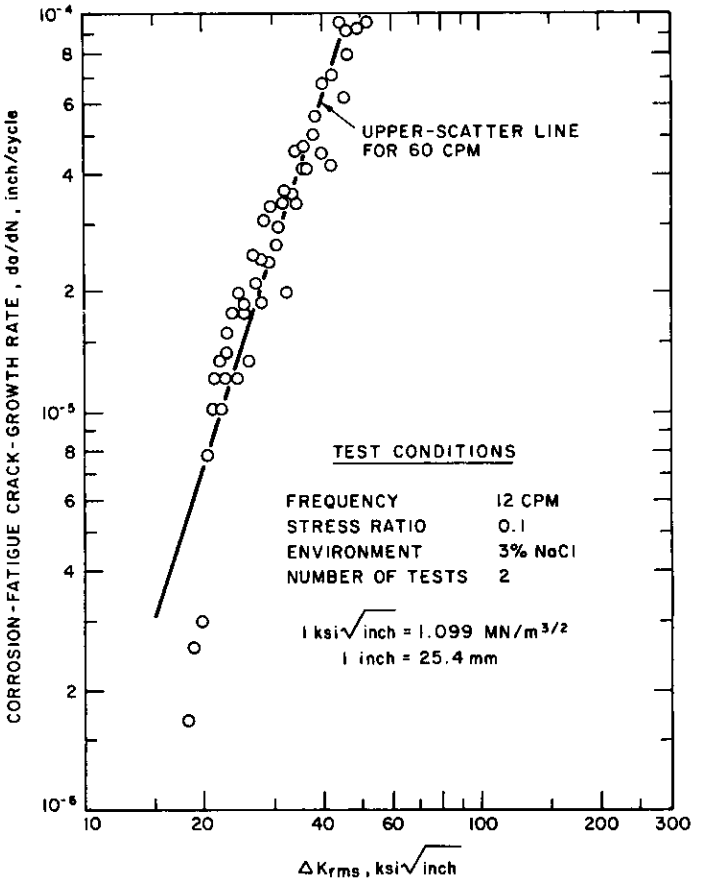

Figure 30. Corrosion fatigue, crack growth rate as a function of the root mean square of the stress intensity factor for A588 Grade A steel.

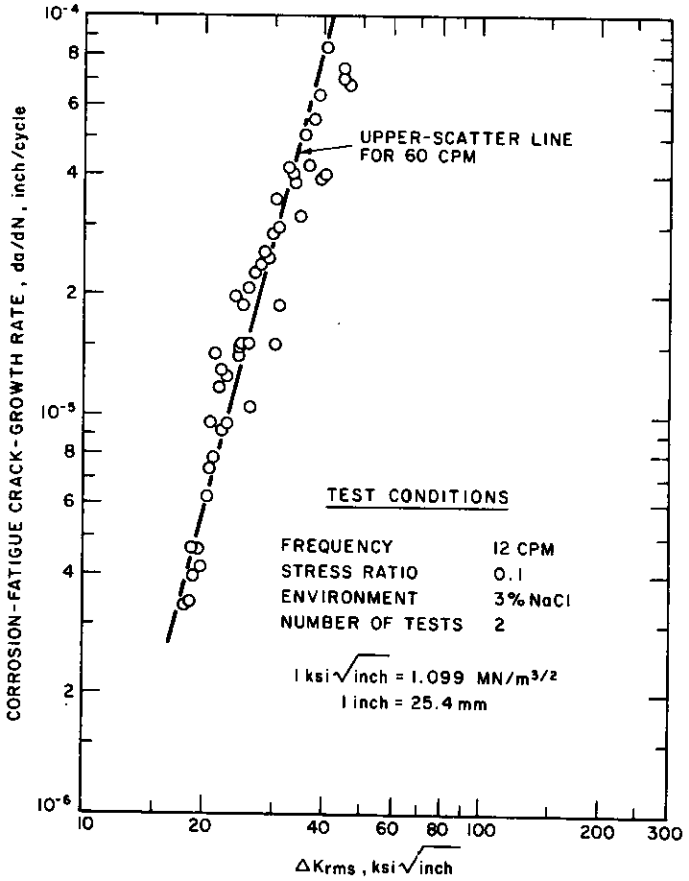

Figure 31. Corrosion fatigue, crack growth rate as a function of the root mean square of the stress intensity factor for A588 Grade B steel.

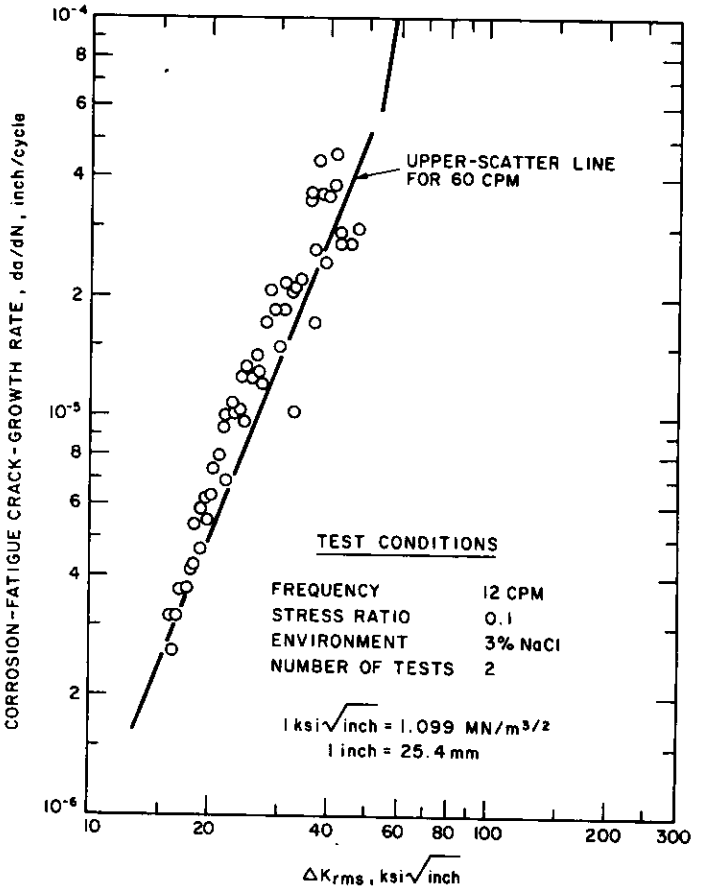

Figure 32. Corrosion fatigue, crack growth rate as a function of the root mean square of the stress intensity factor for A514 Grade E steel.

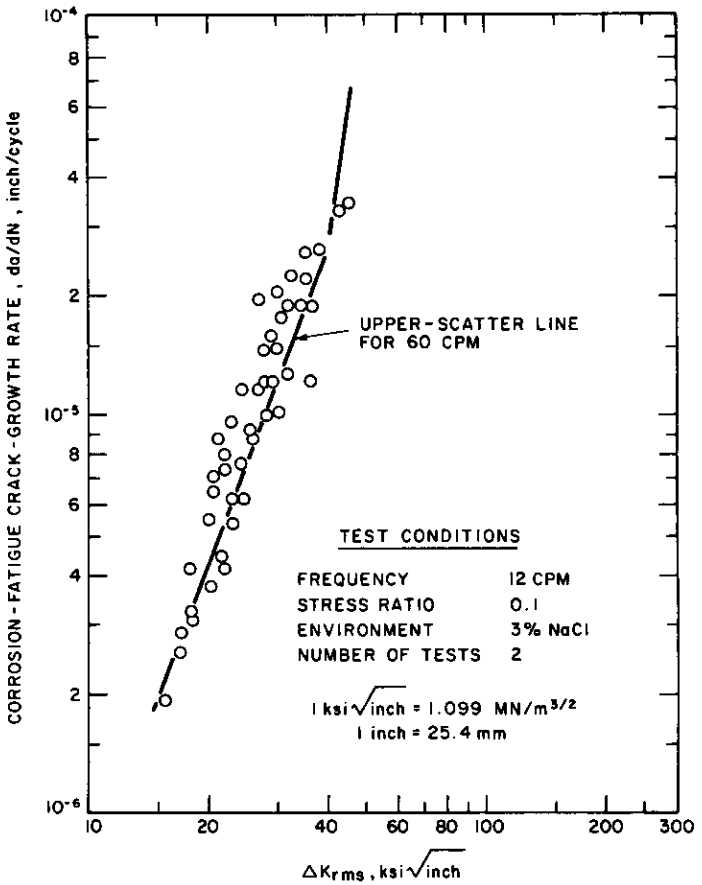

Figure 33. Corrosion fatigue, crack growth rate as a function of the root mean square of the stress intensity factor for A514 Grade F steel.

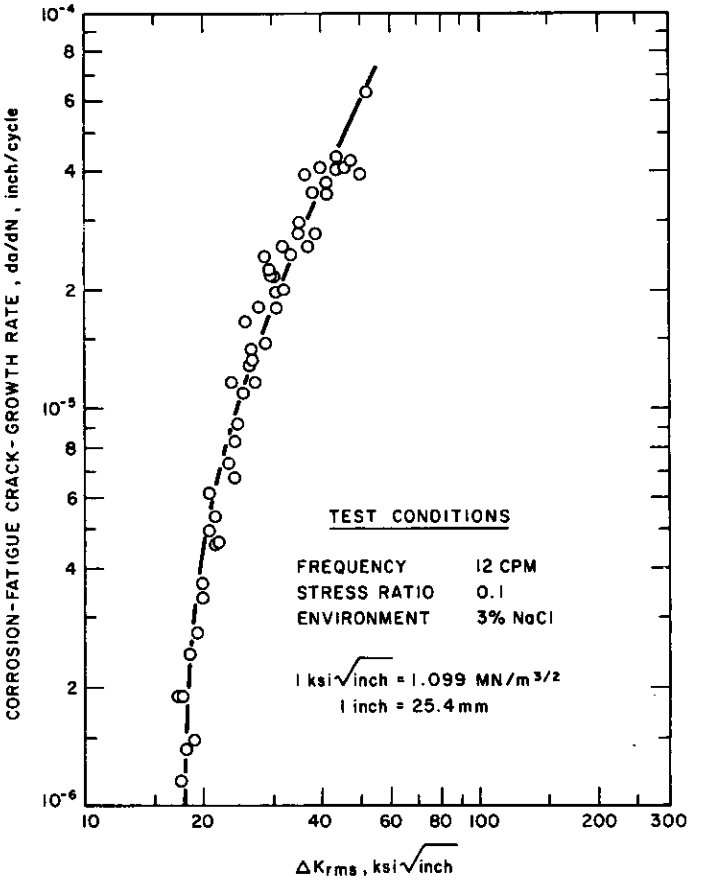

Figure 34. Corrosion fatigue, crack growth rate as a function of the root mean square of the stress intensity factor for A36 steel.

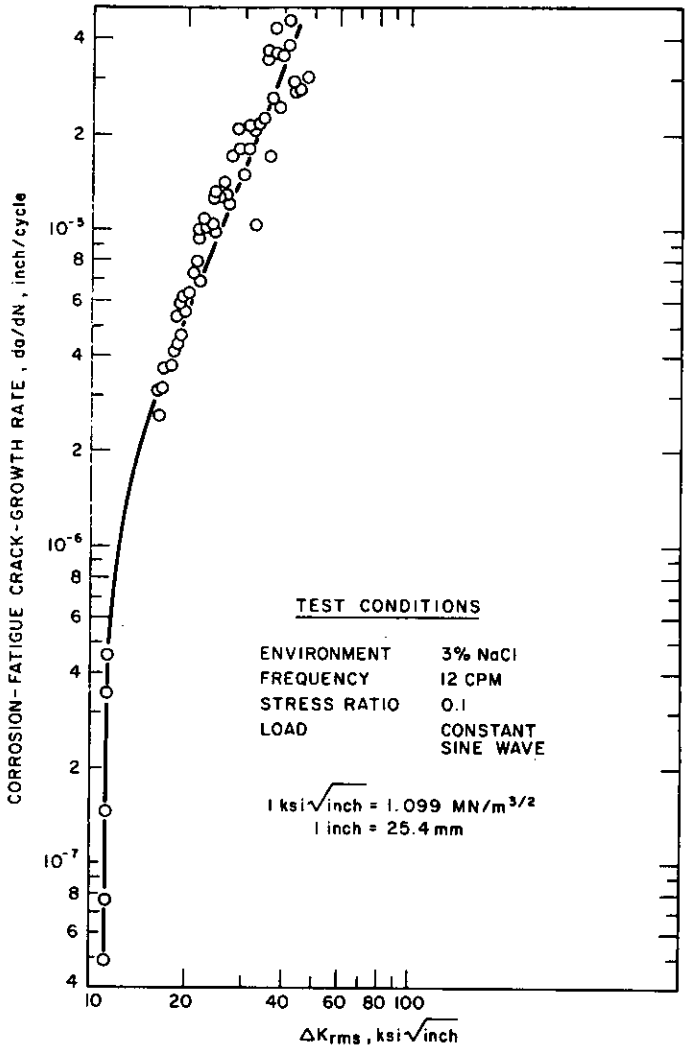

Figure 35. Corrosion fatigue, crack growth rate as a function of the root mean square of the stress intensity factor for A514 Grade E steel.

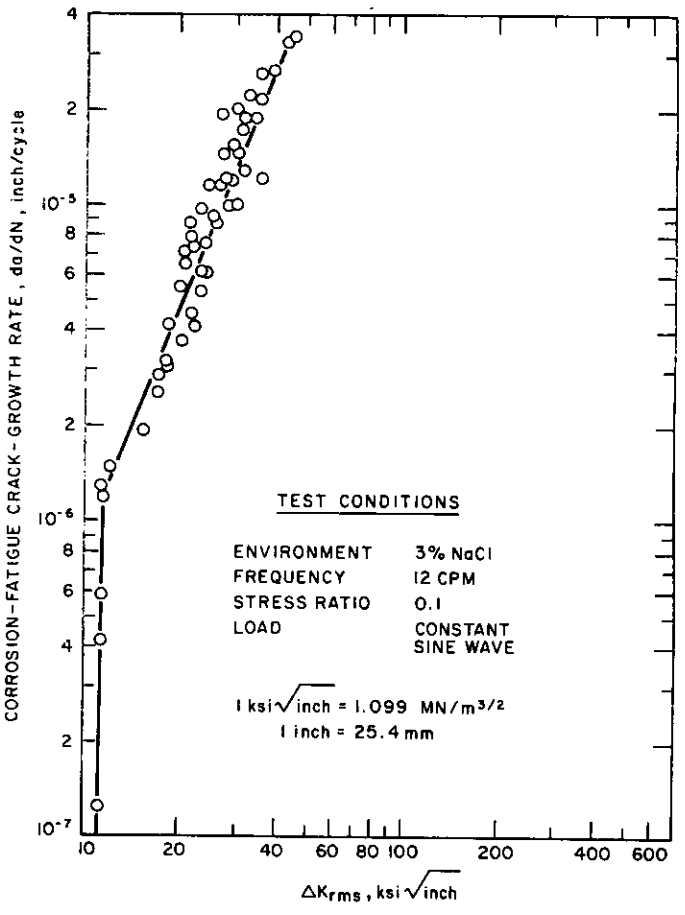

Figure 36. Corrosion fatigue, crack growth rate as a function of the root mean square of the stress intensity factor for A514 Grade F steel.

Bucci and Donald (*33*) observed that the environmental ΔK_{th} in a 200-grade maraging steel forging was higher than the ΔK_{th} in air and that salt water appeared to produce an inhibitive effect on fatigue cracking at very low ΔK levels. Paris et al. (*34*) also observed that the threshold ΔK of ASTM A533 (Grade B Class 1) steel in distilled water was greater than that established in room-temperature air. These investigators noted the following:

> Since the distilled water retardation of very low crack extension rates was a somewhat surprising result, an additional specimen was tested for which a distilled water environment was provided to the crack tip and its surrounding only after an initial slow crack extension rate had been established in room air. Upon application of the distilled water, the rate of crack growth decreased from those initially obtained in air.

The observations by Bucci and Donald and by Paris et al. confirm the results of this investigation.

In an air environment, the fatigue ΔK_I threshold, ΔK_{th}, in various steels tested at a stress ratio of 0.1 is independent of cyclic load frequency and is equal to about 5.5 ksi $\sqrt{\text{in.}}$ Because hostile environmental effects decrease with increased cyclic load frequency, the corrosion fatigue K_{th} at very high cyclic load frequencies would have a value close to that of fatigue in air. A K_{Iscc} test can be considered a corrosion fatigue test at extremely low cyclic load frequency. In such tests, the rate of crack growth at a stress intensity factor fluctuation that is slightly lower than K_{Iscc} is, by definition, equal to zero. Consequently, at very low cyclic load frequencies, ΔK_{th} is equal to K_{Iscc}. Hence, the value of the environmental ΔK_{th} at intermediate cyclic load frequencies must be greater than 5.5 ksi $\sqrt{\text{in.}}$ and less than the value of K_{Iscc} for the environment-steel system under consideration. The test results show that, at 12 cpm, the environmental ΔK_{th} of A514 steels in 3-percent solution of sodium chloride in distilled water was equal to about 11 ksi $\sqrt{\text{in.}}$ Based on the preceding observations, a schematic representation of the corrosion fatigue behavior of bridge steels subjected to different cyclic load frequencies was constructed, as shown in Figure 37. This figure, which

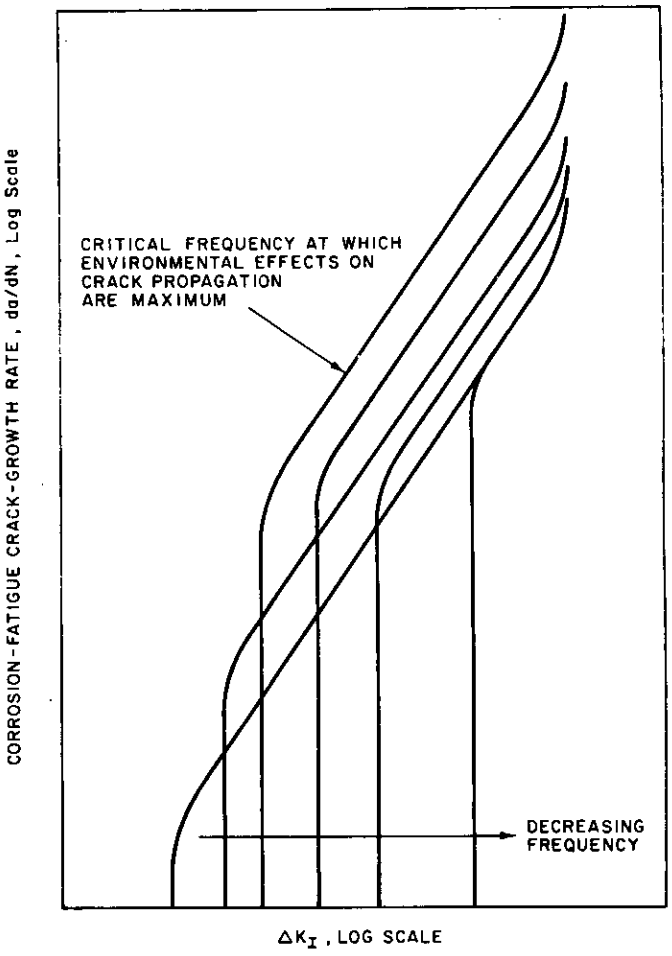

Figure 37. Schematic of idealized corrosion fatigue behavior as a function of cyclic load frequency.

is an oversimplification of a very complex phenomenon, depicts only the effects of cyclic load frequency on the corrosion fatigue, crack growth rate behavior of bridge steels.

Corrosion Fatigue Behavior Under Alternate Wet and Dry Conditions

The foregoing discussion concerned the corrosion fatigue behavior of bridge steels under complete immersion conditions. Under actual operating conditions, bridges are subjected to benign environments (as in the case of painted bridges) or to alternate wet and dry environmental conditions (as in the case of unpainted bridges or improperly maintained bridges). The fatigue behavior of bridge steels in a benign environment (room-temperature air) is covered in a preceding section and is also the subject of investigation in Refs. (*1*), (*2*), and (*24*). The fatigue behavior under alternate wet and dry conditions is described as follows.

The effects of alternate wet and dry environmental conditions on bridge steels were simulated in this study by using a specimen of A514 steel. First, the corrosion fatigue, crack growth rate in the specimen was established at 12 cpm under full-immersion conditions in 3-percent solution of sodium chloride in distilled water. The specimen was then removed from the environmental bath and left overnight to dry in room-temperature air. Finally, the specimen was replaced in 3-percent sodium chloride solution, and the corrosion fatigue, crack growth behavior was again measured at 12 cpm under full-immersion conditions and under the same load fluctuations applied prior to drying the specimen. Figure 38 shows the results obtained from this interrupted test. The data indicate the existence of nonsteady-state crack growth represented by a severe retardation of the rate of corrosion fatigue crack growth and a corresponding substantial increase in the life of the specimen. The data also show that the life of the specimen was *doubled,* because 115,000 cycles were required to reestabilsh the steady state, crack growth rate behavior. Similar retardation behavior and a concomitant increase in the useful life of specimens tested under alternate wet and dry conditions were observed by Miller et al. (*35*) in AISI 4340 steel tempered at 200 F. (93 C), as shown in Figure 39.

Effect of Stress Ratio on the Corrosion Fatigue Behavior of Bridge Steels

The corrosion fatigue data obtained by testing A36, A588 grades A and B, and A514 grades E and F steels in 3-percent solution of sodium chloride in distilled water at a stress ratio, R, of 0.5 and at 60 cpm are given in Appendix G in terms of crack length, a, and the corresponding number of elapsed cycles, N. The data obtained by testing duplicate specimens of these steels at $R = 0.5$ under variable amplitude loading are shown in Figures 40 through 44 in terms of crack growth rate and the corresponding root mean square of the stress intensity factor fluctuation, ΔK_{rms}. Superimposed on these figures are the upper and lower bounds of corrosion fatigue data obtained at $R = 0.1$. It is obvious from these figures that a stress ratio of 0.5 had a negligible effect on the rate of corrosion fatigue crack growth in bridge steels.

Corrosion Fatigue Behavior of A588 Steel from Various Sources

Corrosion fatigue data of four heats of A588 Grade A steel and one heat of A588 Grade B steel were obtained at 60 cpm in 3-percent solution of sodium chloride in distilled water. These five steels (A588 grades A and B) were obtained from two suppliers (Bethlehem Steel Corp. and U.S. Steel Corp.) at three plant locations; the steels were melted by either of two melting processes (open-hearth and basic-oxygen process) over a span of 10 years' time (1964 to 1974). Furthermore, these five steels represent reasonable variation in chemical composition within the ASTM specification (Tables II and IV), as well as reasonable variation in mechanical properties (Tables III and V). The corrosion fatigue data are given in Appendix G in terms of crack length, a, and the corresponding number of elapsed cycles, N; the data shown in Figure 45 are in terms of da/dN and ΔK_I. This figure reveals that the rate of corrosion fatigue crack growth for one heat of the A588 steels tested was equal to the rate of growth for any of the other heats. Thus, despite the variations in melting history, chemical composition, and mechanical properties, the corrosion fatigue, crack growth rates for various A588 grades A and B steels were essentially identical.

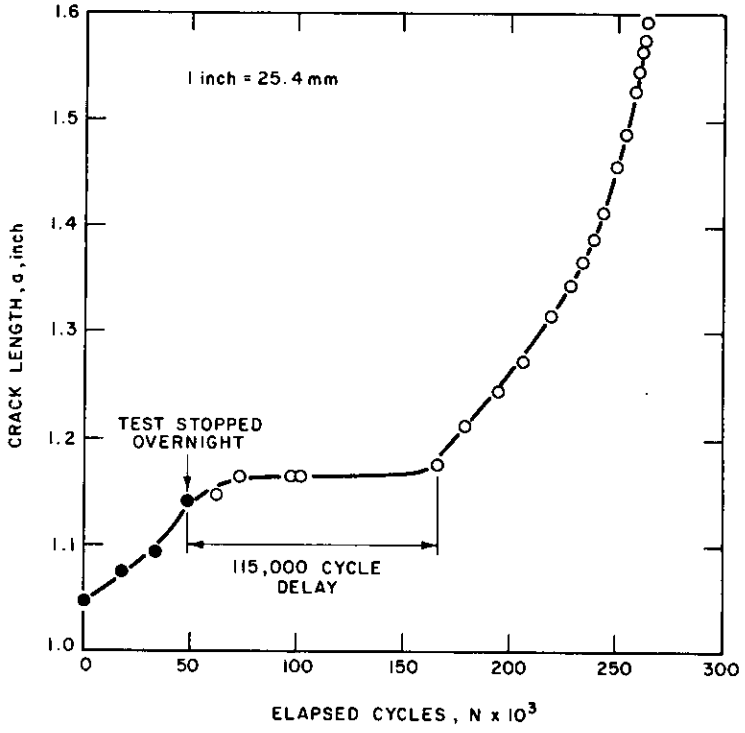

Figure 38. Retardation of corrosion fatigue, crack growth rate under wet and dry environmental conditions for A514 Grade F steel.

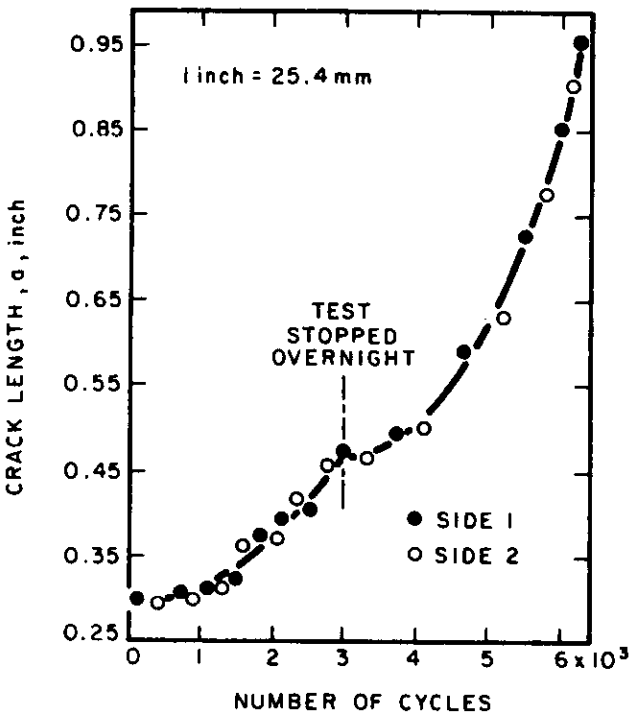

Figure 39. Fatigue crack growth curve for AISI 4340 steel tempered at 200 F (93 C), showing nonsteady-state behavior (from Ref. (35)).

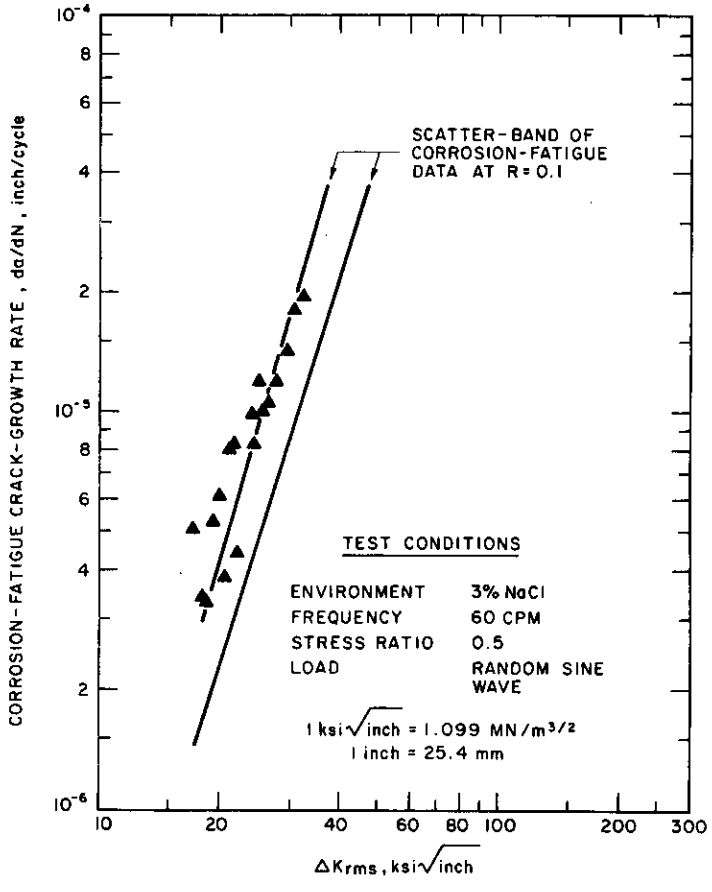

Figure 40. Corrosion fatigue, crack growth rate as a function of the root mean square of the stress intensity factor for A36 steel.

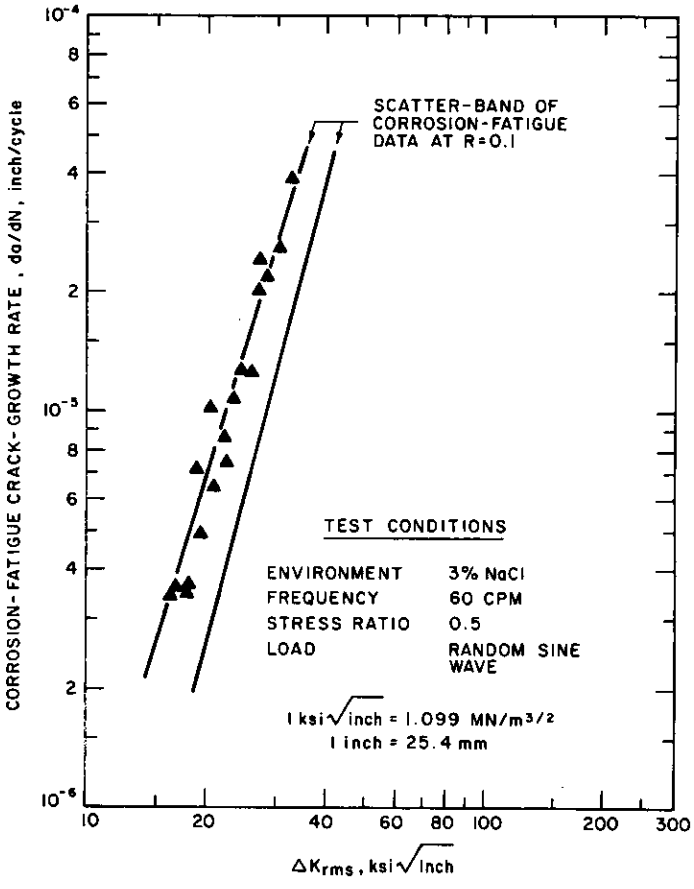

Figure 41. Corrosion fatigue, crack growth rate as a function of the root mean square of the stress intensity factor for A588 Grade A steel.

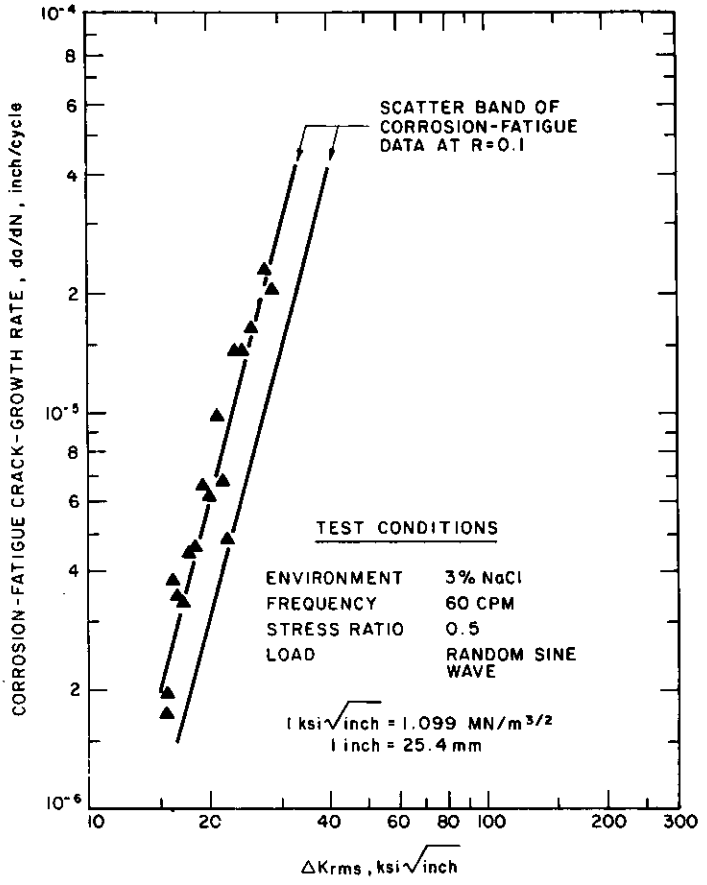

Figure 42. Corrosion fatigue, crack growth rate as a function of the root mean square of the stress intensity factor for A588 Grade B steel.

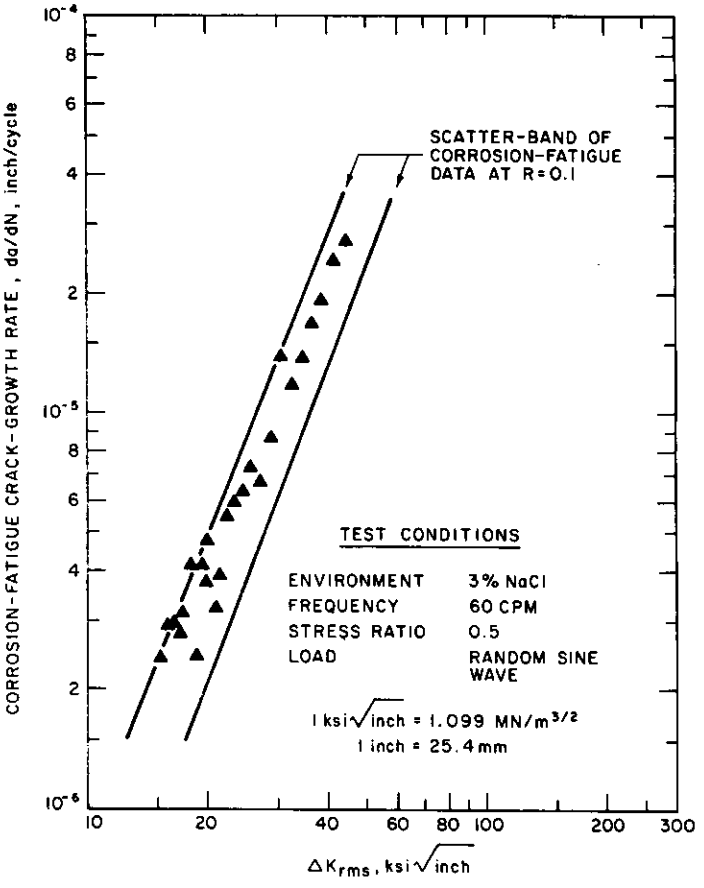

Figure 43. Corrosion fatigue, crack growth rate as a function of the root mean square of the stress intensity factor for A514 Grade E steel.

CHAPTER THREE

INTERPRETATION OF APPRAISAL OF FINDINGS

SIGNIFICANCE OF FRACTURE TEST RESULTS

A summary of the results from the fracture tests conducted at 72 F (22 C) is given in Table 6. These results, discussed in detail in Appendix D, show that no valid K_{Ic} values could be measured for any of the five steels tested. The inability to measure valid K_{Ic} values in the fracture tests was due to the combined effects of both a high level of fracture toughness for each steel and the limitations imposed by the size of the 1T specimen. Because of these circumstances, high levels of plasticity were developed prior to fracture in all tests, thus precluding the direct application of LEFM concepts (at fracture).

Although quantitative assessments of fracture behavior for the steels tested can not be made on the basis of the present results, semiquantitative interpretations can be given based on the K_I-suppression effect concept (*21, 36, 37*). In particular, it has been shown that, when fracture test specimens that are too small are employed in fracture tests of high-toughness steels, the apparent K_{Ic} values (K_Q values) will be *lower* than the true K_{Ic} value. The systematic manner in which the K_Q values decrease and further underestimate the true K_{Ic} value as the test specimens are made smaller is known as the K_I-suppression effect. When the specimen size for a proportional geometry specimen is only 10 percent of that required for a valid K_{Ic} result, the K_Q value measured will be suppressed to less than half (0.50) of the true K_{Ic} value. The indexing point for the occurrence of such behavior is when the observed K_Q value is 60-percent higher than the valid plane-strain measurement capacity for the test conditions employed. (The K_Q value is suppressed to less than one-half (0.50) of K_{Ic} when

$(K_Q/K_{I,\,Lub}) = 1.60$, where $K_{I,\,Lub} = \sigma_{ys}\,(B/2.50)^{1/2}$ and $K_{I,\,Lub}$ is the plane-strain measurement capacity for the particular combination of steel, σ_{ys}, and specimen size, B, tested.) When the size of the fracture test specimen is only moderately inadequate to obtain a valid K_{Ic} result, the corresponding K_Q value will be suppressed below the true K_{Ic} value by only a moderate amount.

Because of the systematic nature of the K_I-suppression effect, this concept can be used in a reverse manner to "correct" the invalid K_{Ic} results. Although precise corrections are not possible at this time, meaningful approximations of the true K_{Ic} behaviors can be made, particularly in relation to the indexing point described earlier.

Such estimates of the true K_{Ic} behavior of the five steels of interest were made and are given in Table 6 together with the summary of actual test results. The estimates of K_{Ic} behavior for the steels tested by using the K_I-suppression effect are believed to be both conservative and realistic. Furthermore, such estimates are the best presently available without using elastic-plastic fracture analysis methods—J-integral (*38, 39*) and equivalent-energy methods (*40, 41*)—which are still under development and for which special test conditions must be provided (such as 6 specimens per evaluation, load-line measurement for V, and metallographic sectioning of specimens).

The realistic nature of the estimates of K_{Ic} behavior (Table 6) is given further credence when such results are compared with those obtained from other estimating techniques developed earlier (*42, 43*). In particular, it can be seen that the singular estimates of K_{Ic} behavior made for the A514 grade E and A514 grade F steels, by using the Charpy V-notch specimen correlation for high-strength martensitic steels (*42*) ($K_{Ic} = 184$ and 156 ksi $\sqrt{\text{in.}}$ (202.2 and 171.4 $\text{MNm}^{-3/2}$), respectively), are contained within the corresponding ranges of K_{Ic} behavior estimated by using the K_I-suppression effect concept. Furthermore, the minimum values cited for the A588 Grade A and A588 Grade B steels are consistent with both actual K_{Ic} results and results of behavior from more extensive studies of an A572 steel of similar strength (σ_{ys}) and mechanical properties (CVN) (*37*). An additional method is also available for estimating the K_{Ic}-transition behavior of ferrite-pearlite steels, such as the A36 and A588 grades A and B steels (*43*). This technique involves the use of CVN test results for predicting the interrelationship of K_{Ic} with test temperature and strain rate. However, this approach is of limited applicability in the present discussion concerning the static K_{Ic} behavior of the steels tested, because only the K_{Ic} transitional behavior can be predicted, and, for the steels tested, this behavior will occur at temperatures well below the 72-F test temperature used in the bulk of the current study.

The results in Table 6 include the minimum thicknesses, $B_{\min}$, required for valid K_{Ic} fracture of each material under two different conditions of crack orientation. For each steel, $B_{\min}$ values are given for both through-thickness cracks and partial-thickness cracks (PTC). These $B_{\min}$ values are calculated on the basis of the minimum estimates of K_{Ic} behavior presently given for each steel. Calculations of the critical flaw size at fracture, a_{cr}, under K_{Ic} conditions are not applicable by using LEFM principles, unless the thicknesses used in the specific structural applications are

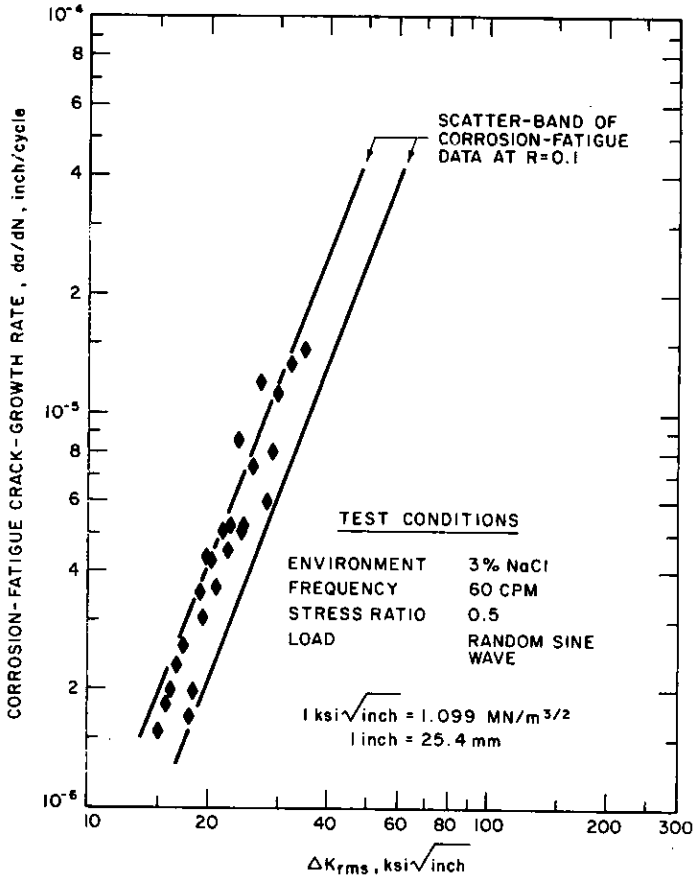

Figure 44. Corrosion fatigue, crack growth rate as a function of the root mean square of the stress intensity factor for A514 Grade F steel.

in excess of the cited $B_{\min}$ values. Thus, as noted in the following discussion, the applicability of the present K_{Ic} estimates for predicting actual structural behavior at fracture depends on the specific service application.

The preceding estimates of K_{Ic} fracture behavior for the steels in Table 6 are largely academic for bridge construction, because the structural members in such applications are generally fabricated from plates ranging in thickness from ½ to 1½ in. (12.7 to 38.1 mm). Thicknesses greater than 1½ inches are used only occasionally in routine bridge construction. However, even the 1½-in. plate thicknesses are still less (considerably less in most cases) than that required ($B_{\min}$) for plane-strain (K_{Ic}) fracture on the basis of the minimum estimated behavior for each steel (Table 6). Plates that are 1½ in. or less in thickness would fracture under so-called plane-stress (K_c) conditions. Because K_c values are generally 2 to 5 times higher than corresponding K_{Ic} values, each of the steels in this study would possess extensive resistance to fracture in such bridge applications and fracture would not be a major criterion of concern. (Although this statement is clearly applicable to all five of the steels tested, it is least applicable to the A514 Grade F steel because of its abnormally high strength ($\sigma_{ys} =$ 126 ksi, or 869 MN/m^2). However, even for this A514-F steel, calculations show that relatively large flaws could be tolerated prior to fracture under normal design conditions. For example, for material behavior of $K_{Ic} = 125$ $\sqrt{\text{in.}}$

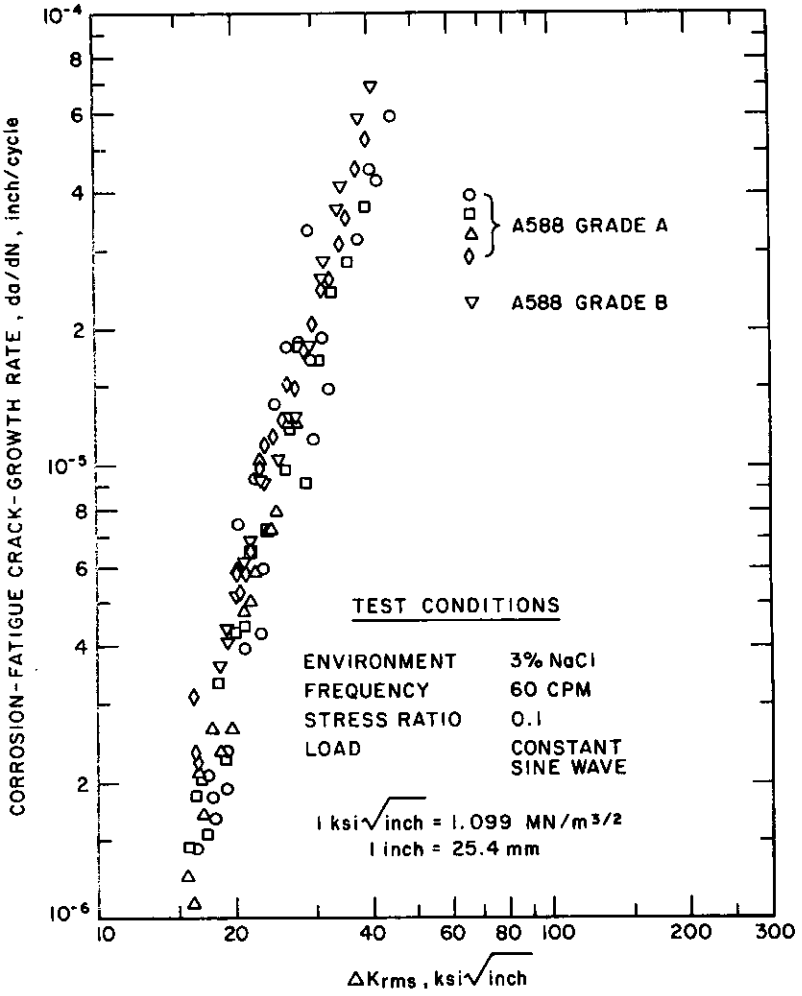

Figure 45. Corrosion fatigue, crack growth rate as a function of the root mean square of the stress intensity factor for A588 steels from various sources.

(138 $MNm^{-3/2}$) and $\sigma_{ys} = 125$ ksi (862 MN/m^2), the dimensions of a typical PTC ($a/2C = 0.25$) contained within a plate of sufficient thickness ($B \geqq B_{min} = 500$ in., or 127 mm) and subjected to a uniform tensile stress field under typical design conditions ($\sigma V_D/\sigma_{ys} = 0.75$) would be $a_{cr} = 0.65$ in. (16.5 mm) and $2c_{cr} = 2.60$ in. (66.0 mm) at fracture. Furthermore, the actual crack dimensions would be even larger, because the calculated a_{cr} value is less than that required (2.50 in., or 63.5 mm) for the strict application of LEFM calculations to K_{Ic} fracture behavior. A semiempirical fracture analysis method in which the K_{Ic} value is corrected to higher effective value, K_{Iu}, currently exists for such conditions (*44*).)

Above and beyond the basic fracture behavior lies the question of over-all structural life. Certainly, the load carrying capacity, and consequently the life of a typical structural member, is virtually nonexistent once a crack penetrates the tension flange of a plate girder. However, the initiation and growth of a crack of this type through the governing processes of fatigue and corrosion fatigue would require many years (30 to 100), even if the crack is at a critical location, such as at the end of a cover plate. Furthermore, because of the multiple load paths available in redundant-bridge construction, H-beams of this type (for which the life is consumed) are generally replaced long before fracture can take place. In other words, because the life of such an H-beam is governed by the initiation of a crack ($K = 0$) and its subsequent propagation from the tension flange into the web ($K \cong 30$ to 40 ksi $\sqrt{\text{in.}}$, or 33.0 to 44.0 $MNm^{-3/2}$), the life is normally consumed well in advance of fracture at a K_{Ic} (or K_c) value that is substantially higher. Consequently, the fracture toughness requirement for bridge steels can be relegated to a position of secondary importance once the particular candidate material has been shown to possess an *adequate level of fracture toughness.*

In predictions of service life for structures, the material behavior considerations must always be viewed in proper context as only a single component of the entire problem. Over-all life is determined by (1) basic material behavior, (2) design, (3) fabrication, and (4) inspection. As discussed elsewhere (*43*), inadequate performance in any of these areas will tend to minimize the actual life of the particular structure considered.

SIGNIFICANCE OF FATIGUE TEST RESULTS

Extensive fatigue crack growth data for various bridge steels were obtained under constant amplitude, cyclic load fluctuations and under variable amplitude, random se-

quence, cyclic load fluctuations such as occur in actual bridges. The test results show that, for various bridge steels, a correlation exists between both the average rate of fatigue crack growth under constant amplitude, cyclic loading conditions and the average rate of fatigue crack growth under variable amplitude, cyclic loading conditions. The data obtained for A36, A588 grades A and B, and A514 grades E and F steels showed that the average rate of fatigue crack growth, da/dN, under variable amplitude, cyclic load fluctuations and under constant amplitude, cyclic load fluctuations agreed closely when da/dN was plotted as a function of the root mean square of the stress intensity factor fluctuation, ΔK_{rms}. Thus, the average rate of fatigue crack growth, da/dN, for various bridge steels subjected to variable amplitude and constant amplitude, cyclic load fluctuations can be represented by the equation

$$da/dN = A(\Delta K_{rms})^n$$

where A and n are material constants. This RMS model for fatigue crack growth is expected to have widespread application in the computation of the useful life of bridge components and other structures. The use of this model requires characterization of the cyclic stress distribution function for the structure of interest. Characterization of the cyclic stress distribution functions for bridges is under consideration in Ref. (*24*).

SIGNIFICANCE OF STRESS CORROSION TEST RESULTS

The results of the 5000-h (30-week) stress corrosion tests with precracked cantilever beam specimens are shown in Figures 19 through 23 and are discussed in detail in Appendix F. The sailent features of these results are summarized in Table 7.

It is apparent from these data that no valid K_{Iscc} values were obtained for any of the five steels examined in this study. As described in Appendix F, the apparent K_{Iscc} values measured for most of the steels correspond to conditions involving substantial crack-tip plasticity. Consequently, LEFM concepts can not be used for quantitative analysis of the respective stress-corrosion-cracking (SCC) behaviors (*21*). Furthermore, the apparent K_{Iscc} values are suppressed to various degrees below the intrinsic K_{Iscc} values for these steels in a manner similar to that described in the previous section on fracture (K_{Ic}) behavior. In other words, the apparent K_{Iscc} values reflect behavior described by the K_I-suppression effect concept because of both a high resistance to SCC for each steel and the limitations in analysis imposed by the size of the 1T specimen.

For such cases the most important parameter for characterizing the SCC behavior is the ratio of the apparent threshold to the value at fracture obtained with an identical size specimen (apparent K_{Iscc}/K_{Ix}) (*21*). This ratio, known as the relative index of SCC susceptibility, can be used to quickly ascertain the degradation in fracture behavior as a result of the test solution and the inherent SCC characteristics of each steel.

General experience with many steels and weldments, some of which are used successfully in long-time environmental service applications, dictates the following broad-based interpretation for assessing the relative SCC index: (1) values ranging from 0.95 to 1.00 represent material behaviors that are immune to SCC; (2) values ranging from 0.80 to 0.95 represent material behaviors that either are moderately susceptible to SCC if the K_{Iscc} value is valid, or are primarily the result of long-time creep that occurs at the crack tip (under the presence of intensely high stress levels) if the apparent K_{Iscc} value measured is not valid and high levels of crack-tip plasticity are involved; and (3) values less than 0.80 are generally the result of true susceptibility to SCC for steels, regardless of whether the apparent K_{Iscc} value is valid or not.

The relative index of SCC susceptibility for each of the five steels tested is contained in Table 7. These results show that each of these steels yielded relative SCC indices of 0.73 or higher for the 5000-h tests in continuously aerated 3-percent sodium chloride solution. In particular, a value of 0.95, representing essentially immune behavior, was found to occur for the A36 steel. Nearly identical values of 0.80 and 0.82 were measured for the A588 grades A and B steels, respectively. These latter values apparently represent primary behavior associated with long-term creep under sustained conditions of high stress level at the crack tip. The two higher strength martensitic steels yielded slightly lower ratios, with specific values of 0.73 and 0.79 for the A514 grades E and F steels, respectively. Although both the fracture-toughness (K_{Ix}) and SCC-threshold (apparent K_{Iscc}) values were higher for the A514 Grade E steel, the relative SCC index was somewhat lower. This difference in behavior of the two A514 steels is somewhat surprising and is illustrative of the complex nature of the SCC mechanism.

Reservations generally held relative to the analysis of SCC test results deal with the time factor. As discussed in more detail elsewhere (*20, 21*), questions often arise, in relation to predictions of long-term structural life (for example, 20 to 50 years), as to whether or not the SCC-evaluation time period for generating baseline data is sufficient. The sigmoidal shapes in the K_{Ii} versus log-time plots obtained for several of the steels tested (Figs. 19 through 23) indicate that the observed thresholds are real, and extrapolations of the same behavior for 1 or 2 additional orders of magnitude (for example, 20 to 50 years) can be made with high levels of confidence. This appears to be particularly true for the A514 Grade F steel, which yielded a marginally invalid K_{Iscc} threshold primarily as a result of its abnormally high strength level. It is of interest to note that the strength level for this steel ($\sigma_{ys} = 126$ ksi, or 869 MN/m^2; $\sigma_{ts} = 134$ ksi, or 924 MN/m^2) was near the specified upper limit of acceptable tensile strength ($\sigma_{ts} =$ 115 to 135 ksi, or 793 to 931 MN/m^2) for the 1-in. plate thickness tested (*45*). Despite this extreme in strength level, the A514 Grade F steel yielded satisfactory performance in the long-term SCC tests.

In summary, the present SCC results indicate a slight, but distinct, degradation in fracture behavior when the steels evaluated are subjected to long-term exposure in an SCC environment. However, both the relative and absolute SCC behaviors (apparent K_{Iscc}/K_{Ix} and apparent K_{Iscc} values reflecting K_I-suppression effects) are at such high levels for each steel that there would appear to be no major problems related to SCC for the use of any of these steels in such long-term structural applications as in bridges. De-

spite the present inability to quantitatively characterize the results in terms of LEFM concepts, the safety and reliability of structures fabricated with any of the present steels would not be impaired due to intrinsic SCC behavior. The existing successful service performance for bridges fabricated with A36 steel and, to a more limited degree, with the A588 grades of steel is, of course, consistent with such expectations and would tend to further confirm the validity of such predictions. In addition, the same criteria described in the preceding section on fracture behaivor are equally applicable here in relation to SCC behavior. Considerations involving typical structural members of ½ to 1½ in. in thickness for bridges resulting in plane-stress behavior (loss of through-thickness constraint) and the general over-all life of a structural member corresponding to the range of $K_I = 0$ to 30 ksi $\sqrt{\text{in.}}$ (33 $\text{MNm}^{-3/2}$) are both still equally valid — even if to a slightly lesser extent because of a token amount of degradation in behavior by SCC as a result of long-term environmental exposure.

It should be noted, in passing, that the 5000-h SCC tests with precracked specimens are among the longest conducted for any class of materials in general. Furthermore, the present results constitute the first such study of significance conducted on structural steels specifically.

SIGNIFICANCE OF CORROSION FATIGUE TEST RESULTS

The effects of variable amplitude loading on the fatigue crack propagation rates in benign environments for bridge steels can be studied by using the RMS model. Consequently, differences between the corrosion fatigue, crack growth rate and the fatigue crack growth rate that are analyzed by using the RMS model must be related, primarily, to environmental effects. The corrosion fatigue, crack growth rate data (Figs. 24 through 28) obtained by testing A36, A588 grades A and B, and A514 grades E and F steels at 60 cpm in distilled water and in 3-percent solution of sodium chloride in distilled water are essentially identical to the data on the rate of fatigue crack growth in air for these steels. Thus, the data indicate that the effects of these more hostile environments on the rate of fatigue crack growth for bridge steels are negligible at 60 cpm. A corollary of this finding is that *the addition of sodium chloride to distilled water has negligible effect on the fatigue behavior of bridge steels.* Moreover, corrosion fatigue data obtained at a stress ratio of 0.5 were identical to those obtained at 0.1, and corrosion fatigue data obtained for five different heats of A588 steel were also identical. Consequently, the corrosion fatigue data at 60 cpm show that specifications for bridge details that are based on fatigue data in benign environments are equally applicable to corrosion fatigue in distilled water and in 3-percent solution of sodium chloride in distilled water.

The corrosion fatigue, crack growth rate data for bridge steels tested at 12 cpm in 3-percent solution of sodium chloride in distilled water resulted in three observations that are of primary importance to the analysis of the corrosion fatigue life of bridge details. The first observation relates to the magnitude of the corrosion fatigue, crack propagation threshold, ΔK_{th} (the value of the stress intensity factor fluctuation below which corrosion fatigue cracks do not propagate), at $R = 0.1$. The corrosion fatigue ΔK_{th} for A36 steel tested at 12 cpm (Fig. 34) appears to be equal to about 15 ksi $\sqrt{\text{in.}}$ (16.5 $\text{MNm}^{-3/2}$). The corrosion fatigue ΔK_{th} for A514 steels at 12 cpm (Figs. 35 and 36) appears to be equal to about 11 ksi $\sqrt{\text{in.}}$ (12.1 $\text{MNm}^{-3/2}$). The value of ΔK_{th} for steels tested in a benign environment at $R = 0.1$ is equal to 5.5 ksi $\sqrt{\text{in.}}$ (6.0 $\text{MNm}^{-3/2}$). These ΔK_{th} values suggest that the corrosion fatigue life of bridge details at low ΔK_I values ($\Delta K_I < 15$ ksi $\sqrt{\text{in.}}$) and at low cyclic load frequencies (cpm $\leq$ 12) could be significantly greater than the corresponding fatigue life. This observation is supported by data reported by Bucci and Donald (*33*) and by Paris et al. (*34*).

The second observation is related to the corrosion fatigue, crack propagation behavior of bridge steels at ΔK_I values greater than about 15 ksi $\sqrt{\text{in.}}$ and at 12 cpm (Figs. 29 through 33). The data show that the rate of crack growth for all the bridge steels tested under these conditions was equal to or slightly greater than that observed at 60 cpm in 3-percent sodium chloride solution or in room-temperature air environments. This behavior suggests that the corrosion fatigue, crack propagation life for A36, A588 grades A and B, and A514 grades E and F steels at 12 cpm and at ΔK_I levels greater than 15 ksi $\sqrt{\text{in.}}$ could be slightly less than the corresponding fatigue crack propagation life. The corrosion fatigue, crack growth rates at ΔK_I values greater than 15 ksi $\sqrt{\text{in.}}$ and at 12 cpm for the five bridge steels investigated were essentially identical. For example, as shown in Figure 46, the superposition of the corrosion fatigue data for the A36 steel and the A514 Grade F steel, which had a tensile strength of 134 ksi (924 MN/m^2) and a yield strength of 126 ksi (869 MN/m^2), shows that the rates of corrosion fatigue crack growth at ΔK_I greater than about 15 ksi $\sqrt{\text{in.}}$ and at 12 cpm are essentially identical.

The third observation is related to the retardation of the corrosion fatigue crack propagation rate that is caused by alternate wet and dry environmental conditions. This transient behavior of corrosion fatigue, crack propagation rates could have a substantial influence on the cyclic life of bridge components. For example, the corrosion fatigue life of an A514 Grade F steel specimen tested at 12 cpm in 3-percent solution of sodium chloride (Fig. 38) was doubled when it was removed *once* from the environment and permitted to dry overnight.

The test results in the transition region are shown in Figure 47 in terms of crack growth rate and the stress intensity factor fluctuation. The data show that the rate of growth was decreased by an order of magnitude from the steady state, corrosion fatigue behavior under full-immersion conditions and that the initial growth rates at the restart of full-immersion testing were well below the rates of growth in room-temperature air environment.

The preceding discussion of the corrosion fatigue behavior for bridge steels tested at 12 cpm in 3-percent solution of sodium chloride indicates that (1) ΔK_{th} in the solution was greater than that in air; (2) corrosion fatigue, crack growth rates at ΔK_I values greater than the environmental ΔK_{th} were equal to or slightly higher than those in air; and (3) crack propagation life was significantly longer under alternate wet and dry environmental conditions than it was under conditions of full immersion in the solution or in air. The combined effects of these findings point out that

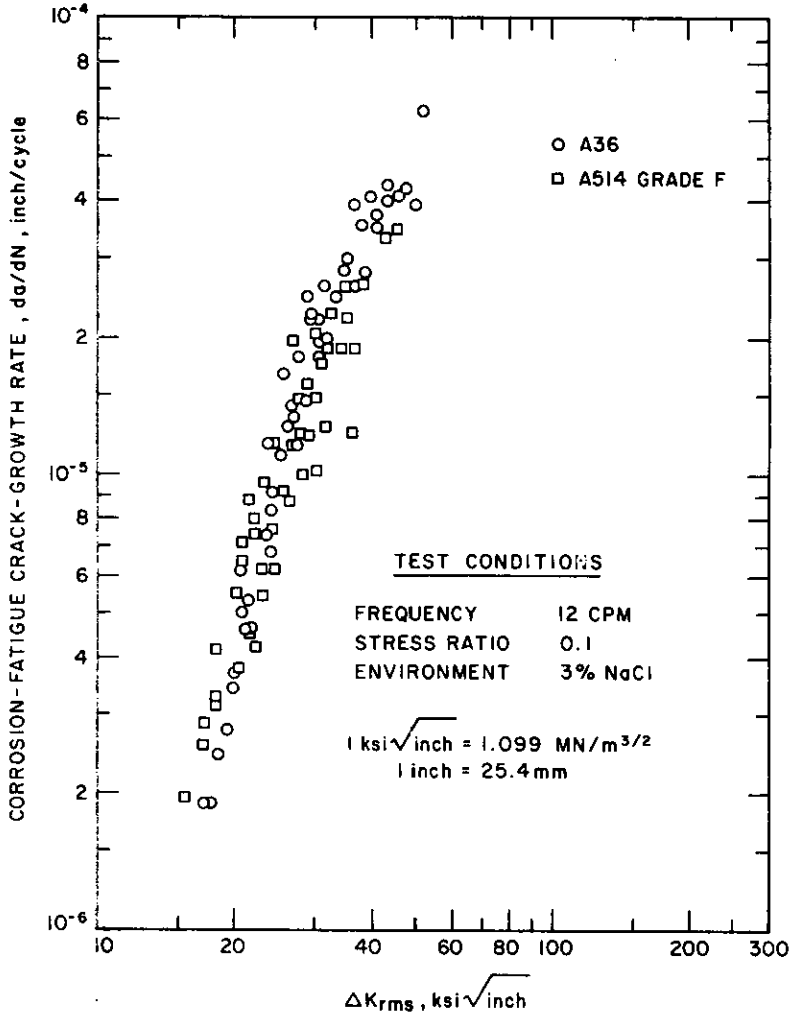

Figure 46. Corrosion fatigue, crack growth rate a a function of the root mean square of the stress intensity factor for A36 and A514 Grade F steels.

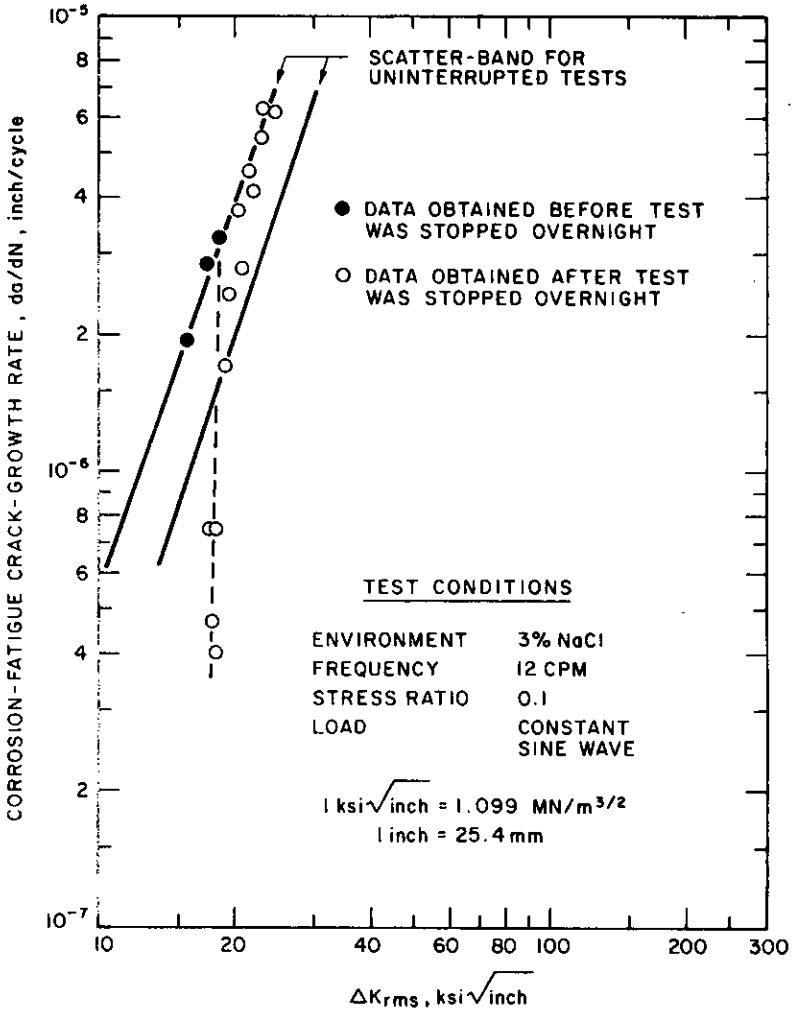

Figure 47. Retardation of corrosion fatigue, crack growth rate under alternate wet and dry environmental conditions for A514 Grade F steel.

the corrosion fatigue aqueous life of steel bridges under actual operating (alternate wet and dry) conditions in the aqueous environments investigated should be equal to or greater than their fatigue life in air.

Specifications for bridge details are currently based on fatigue data in air. The aqueous solutions used in these studies—distilled water and 3-percent solution of sodium chloride in distilled water—represent environmental conditions that are potentially more aggressive than that of air. However, no major effects of these aqueous environments were found in relation to fatigue crack propagation rate. Further work is needed to determine how actual bridge environments affect fatigue crack propagation rate.

CHAPTER FOUR

CONCLUSIONS AND RECOMMENDED RESEARCH

CONCLUSIONS

The conclusions summarized in this chapter are based on the results of an investigation of subcritical crack growth in bridge steels subscribed by benign (air) and aqueous (distilled water and 3-percent solution of sodium chloride in distilled water) environmental conditions.

Fracture Behavior

1. Fracture toughness tests conducted at 72 F (22 C) with fatigue-precracked specimens under static loading conditions showed that no valid K_{Ic} values could be measured for any of the five steels tested.
2. Suppression-effect analysis of the fracture behavior under the test conditions studied indicated that each of the five steels tested would exhibit extensive resistance to fracture in typical structural components used in bridges and that brittle fracture should not be of primary concern in such applications.

Fatigue Behavior

1. The average rate of fatigue crack growth, da/dN, under variable amplitude, random sequence load fluctuations such as occur in actual bridges and under constant amplitude load fluctuations can be represented by the equation

$$da/dN = A(\Delta K_{rms})^n$$

where ΔK_{rms} is the root mean square of the stress intensity factor range and A, n are constants for a given material.
2. This relationship was found to be applicable to the following steels: A36, A588 grades A and B, and A514 grades E and F.
3. The average rate of fatigue crack growth, da/dN, of the various steels studied under variable amplitude, random sequence load fluctuations such as occur in actual bridges are equal to da/dN values obtained under constant amplitude load fluctuations when the stress intensity factor range, ΔK, under constant amplitude load fluctuation is equal in magnitude to the ΔK_{rms} of the variable amplitude fluctuations.

Stress-Corrosion-Cracking Behavior

1. Stress-corrosion-cracking (SCC) tests conducted at 72 F with fatigue-precracked specimens in a 3-percent sodium chloride solution for 5000 h showed that no valid K_{Iscc} values could be measured for any of the five steels tested.
2. The SCC test results obtained showed a general decrease in the relative susceptibility index (apparent K_{Iscc}/K_{Ix}) with increasing strength (σ_{ys}), ranging from a value of 0.95 for A36 steel (representing immune behavior) to values of 0.73 and 0.79 for the A514 Grade E and A514 Grade F steels, respectively (representing slight to moderate SCC susceptibility). Assessments of such behavior indicated that the safety and reliability of typical bridges fabricated with such steels would not be impaired because of intrinsic SCC behavior.

Corrosion Fatigue Behavior

1. Corrosion fatigue, crack propagation rates for bridge steels at 60 cpm were identical in distilled water and in 3-percent solution of sodium chloride in distilled water.
2. Corrosion fatigue, crack propagation rates for bridge steels at 60 cpm in both distilled water and in 3-percent solution of sodium chloride in distilled water were essentially identical to the fatigue crack propagation rates in room-temperature air environment.
3. Corrosion fatigue, crack propagation rates for bridge steels were identical under constant amplitude, sine wave and square wave, cyclic load fluctuations of 60 cpm.
4. Corrosion fatigue, crack propagation rates for bridge steels were identical at stress ratios of 0.1 and 0.5.
5. Corrosion fatigue, crack propagation rates for A588 steels obtained from five sources were identical at 60 cpm in 3-percent solution of sodium chloride in distilled water.
6. Corrosion fatigue, crack propagation rates for bridge

steels at 12 cpm were equal to or slightly greater than the fatigue crack propagation rates in room-temperature air environment, as would be expected because of the high inherent resistance to SCC for these steels.

7. The corrosion fatigue, crack propagation threshold, ΔK_{th} (the value of the stress intensity factor fluctuation below which corrosion fatigue cracks do not propagate), for bridge steels subjected to a stress ratio of 0.1 and at 12 cpm appeared to be greater in 3-percent solution of sodium chloride in distilled water than it was in room-temperature air environment. The environmental ΔK_{th} values appeared to be equal to 15 and 11 ksi $\sqrt{\text{in.}}$ (16.5 and 12.1 $\text{MNm}^{-3/2}$) for A36 and A514 steels, respectively. The value of ΔK_{th} at a stress ratio of 0.1 in room-temperature air environment was 5.5 ksi $\sqrt{\text{in.}}$ (6.0 $\text{MNm}^{-3/2}$) for both steels.

8. Corrosion fatigue, crack propagation rates were retarded significantly by alternate wet and dry environmental conditions. The corrosion fatigue life of an A514 Grade F steel specimen tested at 12 cpm in 3-percent solution of sodium chloride in distilled water was *doubled* when it was removed *once* from the environment and permitted to dry overnight.

9. The corrosion fatigue, crack propagation life of bridge-steel components under actual operating (wet and dry) conditions in the aqueous environments investigated should be equal to or greater than their fatigue life in room-temperature air environment.

Structural Behavior

1. Specifications for bridge details are currently based on fatigue data in air. The aqueous solutions used in the present studies—distilled water and 3-percent sodium chloride in distilled water—represent environmental conditions that are potentially more aggressive than that of air. However, no major effects of these aqueous environments were found in relation to fatigue crack propagation rate in this investigation.

2. Further work is needed to determine how actual bridge environments affect fatigue crack propagation rate.

RECOMMENDATIONS FOR FURTHER RESEARCH

The fatigue crack propagation data for various bridge steels (A36, A588 grades A and B, and A514 grades E and F) showed that the average rate of fatigue crack growth, da/dN, under variable amplitude, random sequence load fluctuation and under constant amplitude load fluctuation agreed closely when da/dN was plotted as a function of the root mean square of the stress intensity factor range, ΔK_{rms}. Thus, within the limits of the present investigation, the average rate of fatigue crack growth, da/dN, of various bridge steels subjected to variable amplitude, random sequence load fluctuations such as occur in actual bridges and to constant amplitude load fluctuations can be represented by the equation

$$da/dN = A\ (\Delta K_{rms})^n$$

where ΔK_{rms} is the root mean square of the stress intensity factor fluctuation and A, n are material constants. The applicability of this RMS model for predicting the useful cyclic life of simulated bridge-steel components has been studied under NCHRP Project 12-12.

The corrosion fatigue, crack propagation data for these bridge steels indicated, however, that the corrosion fatigue, crack propagation life of bridge-steel components under actual operating (wet and dry) conditions in distilled water and in 3-percent solution of sodium chloride in distilled water is equal to or greater than their fatigue crack propagation life in room-temperature air environment. It is therefore recommended that consideration be given to a further study of the effect of alternate wet and dry environmental conditions on the life of laboratory specimens and simulated bridge details. It is also recommended that such tests be conducted at relatively low cyclic load frequency.

REFERENCES

1. FISHER, J. W., FRANK, K. H., HIRT, M. A., and MCNAMEE, B. M., "Effect of Weldments on the Fatigue Strength of Steel Beams." *NCHRP Report 102*, 114 pp. (1970).
2. FISHER, J. W., ALBRECHT, P. A., YEN, B. T., KLINGERMAN, D. J., and MCNAMEE, B. M., "Fatigue Strength of Steel Beams with Welded Stiffeners and Attachments." *NCHRP Report 147*, 85 pp. (1974).
3. IRWIN, G. R., "Analysis of Stresses and Strains Near the End of a Crack Traversing a Plate." *J. Appl. Mech.*, Vol. 24 (1957).
4. TADA, H., PARIS, P. C., and IRWIN, G. R., eds., *Stress Analysis of Cracks Handbook*. Del Res. Corp., Hellertown, Pa. (1973).
5. SIH, G. C., *Handbook of Stress-Intensity Factors for Researchers and Engineers*. Inst. of Fracture and Solid Mech., Lehigh Univ. (1973).
6. PARIS, P. C., and ERDOGAN, F., "A Critical Analysis of Crack Propagation Laws." *J. Basic Eng.*, Series D, Vol. 85, No. 3 (1963).
7. BARSOM, J. M., "Fatigue-Crack Propagation in Steels of Various Yield Strengths." *J. Eng. Industry*, Series B, Vol. 93, No. 4 (Nov. 1971) pp. 1190-1196.
8. BARSOM, J. M., "Effect of Cyclic-Stress Form on Corrosion-Fatigue Crack Propagation Below K_{Iscc} in a High-Yield-Strength Steel." *Corrosion Fatigue: Chemistry, Mechanics, and Microstructure*, International Corrosion Conference Series, Vol. NACE-2 (1972) pp. 424-436.

9. CLARK, W. G., JR., and TROUT, H. E., JR., "Influence of Temperature and Section Size on Fatigue Crack Growth Behavior in Ni-Mo-V Alloy Steel." *J. Eng. Fracture Mech.*, Vol. 2, No. 2 (Nov. 1970).
10. JOHNSON, H. H., and PARIS, P. C., "Sub-critical Flaw Growth." *J. Eng. Fracture Mech.*, Vol. 1, No. 3 (June 1968).
11. WEI, R. P., "Some Aspects of Environment-Enhanced Fatigue-Crack Growth." *J. Eng. Fracture Mech.*, Vol. 1, No. 4 (Apr. 1970).
12. BARSOM, J. M., and MCNICOL, R. C., "Effect of Stress Concentration on Fatigue-Crack Initiation in HY-130 Steel." *Proc. Seventh Annual Symposium on Fracture Mechanics*, Univ. of Maryland (Aug. 1973).
13. CLARK, W. G., JR., "An Evaluation of the Fatigue Crack Initiation Properties of Type 403 Stainless Steel in Air and Steam Environments." *Proc. Seventh Annual Symposium on Fracture Mechanics*, Univ. of Maryland (Aug. 1973).
14. CLARK, W. G., JR., "Effect of Temperature and Section Size on Fatigue Crack Growth in A533 Grade B, Class 1 Pressure Vessel Steel." *J. Materials*, Vol. 6, No. 1 (Mar. 1971).
15. SHANINIAN, P., WATSON, H. E., and SMITH, H. H., "Fatigue Crack Growth in Selected Alloys for Reactor Applications." *J. Materials*, Vol. 7, No. 4 (1972).
16. WEBER, J. H., and HERTZBERG, R. W., "Effect of Thermomechanical Processing on Fatigue Crack Propagation." *Metallurgical Trans.*, Vol. 4 (Feb. 1973).
17. BROWN, B. F., "A New Stress-Corrosion Cracking Test for High-Strength Alloys." *Materials Res. and Standards*, Vol. 6, No. 3 (Mar. 1966).
18. NOVAK, S. R., and ROLFE, S. T., "Modified WOL Specimen for K_{Iscc} Environmental Testing." *J. Materials*, Vol. 4, No. 3 (Sept. 1969) pp. 701-728.
19. WEI, R. P., and LANDES, J. D., "Correlation Between Sustained-Load and Fatigue-Crack Growth in High-Strength Steels." *Materials Res. and Standards*, Vol. 9, No. 7 (July 1969).
20. WEI, R. P., NOVAK, S. R., and WILLIAMS, D. P., "Some Important Considerations in the Development of Stress Corrosion Cracking Test Methods." *Materials Res. and Standards*, Vol. 12, No. 9 (1972) p. 25.
21. NOVAK, S. R., "Effect of Prior Uniform Plastic Strain on the K_{Iscc} of High-Strength Steels in Sea Water." *Eng. Fracture Mech.*, Vol. 5 (1973) pp. 727-763.
22. AMERICAN SOCIETY FOR TESTING AND MATERIALS, "Standard Methods for Notched-Bar Impact Testing of Metallic Materials." *ASTM E23-72*, Part 31 (1973).
23. LANGE, E. A., PUZAK, P. P., and COOLEY, L. A., "Standard Method for the 5/8-Inch Dynamic-Tear Test." *NRL Report 7159*, Naval Research Laboratory (Aug 27, 1970).
24. "NCHRP Project 12-12: Interim Report," *U.S. Steel Res. Lab. Rep. 76.019-001* (Oct. 1, 1972).
25. WILSON, W. K., "Review of Analysis and Development of WOL Specimen." *Westinghouse Res. Lab. Rep. 67-7D7-BTLPV-R1* (Mar. 8, 1967).
26. BARSOM, J. M., "Fatigue-Crack Growth Under Variable-Amplitude Loading in ASTM A514 Grade B Steel." *Progress in Flaw Growth and Fracture Toughness Testing, ASTM STP 536* (1973) pp. 147-167.
27. HARDRATH, H. F., and MCEVILY, A. T., "Engineering Aspects of Fatigue-Crack Propagation." *Proc. Crack Propagation Symposium*, Vol. 1, Cranfield, England (Oct. 1961).
28. SCHIJVE, J., JACOBS, F. A., and TROMP, P. J., "Crack Propagation in Clad 2024-T3A1 Under Flight Simulation Loading. Effect of Truncating High Gust Loads." *NLR TR-69050-U*, National Lucht-En Ruimtevaart-Laboratorium (National Aerospace Laboratory NLR—The Netherlands) (June 1969).
29. HUDSON, C. M., and HARDRATH, H. F., "Effects of Changing Stress Amplitude on the Rate of Fatigue-Crack Propagation of Two Aluminum Alloys." *NASA Technical Note D-960* (Sept. 1961).
30. MCMILLAN, J. C., and PELLOUX, R. M. N., "Fatigue-Crack Propagation Under Program and Random Loads." *Fatigue-Crack Propagation, ASTM STP 415* (1967) p. 505.
31. WHEELER, O. E., "Spectrum Loading and Crack Growth." *General Dynamics Rep. FZM-5602* (June 30, 1970).
32. BARSOM, J .M., "Fatigue Behavior of Pressure-Vessel Steels." *WRC Bulletin 194* (May 1974).
33. BUCCI, R. J., and DONALD J. K., "Fatigue and Fracture Investigation of a 200 Grade Maraging Steel Forging." Del Res. Corp. Rep. (Oct. 1972).
34. PARIS, P. C., BUCCI, R. J., WESSEL, E. T., CLARK, W. G., and MAGER, T. R., "Extensive Study of Low Fatigue-Crack-Growth Rates in A533 and A508 Steels." *Stress Analysis and Growth of Cracks, Proc. 1971 National Symposium on Fracture Mech., Part I; ASTM STP 513* (1972).
35. MILLER, G. A., HUDAK, S. J., and WEI, R. P., "The Influence of Loading Variables on Environment-Enhanced Fatigue-Crack Growth in High Strength Steels." *J. Testing and Evaluation*, Vol. 1, No. 6 (1973).
36. BARSOM, J. M., SOVAK, J. F., and NOVAK, S. R., "AISI Project 168-Toughness Criteria for Structural Steels: Fracture Toughness of A36 Steel." *U.S. Steel Res. Lab. Rep. 97.021-001(1)* (May 1, 1972).
37. BARSOM, J. M., SOVAK, J. F., and NOVAK, S. R., "AISI Project 168-Toughness Criteria for Structural Steels: Fracture Toughness of A572 Steels." *U.S. Steel Res. Lab. Rep. 97.021-001(2)* (Dec. 29, 1972).
38. LANDES, J. D., and BEGLEY, J. A., "The Effect of Specimen Geometry on J_{Ic}." *Fracture Toughness, Part II, ASTM STP 514* (Sept. 1972) pp. 24-40.
39. BUCCI, R. J., PARIS, P. C., LANDES, J. D., and RICE, J. R., "J-Integral Estimation Procedures." *Fracture Toughness, Part II, ASTM STP 514* (Sept. 1972) pp. 40-70.
40. WITT, F. J., "The Equivalent Energy Method for Calculating Elastic-Plastic Fracture." *Proc. 5th Annual Meeting of the Heavy Section Steel Technology Program*, March 25-26, Oak Ridge National Laboratory, Oak Ridge, Tennessee (1971).
41. WITT, F. J., "The Application of the Equivalent Energy Procedure for Predicting Fracture in Thick Pressure Vessels." *Practical Application of Fracture Me-*

chanics to Pressure Vessel Technology, The Institution of Mechanical Engineers (1971) pp. 163-168.

42. ROLFE, S. T., and NOVAK, S. R., "Slow-Bend K_{Ic} Testing of Medium-Strength High-Toughness Steels." *Review of Developments in Plane Strain Fracture Toughness Testing, ASTM STP 463* (1970) pp. 124-159.
43. BARSOM, J. M., "AISI Project 168—Toughness Criteria for Structural Steels: Investigation of Toughness Criteria for Bridge Steels." *U.S. Steel Res. Lab. Rep. 97.018-001(5)* (Feb. 8, 1973).
44. ORANGE, T. W., "A Semiempirical Fracture Analysis for Small Surface Cracks." *Eng. Fracture Mech.,* Vol. 3, No. 1 (July 1971) pp. 53-70.
45. AMERICAN SOCIETY FOR TESTING AND MATERIALS, "Standard Specification for High-Yield-Strength, Quenched and Tempered Alloy Steel Plate, Suitable for Welding." *ASTM A514-70, Annual Book of ASTM Standards* (1972) pp. 575-579.
46. BUCCI, R. J., CLARK, W. G., JR., and PARIS, P. C., "Fatigue-Crack-Propagation Growth Rates Under a Wide Variation of ΔK for an ASTM A517 Grade F (T-1) Steel." *Stress Analysis and Growth of Cracks, ASTM STP 513* (1972).
47. SCHMIDT, R. A., "A Threshold in Metal Fatigue." Master of Science thesis, Lehigh Univ. (1970).
48. PARIS, P. C., "Testing for Very Slow Growth of Fatigue Cracks." *MTS Closed Loop Magazine,* Vol. 2, No. 5 (1970).
49. HARRISON, J. D., "An Analysis of Data on Non-Propagating Fatigue Cracks on a Fracture Mechanics Basis." *Brit. Welding J.,* Vol. 2, No. 3 (Mar. 1970).
50. POOK, L. P., "Fatigue Crack Growth Data for Various Materials Deduced From the Fatigue Lives of Precracked Plates." *Stress Analysis and Growth of Cracks, Proc. 1971 National Symposium on Fracture Mech., Part I; ASTM STP 513* (1972).
51. BARSOM, J. M., IMHOF, E. J., JR., and ROLFE, S. T., "Fatigue-Crack Propagation in High-Yield-Strength Steels." *Eng. Fracture Mech.,* Vol. 2, No. 4 (June 1971).
52. BARSOM, J. M., "The Dependence of Fatigue Crack Propagation on Strain Energy Release Rate and Crack Opening Displacement." *Damage Tolerance in Aircraft Structures, ASTM STP 486* (1971).
53. CROOKER, T. W., "Crack Propagation in Aluminum Alloys Under High-Amplitude Cyclic Load." *NRL Report 7286* (July 12, 1971).
54. IMHOF, E. J., and BARSOM, J. M., "Fatigue and Corrosion-Fatigue Crack Growth of 4340 Steel at Various Yield Strengths." *Progress in Flaw Growth and Fracture Toughness Testing, ASTM STP 536* (1973).
55. PARIS, P. C., and SIH, G. C., "Stress Analysis of Cracks." *Fracture Toughness Testing and Its Applications, ASTM STP 381* (Apr. 1965) pp. 30-83.
56. AMERICAN SOCIETY FOR TESTING AND MATERIALS, "Standard Method of Test for Plane-Strain Fracture Toughness of Metallic Materials." *ASTM E-399-72, Annual Book of ASTM Standards, Part 31* (1973) pp. 960-980.
57. NOVAK, S. R., and ROLFE, S. T., "Comparison of Fracture Mechanics and Nominal Stress Analyses in Stress Corrosion Cracking." *Corrosion,* Vol. 26, No. 4 (Apr. 1970) pp. 121-130.
58. SCHILLING, C. G., KLIPPSTEIN, K. H., BLAKE, G. T., NOVAK, S. R., and BARSOM, J. M., "AISI Project 168—Toughness Criteria for Structural Steels: Low-Temperature Tests of Simulated Bridge Members." *U.S. Steel Res. Lab. Rep. 97.021-001(3)* (Dec. 31, 1972).
59. WELLS, A. A., "Crack Opening Displacements from Elastic-Plastic Analyses of Externally Notched Tension Bars." *Eng. Fracture Mech.,* Vol. 1, No. 3 (Apr. 1969) pp. 399-410.
60. MCCABE, D. E., and HEYER, R. H., "R-Curve Determination Using a Crack-Line-Wedge-Loaded (CLWL) Specimen." *Fracture Toughness Evaluation by R-Curve Methods, ASTM STP 527,* pp. 17-35.
61. NOVAK, S. R., "AISI Project 168—Toughness Criteria for Structural Steels: Resistance to Plane-Stress Fracture (R-Curve Behavior) of A572 Structural Steel." *U.S. Steel Res. Lab. Rep. 97.018-001(4)* (Sept. 27, 1973).
62. BARSOM, J. M., and ROLFE, S. T., "K_{Ic} Transition-Temperature Behavior of A517-F Steel." *Eng. Fracture Mech.,* Vol. 2 (1971) pp. 341-357.

APPENDIX A

SUBCRITICAL CRACK PROPAGATION BEHAVIOR

INTRODUCTION

This appendix presents the general behavior of subcritical crack propagation in steels and the available literature information that is pertinent to this investigation.

The behavior of subcritical crack propagation for steels subjected to cyclic load fluctuations can be divided into three regions, as shown in Figure A-1 (*8*). The behavior in Region I exhibits a "fatigue threshold," cyclic, stress intensity factor fluctuation, ΔK_{th}, below which cracks do not propagate under cyclic stress fluctuations (*46-50, 34*). Region II represents the behavior of fatigue crack propagation above ΔK_{th} (*7*), which can be represented by the equation

$$da/dN = A(\Delta K)^n \qquad \text{(A-1)}$$

where a is the crack length, N is the number of cycles, ΔK is the stress intensity factor fluctuation, and A, n are constants.

In Region III, the fatigue crack growth per cycle is higher than that predicted by Eq. A-1. The data (*7, 51-53*) show that the rate of fatigue crack growth increases and that,

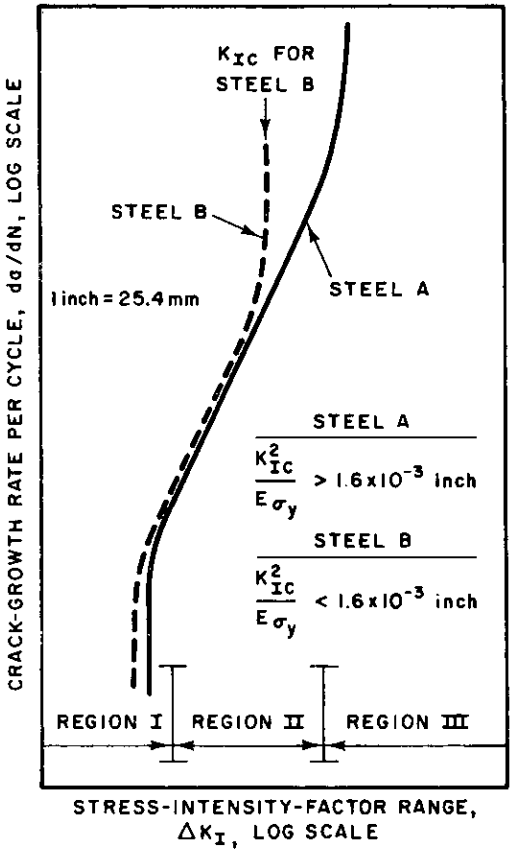

Figure A-1. Schematic representation of fatigue crack growth in steel.

under zero-to-tension loading (that is, $\Delta K = K_{\max}$), this increase occurs at a stress intensity factor value, K_T, given by the equation

$$K_T^2/E\sigma_y = 1.6 \times 10^{-3} \text{ in. } (0.04 \text{ mm}) \qquad \text{(A-2)}$$

where K_T is the value of the stress intensity factor range corresponding to the onset of acceleration in fatigue crack growth rates, E is Young's modulus, and σ_y is yield strength (0.2 percent offset). (The available data indicate that the value of K_T can be predicted more closely by using a flow stress, σ_f, rather than σ_y, where σ_f is the average of the yield and tensile strengths.)

Eq. A-2 is used to calculate the stress intensity factor value corresponding to the onset of fatigue-rate transition, ΔK_T (or K_T for zero-to-tension loading), which also corresponds to the point of transition from Region II to Region III in materials that have high fracture toughness (steel A in Figure A-1—that is, materials for which the critical stress intensity factor, K_{Ic} (or K_c), is higher than the K_T value calculated by using Eq. A-2). Acceleration in the rate of fatigue crack growth occurs at a stress intensity factor value slightly below the critical stress intensity factor, K_{Ic}, when the K_{Ic} (or K_c) of the material is less than K_T (steel B in Figure A-1) (*54*). Furthermore, acceleration in the rate of fatigue crack growth in an aggressive environment may occur at the threshold stress intensity factor, K_{Iscc}, below which cracks do not propagate under sustained load in the environment of interest.

The effects of stress ratio (ratio of applied minimum stress to maximum applied stress) and aggressive environments, as well as of other parameters, are observed as modifications of the basic behavior shown in Figure A-1.

NONPROPAGATING FATIGUE CRACKS (REGION I)

The fatigue crack propagation threshold, ΔK_{th}, is the stress intensity factor range below which fatigue cracks do not propagate under cyclic loading. For steel specimens tested under tension-to-tension loading at a stress ratio $R = 0$, $\Delta K_{th} \sim 6$ ksi $\sqrt{\text{in.}}$ (6.6 MNm$^{-3/2}$) (*46-48*).

An analysis of experimental results published in the literature on nonpropagating fatigue cracks in various metals was conducted by Harrison (*49*). The fatigue crack propagation threshold for a number of materials was found to occur in the range

$$1.5 \times 10^{-4} \sqrt{\text{in.}} \leqslant \Delta K_{th}/E \leqslant 1.8 \times 10^{-4} \sqrt{\text{in.}} \qquad \text{(A-3)}$$

where E is Young's modulus.

Figure A-2 (*32*) shows data published by various investigators (*46-50, 34*) on fatigue-crack-propagation threshold values of steels. The data show that conservative estimates of ΔK_{th} for martensitic steels, ferrite-pearlite steels, and austenitic steels subjected to various R values larger than +0.1 can be predicted from the equation

$$\Delta K_{th} = 6.4\ (1 - 0.85R) \qquad \text{(A-4)}$$

where K_{th} is in ksi $\sqrt{\text{in.}}$ The value of ΔK_{th} for $R < 0.1$ is a constant equal to 5.5 ksi $\sqrt{\text{in.}}$ (6 MNm$^{-3/2}$).

Eq. A-4 indicates that the fatigue crack propagation threshold of steels is primarily a function of the stress ratio and is essentially independent of chemical composition or mechanical properties.

FATIGUE CRACK PROPAGATION (REGIONS II AND III)

Martensitic Steels

Extensive data on the rate of fatigue crack growth for various high-yield-strength (σ_y greater than 80 ksi, or 552 MN/m^2) martensitic steels show that the primary parameter affecting growth rate in Region II is the range of fluctuation in the stress intensity factor and that the mechanical and metallurgical properties of these steels have negligible effects on the rate of fatigue crack growth in a room-temperature air environment (*7, 51*). The data for these steels fall within a single band, as shown in Figure A-3, and the upper bound of the scatter of the fatigue crack propagation rate for martensitic steels in an air environment can be obtained from the equation

$$da/dN = 0.66 \times 10^{-8}\ (\Delta K_I)^{2.25} \qquad \text{(A-5)}$$

where a is in inches and K_I is in kis $\sqrt{\text{inch.}}$ The applicability of Eq. A-5 to martensitic steels ranging in yield strength from 80 to 300 ksi (552 to 2068 MN/m^2) has been established in Refs. (*7*), (*32*), and (*51*).

Eq. A-5 may be used to estimate the fatigue crack propagation rate for martensitic steels in a benign environment in Region II (Fig. A-1). However, the rate of fatigue crack growth increases markedly when the fluctuation of the stress

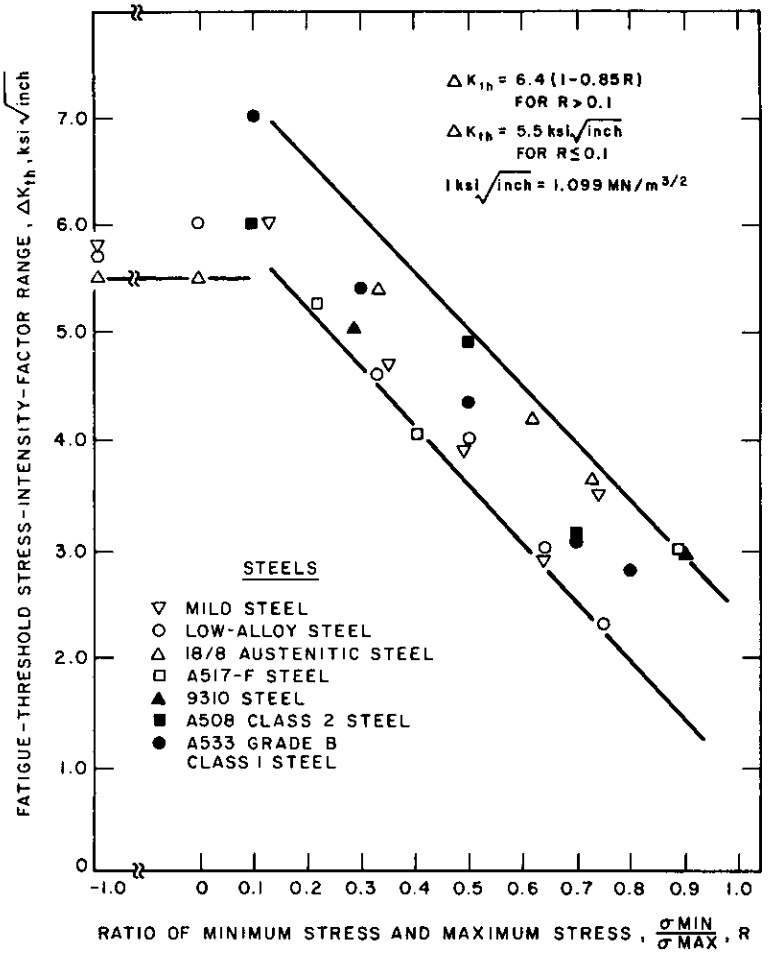

Figure A-2. Dependence of fatigue threshold, stress intensity factor range on stress ratio.

intensity factor, ΔK_I, becomes larger than the value calculated by using Eq. A-2 or when the value of the maximum stress intensity factor becomes close to the K_{Ic} (or K_c) of the material. Under these conditions, the rate of fatigue crack growth can not be predicted by Eq. A-5. The useful cyclic life of a structural component subjected to stress fluctuations corresponding to Region III-type behavior is of practical interest in short-life structural applications. Further work is necessary to characterize the fatigue crack propagation behavior in Region III.

Ferrite-Pearlite Steels

The behavior of the rate of fatigue crack growth in ferrite-pearlite steels (7) prior to the onset of fatigue-rate transition and above ΔK_{th} is shown in Figure A-4. The data indicate that realistic estimates of the rate of fatigue crack growth in these steels can be calcualted from the equation

$$da/dN = 3.6 \times 10^{-10} (\Delta K_I)^{3.0} \qquad \text{(A-6)}$$

where a is in inches and ΔK_I is in ksi $\sqrt{\text{inch}}$.

The data shown in Figures A-3 and A-4 and represented by Eqs. A-5 and A-6 indicate that the rate of fatigue crack growth at a given ΔK_I value below the fatigue rate transition is lower in ferrite-pearlite steels than it is in martensitic steels. The reason for the differences in the behavior of the rate of fatigue crack growth between martensitic steels and ferrite-pearlite steels is explained in Ref. (7).

General Discussion

The preceding discussion of the rate of fatigue crack growth in steels was divided into three groups that reflect microstructural differences. These groups also reflect broad variations in mechanical properties. Because of the wide variation of the chemical compositions and tensile properties of ferrite-pearlite steels and martensitic steels, and the relatively small variation in their fatigue crack growth rates, the use of a single equation to predict the rate of fatigue crack growth for these steels can be justified. Further, because of the difficulties encountered in the determination of the magnitude of stresses and stress fluctuations in complex structural details, the use of Eq. A-5 to calculate conservative estimates of the rate of fatigue crack growth in various steels can be justified.

The number of cycles required to propagate a fatigue crack from a given size to a larger size can be obtained by integrating Eqs. A-5 or A-6. These equations show that the rate of fatigue crack propagation is related to the stress intensity factor range raised to a power that is greater than 2. Consequently, the useful cyclic life to propagate a fa-

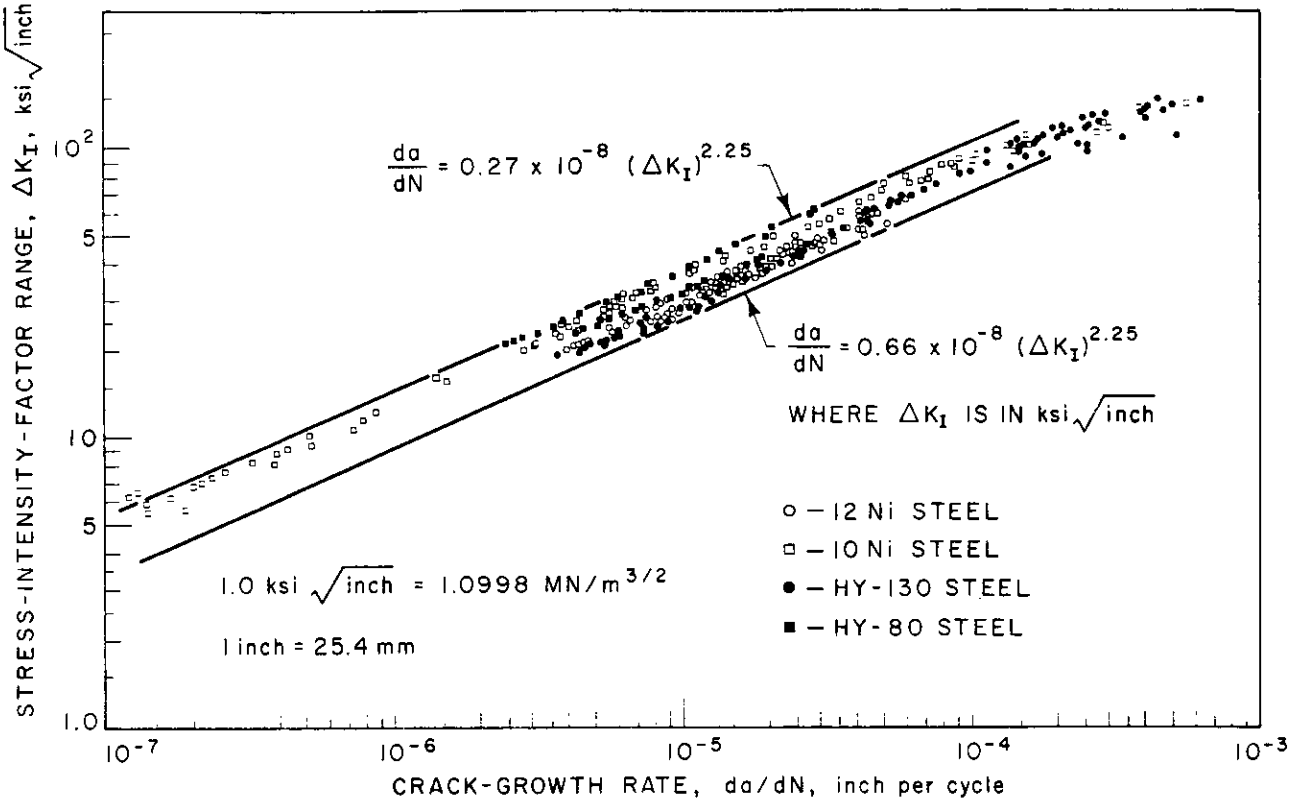

Figure A-3. Summary of fatigue crack propagation data for martensitic steels.

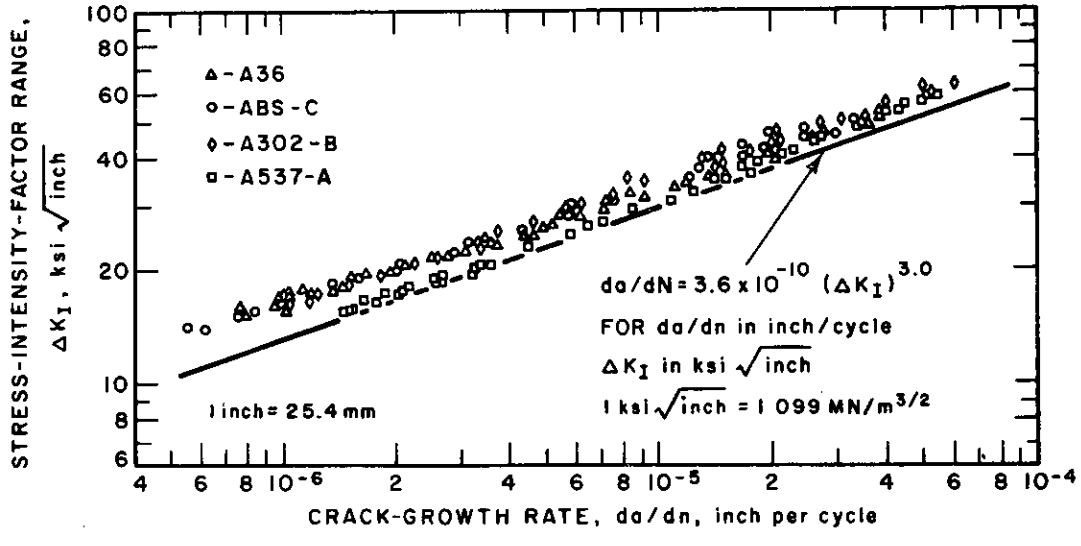

Figure A-4. Summary of fatigue crack growth data for ferrite-pearlite steels.

tigue crack a given increment of length is much greater at low ΔK_I values than at high ΔK_I values. In other words, most of the useful cyclic life of structural components subjected to constant load fluctuations is expended in initiating and propagating fatigue cracks at ΔK_I levels less than 40 ksi $\sqrt{\text{in.}}$ (44 MN/m$^{3/2}$) rather than at higher ΔK_I values.

CORROSION FATIGUE, CRACK PROPAGATION BEHAVIOR

Most corrosion fatigue, crack propagation investigations have been conducted on high-yield-strength steels (*8, 35*). The first systematic published investigation into the effect of environment on the rate of fatigue crack growth was conducted on 12Ni-5Cr-3Mo maraging steel (yield strength = 180 ksi) in 3-percent sodium chloride solution (*8*). The data showed that environmental acceleration of fatigue crack growth does occur below K_{Iscc} (see Fig. A-5) and that the magnitude of this acceleration depends on the frequency of the cyclic stress fluctuations. Because these results were obtained below K_{Iscc}, Barsom (*8*) concluded that the corrosion fatigue, crack growth rate increases to a maximum value and then decreases as the cyclic stress frequency decreases from 600 cpm to frequencies below 6 cpm. Moreover, other published data (*8, 35*) indicate that the environmental effects on the rate of fatigue crack growth in corrosion fatigue are highly dependent on the shape of the cyclic stress wave, as shown in Figure A-6 (*8*). Figure A-7 shows that the fatigue crack growth rates in room-temperature air environment were identical under the various stress fluctuations and are independent of frequency. However, in the sodium chloride solution (Fig. A-8), the crack growth rates per cycle under sinusoidal, triangular, and positive-sawtooth stress fluctuations were identical, but they were three times higher than the fatigue crack growth rate determined in air. Moreover, the data show that the corrosion fatigue, crack growth rates determined with the negative-sawtooth wave and with the square wave were the same as the rate of fatigue crack growth determined in air. Therefore, the negative-sawtooth type of loading and the square-wave type of loading had no corrosive effects.

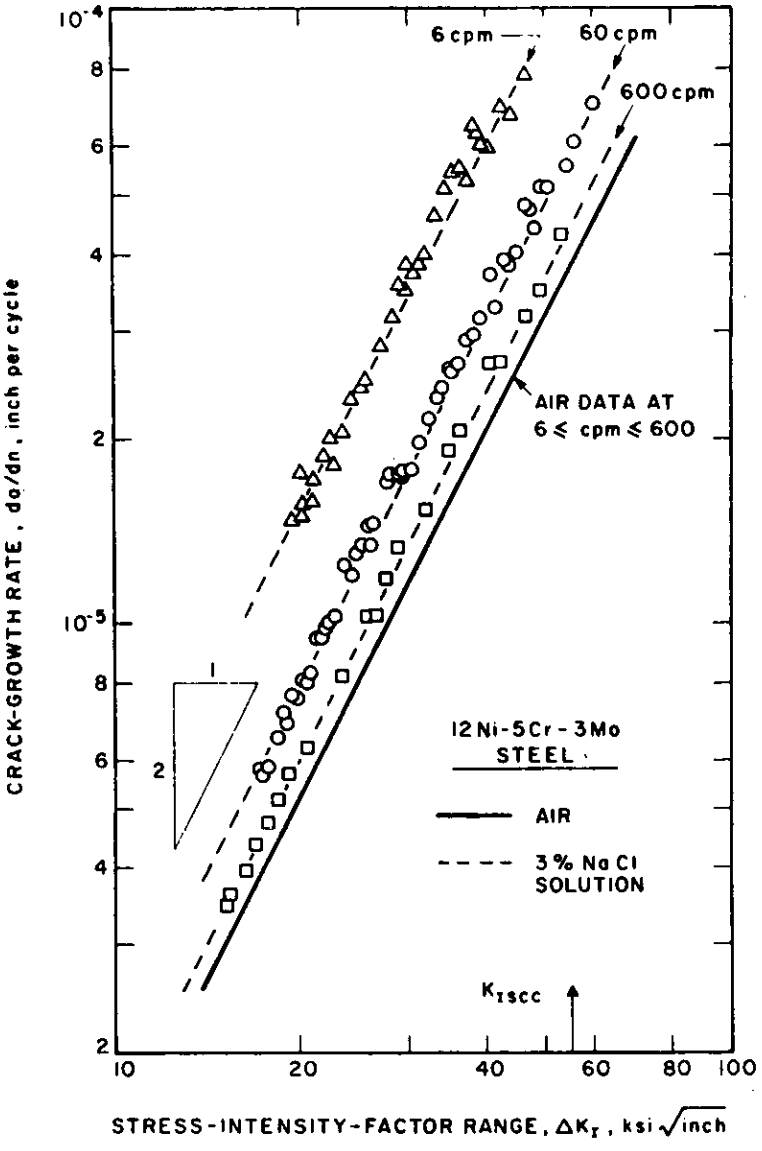

Figure A-5. Corrosion fatigue, crack growth data as a function of test frequency.

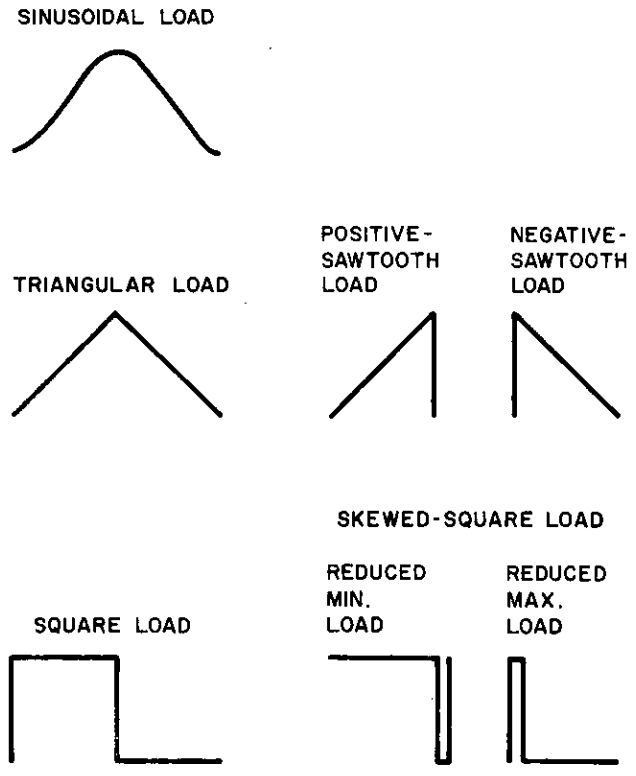

Figure A-6. Various forms of cyclic stress fluctuations used for steel investigated.

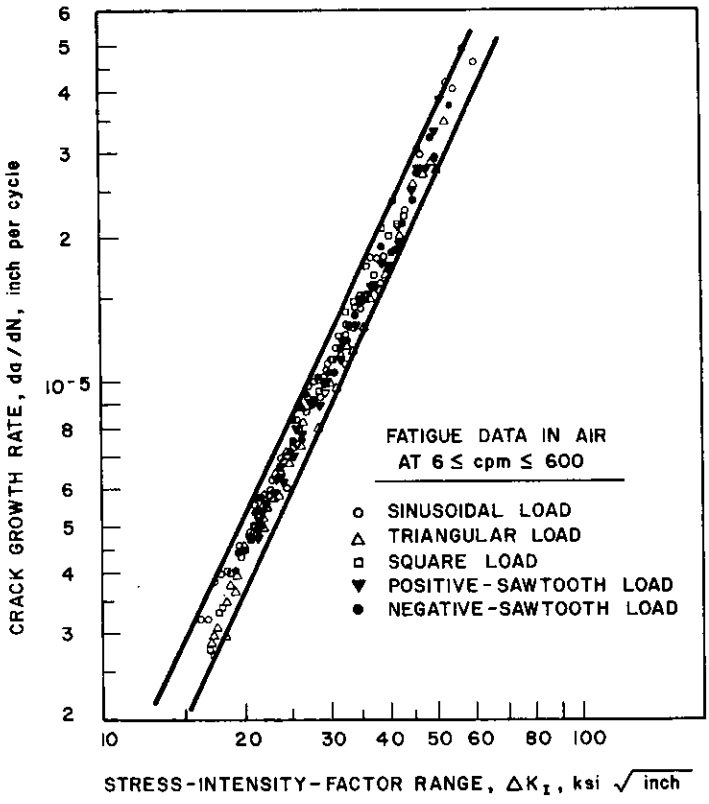

Figure A-7. Fatigue crack growth rates in 12Ni-5Cr-3Mo steel under various cyclic stress fluctuations with different stress-time profiles.

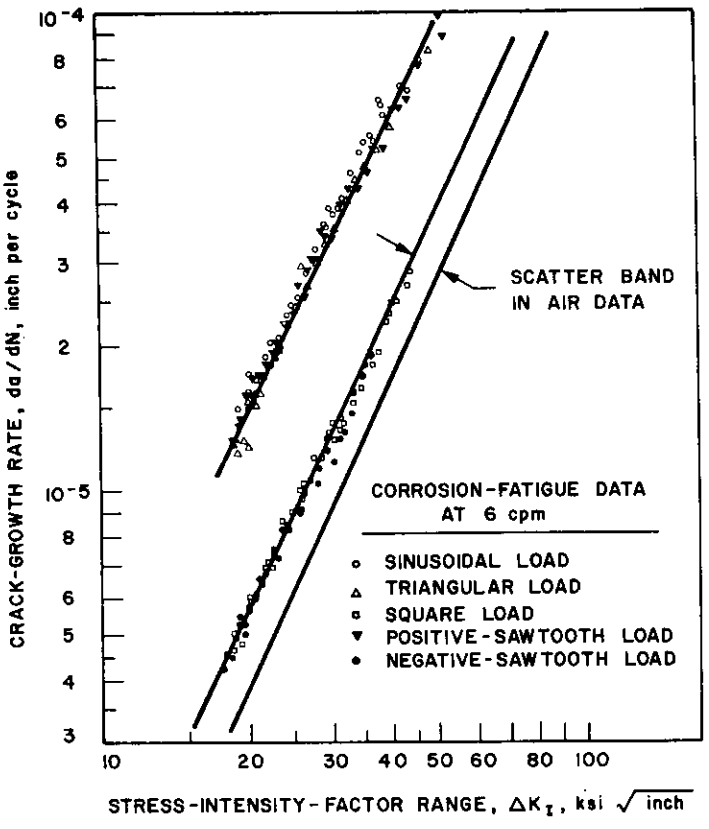

Figure A-8. Corrosion fatigue, crack growth rates in 12Ni-5Cr-3Mo steel in 3-percent solution of sodium chloride under various cyclic stress fluctuations with different stress-time profiles.

The complexity of the corrosion fatigue behavior of high-yield-strength steels is evidenced in the foregoing discussion. Despite these complexities, the systematic study of this behavior has been valuable in predicting the life of structural components subjected to cyclic loading in an aggressive environment. The most important finding is that environmental effects below K_{Iscc} in corrosion fatigue of high-yield-strength steels subjected to constant amplitude or to random cyclic stress fluctuations occur only during the loading part of the transient tensile load in each cycle rather than by the time spent at peak load or during unloading.

STRESS-CORROSION-CRACKING BEHAVIOR

Stress-corrosion crack growth in a statically loaded structure is caused by interaction between the chemical and mechanical processes at the crack tip. The highest stress intensity factor value at which subcritical crack growth does not occur in a material loaded statically in an aggressive environment is designated K_{Iscc}. The corrosion fatigue behavior below K_{Iscc} is of greatest practical interest in bridges. Consequently, to understand the corrosion fatigue behavior below K_{Iscc} in an environmental-material system, the fatigue crack growth behavior of the material in a benign environment and the K_{Iscc} for the environment-material systems should be established first as references.

The apparent K_{Iscc} behavior measured in the laboratory was divided into three types, as shown in Figure A-9 (*20, 21*). The Type I, K_{Iscc} (valid), behavior is that for which the conservative geometrical requirements necessary for ensuring plane-strain conditions in fracture testing (K_{Ic}) are satisfied, LEFM principles are wholly applicable, and corresponding a_{cr} calculations are precise (see Table A-1). The Type II, K_{Iscc} (partially valid), behavior is that for which both environmental plane-strain conditions are satisfied and LEFM principles are applicable to a currently unknown extent; furthermore, it is that for which corresponding a_{cr} calculations are only approximate because of the occurrence of moderate K_I-suppression effects. The Type III, K_{Iscc} (invalid), behavior is that corresponding to a nonplanar stress state (neither plane strain nor plane stress) for which LEFM principles and a_{cr} calculations are both *totally inapplicable* because of the occurrence of severe K_I-suppression effects. Despite the present shortcomings in analysis, this Type III, K_{Iscc} (invalid), behavior is the most desirable in SCC evaluations in the laboratory, because extreme environmental toughness is correspondingly indicated for the associated structural components in the field.

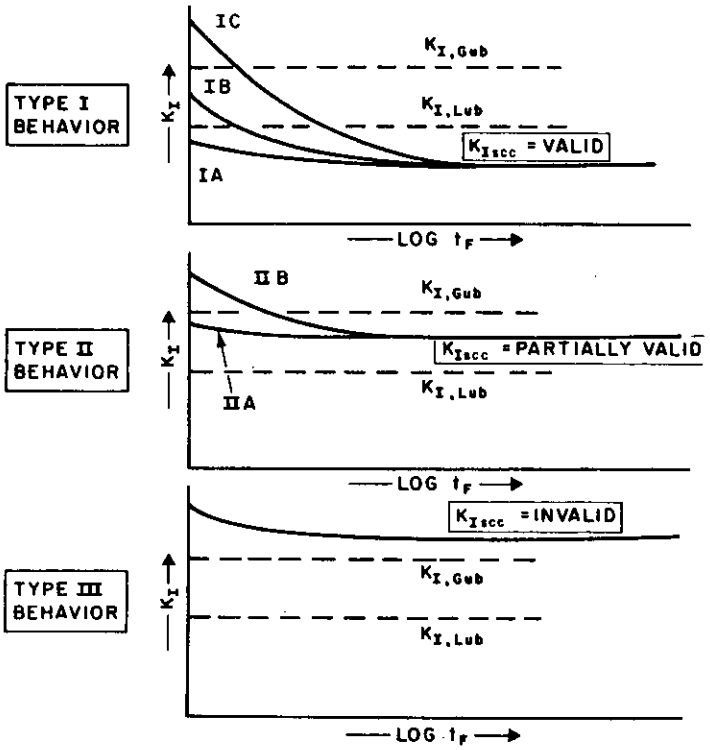

Figure A-9. Three basic types of apparent K_{Iscc} behavior and classification.

TABLE A-1

ANALYSIS OF SCC SUSCEPTIBILITY IN TERMS OF GEOMETRY AND STRESS STATE

Environmental Behavior	K_{Iscc} Designation and Limits	Extent of Plane-Strain Validity	Applicability of "a_{cr}"* Calculations	Extent of Suppression on Apparent K_{Iscc}
Type I	$\underline{K_{Iscc}(\text{VALID})} < K_{I,Lub}$	100% Valid	Precise	None
Type II	$K_{I,Lub} < \underline{K_{Iscc}(\text{PART. VALID})} < K_{I,Gub}$	Mixed validity	Approximate	Moderate
Type III	$K_{I,Gub} < \underline{K_{Iscc}(\text{INVALID})}$	100% Invalid	Inapplicable**	Severe**

* $a_{cr} = A \left(\frac{K_{Iscc}}{\sigma_{ys}}\right)^2$

** Severe suppression effects reflected by grossly inadequate specimen dimensions of a proportional-geometry type (see Table III) and consequent gross underestimates of intrinsic a_{cr}.

APPENDIX B

SPECIMEN PREPARATION AND EXPERIMENTAL PROCEDURES FOR FRACTURE MECHANICS STUDIES

SPECIMEN TYPE AND ANALYSIS

WOL Specimens

With the exception of the tests conducted for K_{Iscc}, the specimen type used throughout the study for fracture mechanics evaluation was the wedge-opening-loading (WOL) specimen. All such WOL specimens were 1-in. thick (1T). They were machined in the same manner (Type B), as shown in Figure 5, and in the same longitudinal crack orientation (RT designation) for each of the five steels investigated (A36, A588 grades A and B, and A514 grades E and F). All WOL specimens were prepared similarly in order to be used for investigation of three different types of material behavior for each of the five steels, including: (1) fracture behavior (static); (2) fatigue-crack-growth rate tests in air; and (3) corrosion fatigue, crack growth rate tests in both distilled water and 3-percent solution of sodium chloride in distilled water. The basic machining of these WOL specimens was the same in the sense that they were machined to ±0.002-in. (0.051-mm) tolerances and a 0.007–in.–root-radius notch was employed using an electrical discharge machine (EDM) process in order to facilitate fatigue precracking. Subsequent preparations of the specimens are described, as follows, in the appropriate descriptions of the experimental procedure for each type of evaluation.

The stress intensity, K_I, at the crack tip was calculated using the following equation (*18*):

$$K_I = \frac{C_3 P}{B\sqrt{a}} \qquad \text{(B-1)}$$

where P is the applied load, B is the specimen thickness, a is crack length measured from the loading plane, and C_3 is a function of the dimensionless crack length, a/W (see Fig. B-1), in which W is the specimen length measured from the loading plane. Expressed in a polynomial form, C_3 can be represented as:

$$C_3\,(a/W) = [30.96\,(a/W) - 195.8\,(a/W)^2 + 730.6\,(a/W)^3 - 1186.3\,(a/W)^4 + 754.6\,(a/W)^5] \qquad \text{(B-2)}$$

In the range $0.25 < a/W < 0.75$, the polynomial is accurate to within 0.5 percent of the experimental compliance.

Cantilever Beam Specimens

Single-edge notched specimens tested in cantilever bending (so-called cantilever beam specimens) were prepared for each of the five steels. These specimens (Fig. 4) were used to evaluate both the resistance to fracture (K_{Ix}) and stress-corrosion cracking (K_{Iscc}) for each of the five steels tested. In a manner similar to that for the WOL specimens, the crack orientation for all cantilever beam specimens was RT (longitudinal). The specimens were 1-in. thick (1T) and were machined to tolerances of ±0.005 in. In addition, an EDM notch starter (0.007-in. root radius) was used for these specimens in order to facilitate fatigue precracking. All specimens were face notched (V notched) 5 percent.

K_I values were calculated for the cantilever beam specimens by using the following equation, developed by Bueckner (*55*), for an edge crack in a strip subjected to in-plane bending and modified to account for reduction of thickness due to the face notches:

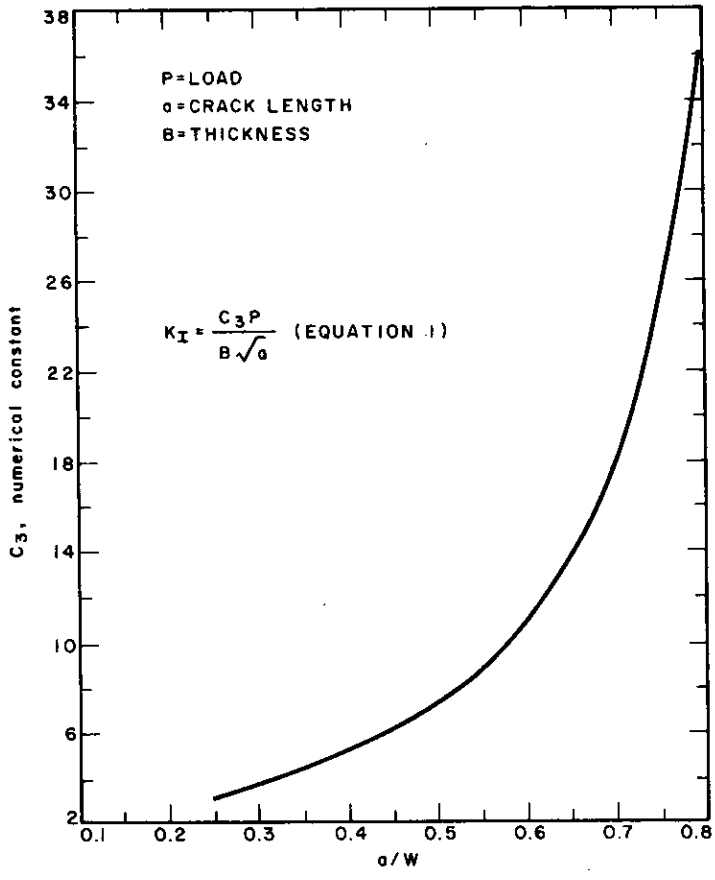

Figure B-1. Relation between constant C_3 used in calculating K_I and a/W ratio.

$$K_I = \frac{6M}{(B \cdot B_N)^{1/2} (W - a)^{3/2}} F(a/W) \qquad \text{(B-3)}$$

where K_I is the stress intensity factor, M is the bending moment, B is the gross specimen thickness, B_N is the net specimen thickness, W is the specimen depth, a is the total crack length, and $F(a/W)$ equals:

0.36 for $(a/W) = 0.05$
0.49 for $(a/W) = 0.10$
0.60 for $(a/W) = 0.20$
0.66 for $(a/W) = 0.30$
0.69 for $(a/W) = 0.40$
0.72 for $(a/W) = 0.50$
0.73 for $(a/W) = 0.60$ and larger.

EXPERIMENTAL TEST PROCEDURES

Fracture (K_{Ix}) Test Procedure

The basic fracture behavior was investigated for each of the five steels by using both WOL and cantilever beam specimens. Duplicate specimens of each type were prepared and tested to fracture for each steel in the same basic manner as that of the standard K_{Ic} test method, described in detail elsewhere (*56*).

After machining, the specimens were cleaned in an ultrasonic bath (to eliminate machining oil) and were fatigue precracked in the same manner. In each case, a fatigue crack was extended approximately 0.15 in. (3.80 mm) beyond the EDM notch tip by using constant amplitude sinusoidal loading under zero-to-tension ($R \cong 0$) conditions; all such fatigue precracking was done on an Amsler High-Frequency Vibraphore test machine at a frequency of approximately 8000 cpm. The final fatigue precracking condition (based on the final crack length) for all specimens corresponded to the range $\Delta K = 20$ to 25 ksi $\sqrt{\text{in.}}$ (22 to 27.5 $\text{MNm}^{-3/2}$).

The specimens were tested to fracture under "static" loading conditions—that is, in a period of approximately 2 to 3 min. For each fracture test, a standard load-displacement (P versus V) test record was obtained. The WOL specimens were tested in tension with a 440-kip-capacity Baldwin tension machine equipped with a hydraulic pressure cell (for measurements of P). The cantilever beam specimens were tested in cantilever bending in a special test rack equipped with a hydraulic elevator apparatus for load application (uniform transfer of load, P, provided by lead weights from the elevator to the arm attached to the specimen). This apparatus applied the load, P, continuously, while a record of this load application was obtained using a load cell (located in the rod connecting the specimen arm and the pedestal on which the lead weights rest). In the case of the fracture tests for both the WOL and cantilever beam specimens, a continuous record of P versus V was obtained using a double-size NASA-type clip gage (for V) and an X-Y recorder.

Additional preparation of the WOL specimens beyond that reported previously included the machining of a clip-gage slot into the specimen edge (same as that for the cantilever beam specimens, Fig. 4) and inserting high strength steel (18Ni(190 grade) maraging steel) into the pin holes to minimize plastic bending of the WOL specimen arms. The specimens were subsequently drilled and tapped to accommodate stud loading during the fracture tests.

Stress-Corrosion-Cracking (K_{Iscc}) Test Procedure

Approximately eight precracked cantilever beam specimens were prepared for each of the five steels tested. The general procedure used in these tests is the same as that described in Refs. (*21*) and (*57*). The fatigue precracking procedure for these specimens is also identical to that described in the previous section on fracture. Two cantilever beam specimens of each steel were tested to fracture in air to provide a detailed history of the basic fracture behavior. This included measurement of the stress intensity level at fracture, K_{Ix}, which is the primary level from which degradation due to SCC is measured for the environmental tests.

The remaining six cantilever beam specimens were immersed in a continuously aerated 3-percent solution of sodium chloride in distilled water contained within a polyethylene cell, as shown in Figure B-2. After first being subjected to the environment, the specimens were loaded individually to different values of the initial stress intensity, K_{Ii}, ranging between K_{Ix} and $K_{I,\,Lub}$, the least upper bound for valid plane-strain conditions. The specimens were dead-weight loaded in cantilever bending with the use of lead weights. Precision digital timers and limit switches provided a means for automatically recording the time to failure.

The nominal test duration for the SCC specimens was 5000 h (30 weeks). Specimens that survived the 5000-h test period (run-outs) were removed from test and subsequently fractured at liquid nitrogen temperature (—320 F). The fracture surfaces of such specimens were inspected carefully for any evidence of crack extension. The apparent K_{Iscc} value (the threshold stress intensity factor below which subcritical crack growth does not occur under sustained loading in the test environment) was then established for each steel on the basis of essentially no-crack extension ($0 \leqq \Delta a \leqq 5$ mils). Careful analysis of such results was necessary in order to distinguish crack extension (Δa) due to SCC from that due to "tearing." This was particularly true for specimens initially loaded to high levels ($K_{Ii} \geqq K_{I,\,Gub}$) and for which gross levels of plastic deformation and tearing occurred in the initial loading process.

Fatigue and Corrosion Fatigue Test Procedures

Approximately twenty-two 1T WOL specimens were machined for each of the five steels in accordance with the procedure outlined earlier. However, additional preparation was necessary for these specimens prior to the subsequent evaluation of the fatigue (*7, 26*) and corrosion fatigue (*8, 54*) crack growth rate behaviors of the five steels. For each specimen used in these studies, the specimen surface adjacent to the expected plane of crack propagation was polished to eliminate machining marks. To provide a means of measuring the rate of crack extension, a

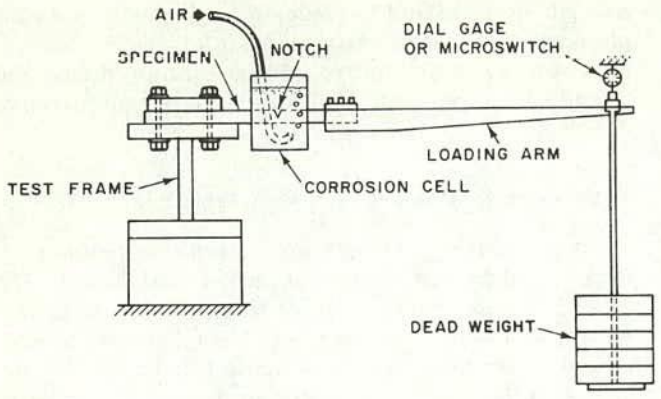

Figure B-2. Schematic drawing of fatigue cracked, cantilever beam test specimen and fixtures.

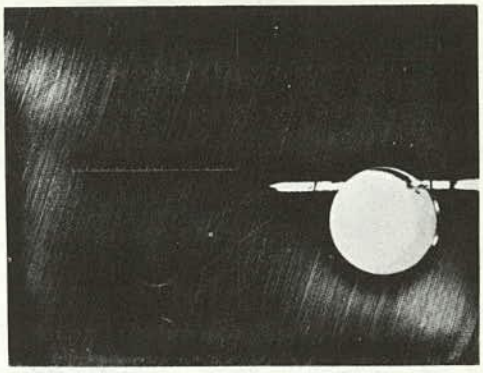

A. Location of hardness identations. X1.

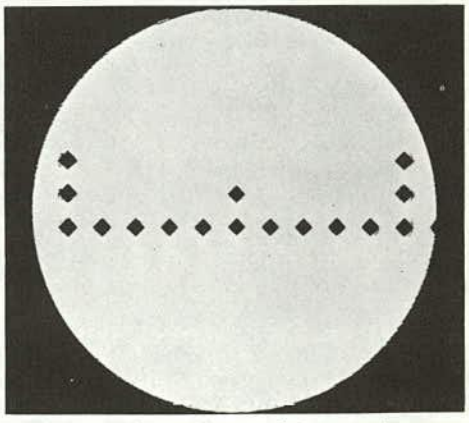

B. Close-up of hardness identations. X25.

Figure B-3. Hardness indentations used to measure crack length in WOL specimens.

series of indentations was made on the specimen surface (with a Vickers Pyramid Hardness Testing Machine) along a line parallel to the plane of the initial crack and in the direction of expected crack extension, as shown in Figure B-3. To ensure that crack extension was not affected by the indentations, the distance between the line of indentations and the crack plane was about ⅛ in. The distance between neighboring indentations was 0.010 ± 0.0002 in. (0.25 ± 0.0051 mm). Each specimen in the crack growth studies was prepared using this procedure on one side (only). Finally, the specimen was cleaned by immersion in an ultrasonically agitated bath.

All crack propagation tests were conducted at room temperature either in air or in distilled water, or in a 3-percent solution of sodium chloride in distilled water, by using 100-, 50-, and 25-kip (444.8-, 222.4-, and 111.2-MN) Materials Testing Systems (MTS) machines. The fatigue crack growth data in air were obtained at cyclic stress frequencies primarily at 60 cpm (with one set of data for each steel), and additionally at 12 cpm to specifically study frequency effects. Alignment was achieved both by careful machining of specimens and other auxiliary parts and by loading the specimens through universal joints.

In most tests, the fatigue crack was initiated and propagated in the test environment under tension-to-tension sinusoidal loading at a constant maximum load and constant minimum load, which were controlled within ±1.0 percent. Prior to making crack-length measurements, the fatigue cracks were extended in the test environment a distance of 0.25 in. (6.4 mm) from the notch root. Thus, at the time crack-length measurements were begun, the total crack length, a, was approximately equal to the specimen thickness (~1.00 in., or 25.4 mm).

Crack extension was measured optically at X17 magnification with an M-101 type Gaertner microscope mounted in a micrometer slide. The average crack extension between consecutive measurements was less than 0.03 in. (0.76 mm).

The environmental bath was built of plexiglass and had a 5-gal (0.019-m^3) capacity to minimize temperature and pH fluctuations (see Fig. B-4). Periodic measurements of pH and temperature were made to assure the stability of the bulk environment. All tests were conducted at 7.0 ± 0.5 pH and at 74 ± 2 F (23 ± 1 C). To minimize galvanic or crevice corrosion effects, the universal joints were coated with an epoxy enamel. For the corrosion fatigue tests the test solution was aerated continuously throughout the course of the tests.

Tests of fatigue crack growth rate in air were conducted for each steel under both constant amplitude, sinusoidal loading and variable amplitude, random sequence, sinusoidal loading. All such tests in air were conducted at a frequency of 300 cpm and at a 10-percent stress ratio 0.10. For the constant amplitude, sinusoidal loading tests, the specimens were subjected to sinusoidal cyclic loads to 3200-lb (14.2-kN) constant maximum load and 200-lb 0.89-kN) constant minimum load. At the start of data recording ($a \cong B \cong 1.00$ in.), this condition corresponded to an initial stress intensity $\Delta K \cong 15.0$ ksi $\sqrt{\text{in.}}$ (16.5 $MNm^{-3/2}$). The stress intensity range gradually increased (and crack propagation rate was determined) as the crack grew to test termination under the prescribed (constant) cyclic loading conditions.

This same basic procedure was also applied for the variable amplitude, random sequence, sinusoidal loading tests conducted in air. However, in these tests, it was necessary to electronically couple an external unit to the MTS testing machines in order to provide the proper random

spectrum of variable amplitude, sinusoidal loading history. This was accomplished with the use of a Weston Instruments EMR 1641 Profiler (random function generator), which was programmed using a continuous loop of metal Mylar tape. The metal tape was prepunched to simulate a 500-cycle block of variable amplitude, sinusoidal loading history under the appropriate random conditions. The specific distribution function used to mathematically describe the frequency (of occurrence for each) of the variable amplitude, sinusoidal waveform cycles was the Rayleigh distribution function.

The corrosion fatigue, crack growth rate tests were conducted in a manner similar to that described for the fatigue-crack-growth rate tests in air. However, the test environment for the corrosion fatigue tests was either distilled water or a 3-percent solution of sodium chloride in distilled water; the test frequency was somewhat slower, being either 60 or 12 cpm. These tests also included additional excursions to investigate the behavior of each of the five steels under both constant amplitude, square waveform conditions (at $R = 0.10$) and variable amplitude, sinusoidal waveform conditions (at $R = 0.50$). These latter tests represent conditions more closely simulating actual material conditions for long-span bridges. The various primary test conditions have been described earlier and are summarized in Table 1. The Weston Instruments EMR 1641 Profiler and continuous Mylar tape system were both used to provide the primary signals for all of the corrosion fatigue, crack growth rate tests conducted under both variable amplitude, sinusoidal loading and constant amplitude, square wave loading.

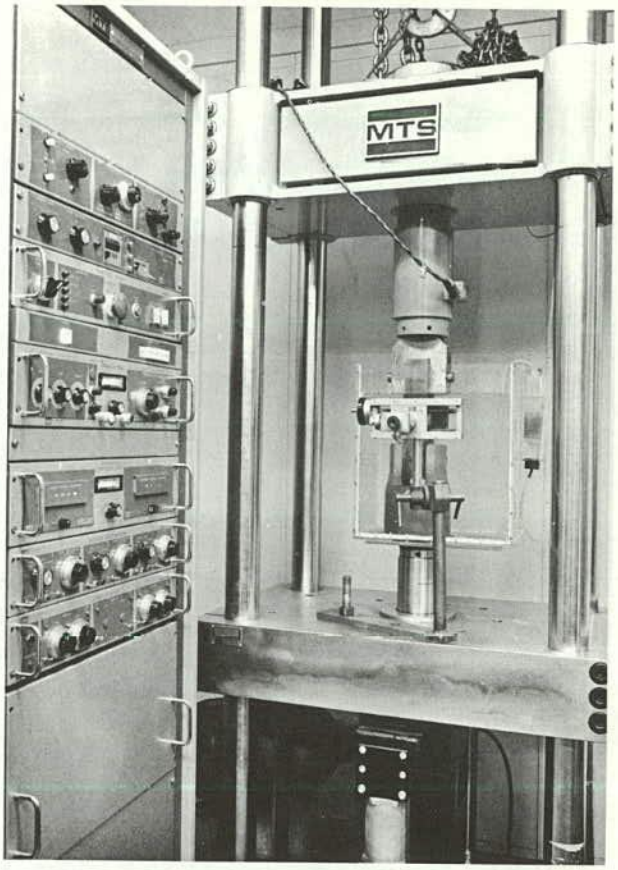

Figure B-4. Experimental setup for corrosion fatigue tests.

APPENDIX C

CHARPY V-NOTCH AND DYNAMIC TEAR DATA

The results of fracture toughness tests for the five steels investigated (A36, A588 grades A and B, and A514 grades E and F) using Charpy V-notch and dynamic tear specimens are summarized in the following Figures C-1 through C-25.

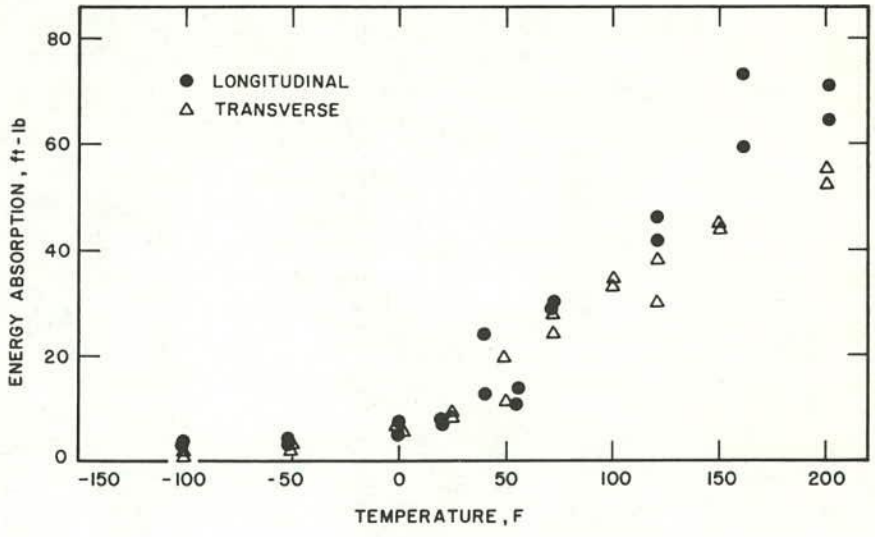

Figure C-1. Charpy V-notch energy absorption for A36 steel.

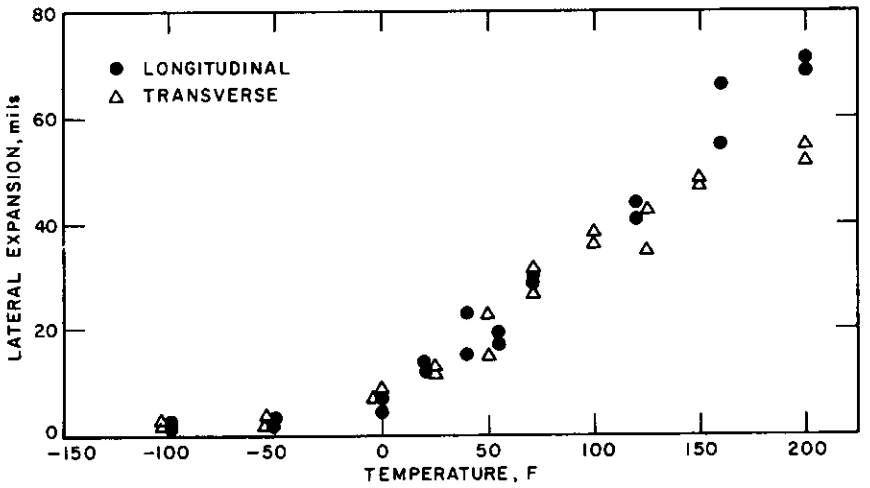

Figure C-2. Charpy V-notch lateral expansion for A36 steel.

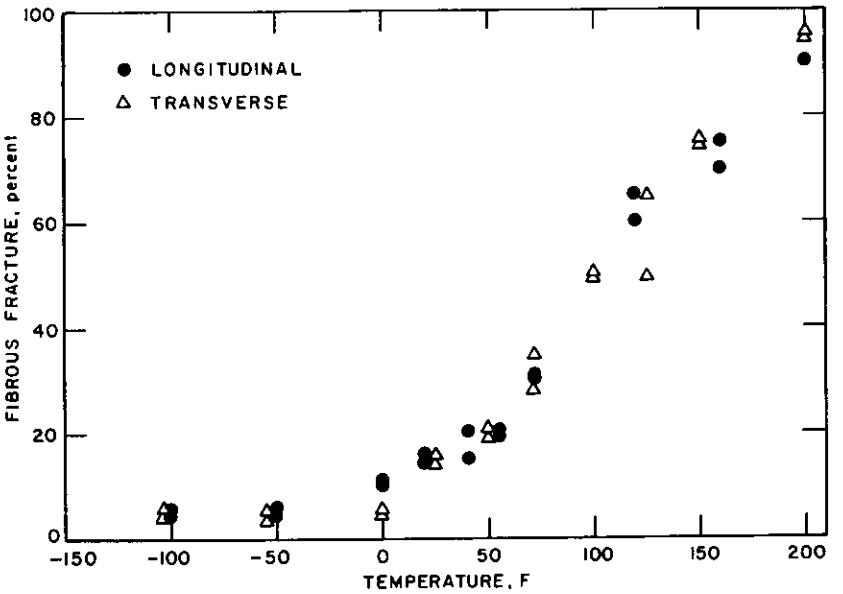

Figure C-3. Charpy V-notch fibrous fracture for A36 steel.

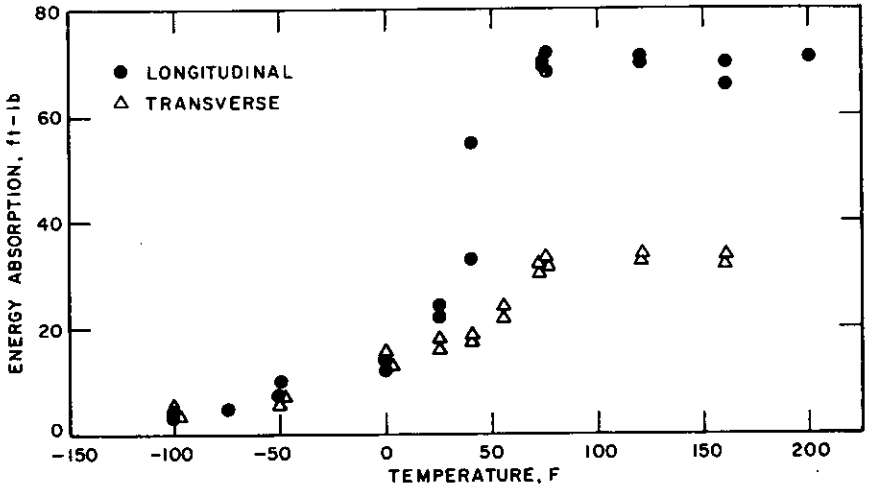

Figure C-4. Charpy V-notch energy absorption for A588 Grade A steel.

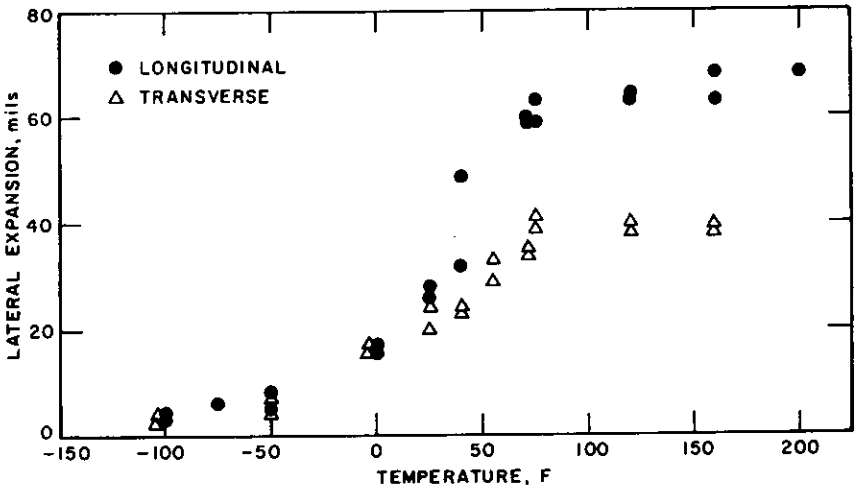

Figure C-5. Charpy V-notch lateral expansion for A588 Grade A steel.

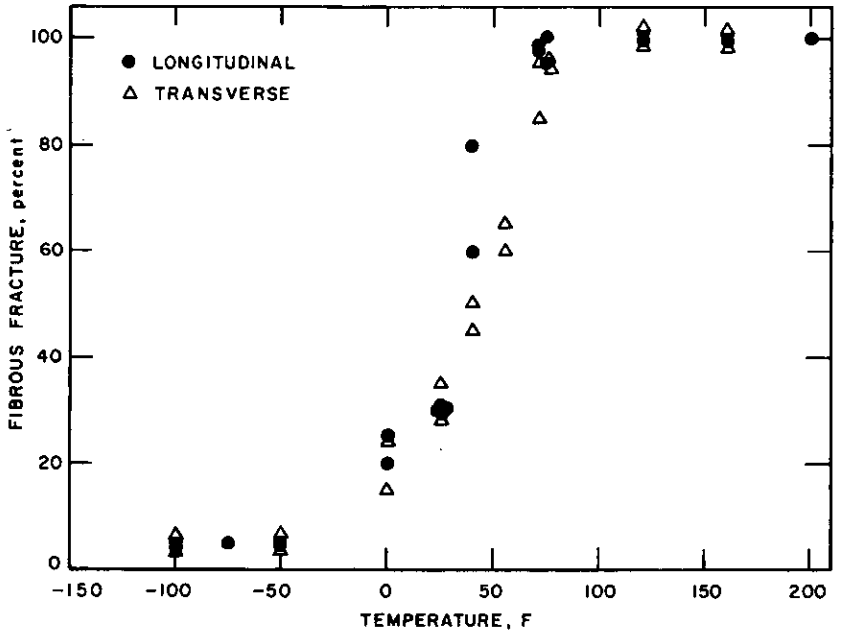

Figure C-6. Charpy V-notch fibrous fracture for A588 Grade A steel.

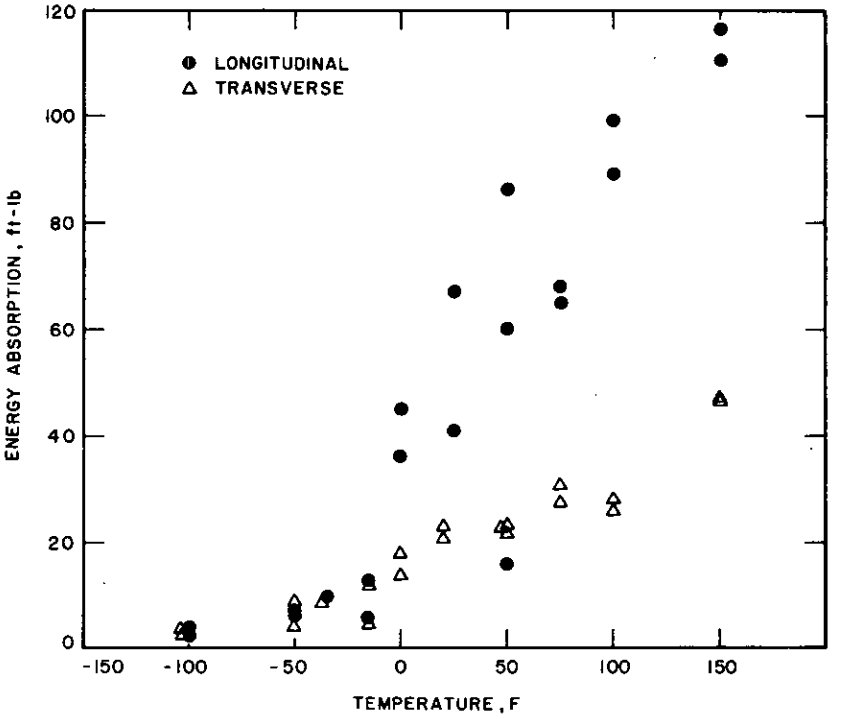

Figure C-7. Charpy V-notch energy absorption for A588 Grade B steel.

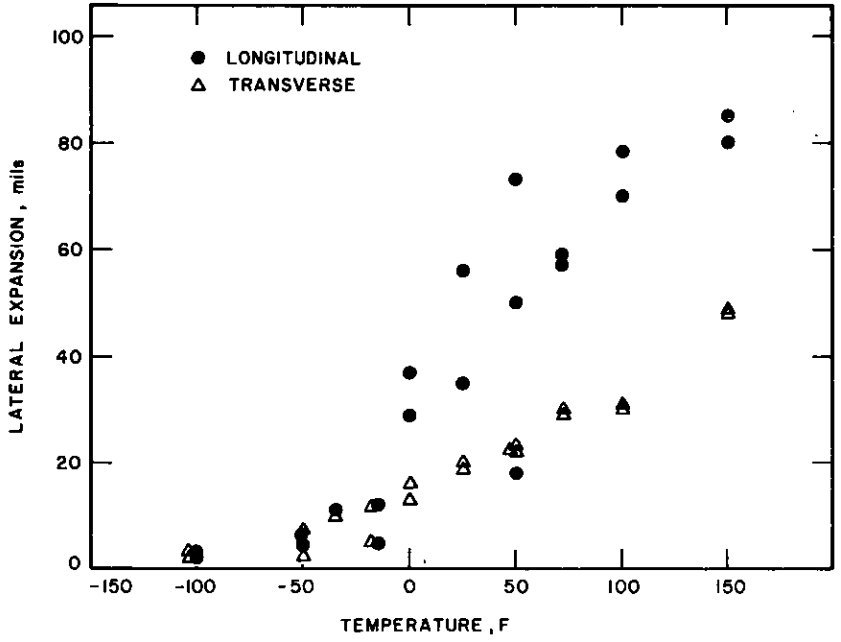

Figure C-8. Charpy V-notch lateral expansion for A588 Grade B steel.

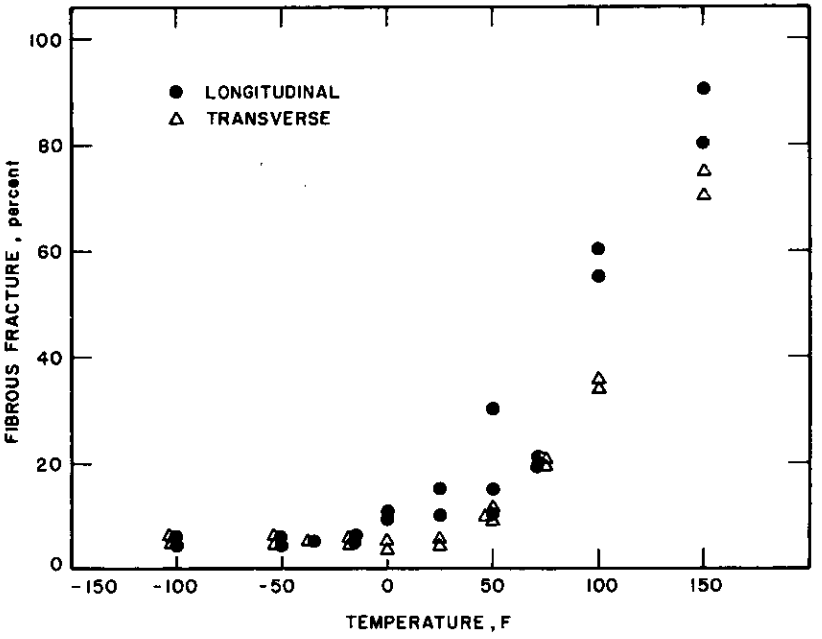

Figure C-9. Charpy V-notch fibrous fracture for A588 Grade B steel.

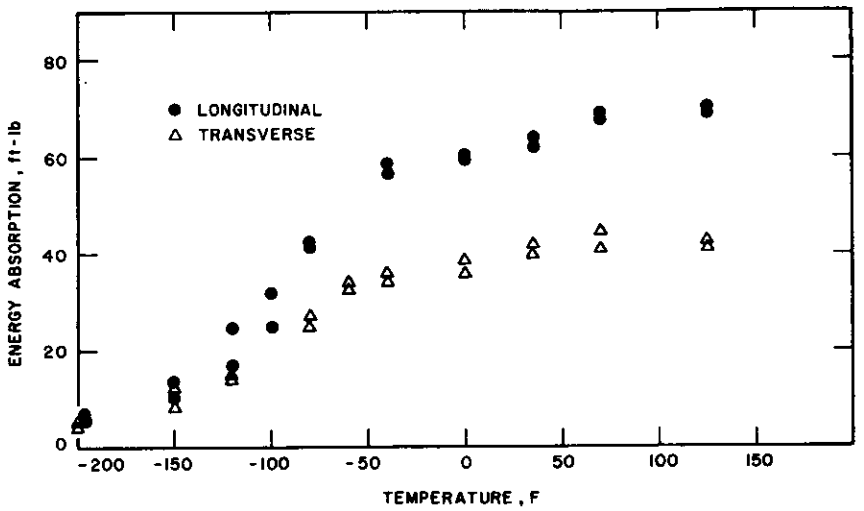

Figure C-10. Charpy V-notch energy absorption for A514 Grade E steel.

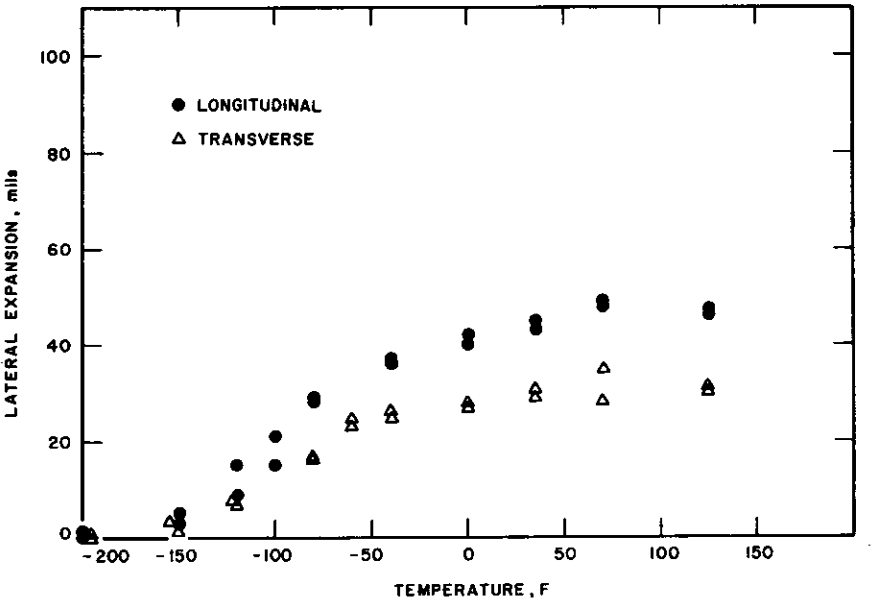

Figure C-11. Charpy V-notch lateral expansion for A514 Grade E steel.

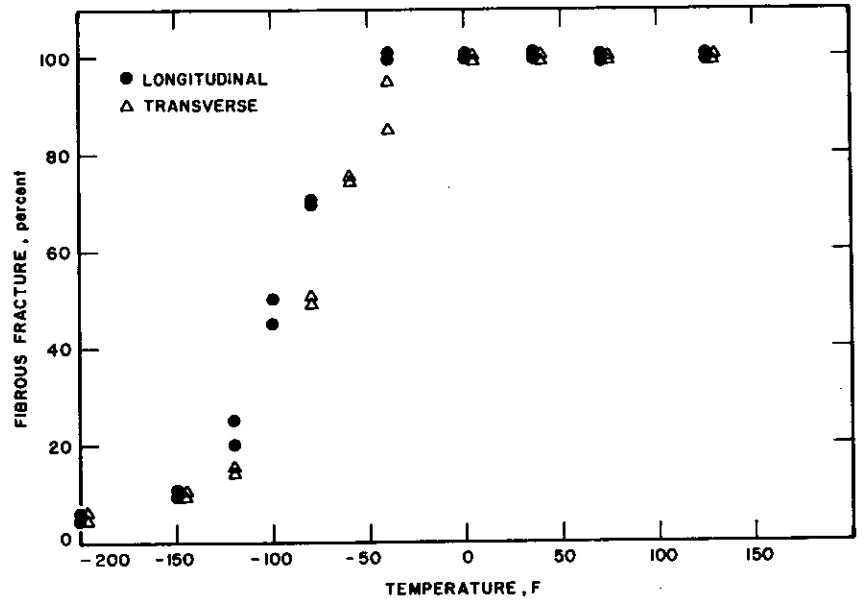

Figure C-12. Charpy V-notch fibrous fracture for A514 Grade E steel.

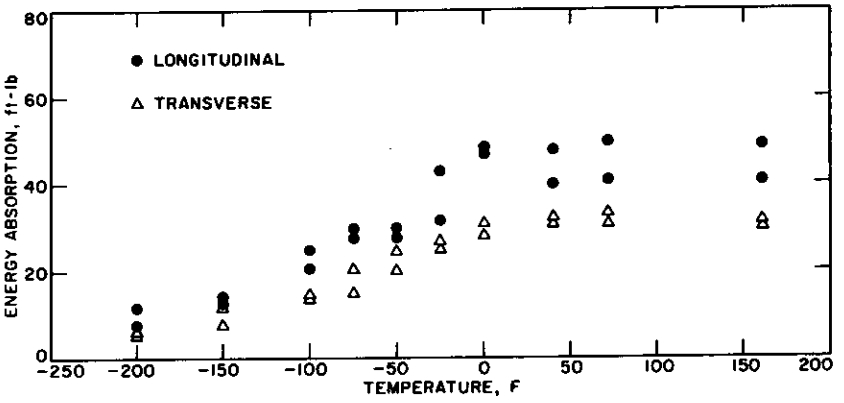

Figure C-13. Charpy V-notch energy absorption for A514 Grade F steel.

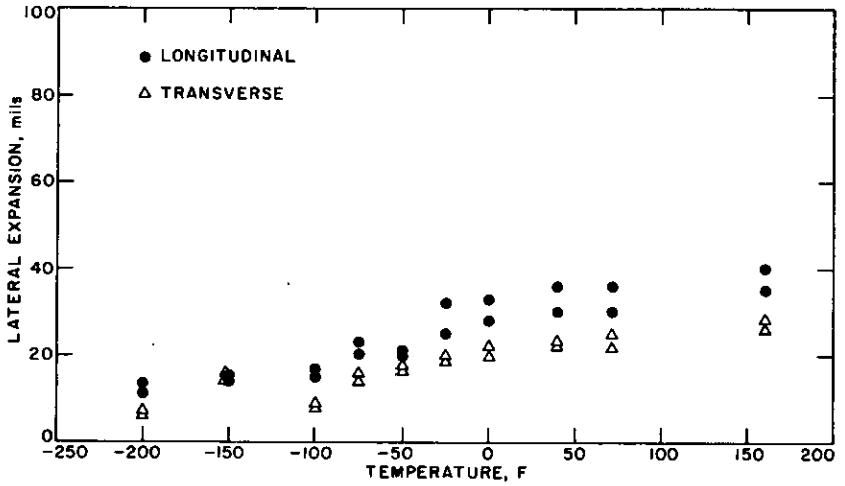

Figure C-14. Charpy V-notch lateral expansion for A514 Grade F steel.

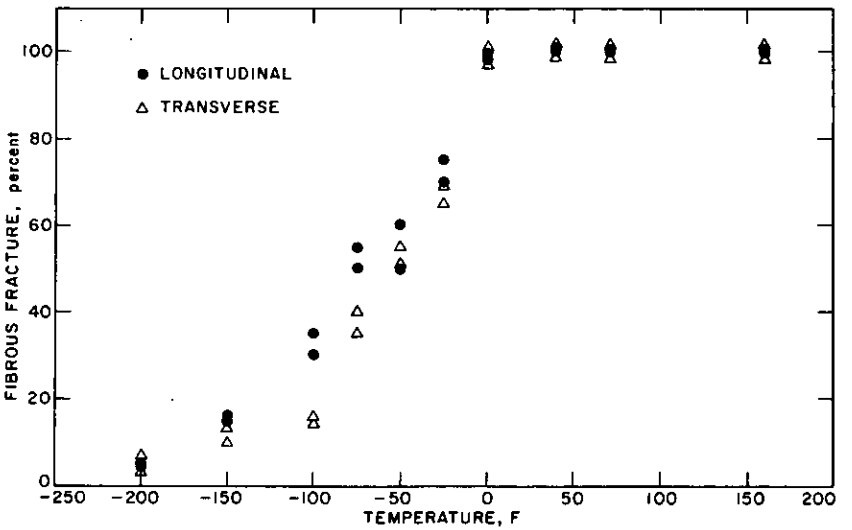

Figure C-15. Charpy V-notch fibrous fracture for A514 Grade F steel.

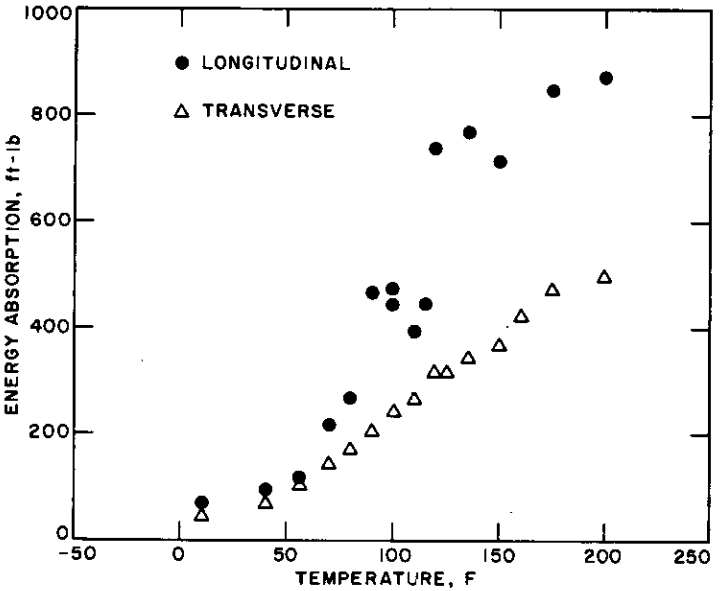

Figure C-16. Dynamic tear energy absorption for A36 steel.

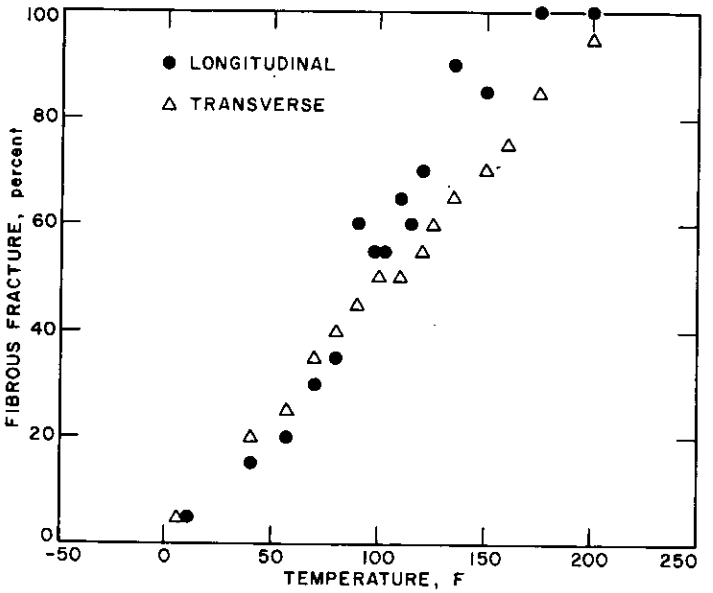

Figure C-17. Dynamic tear fibrous fracture for A36 steel.

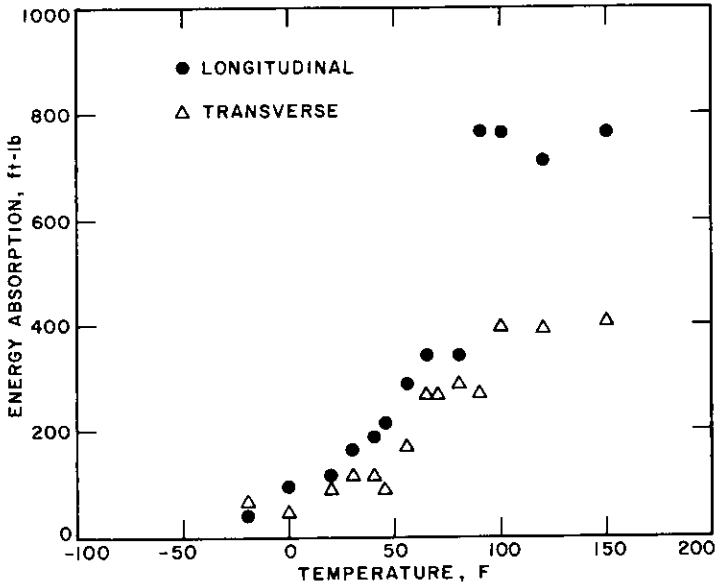

Figure C-18. Dynamic tear energy absorption for A588 Grade A steel.

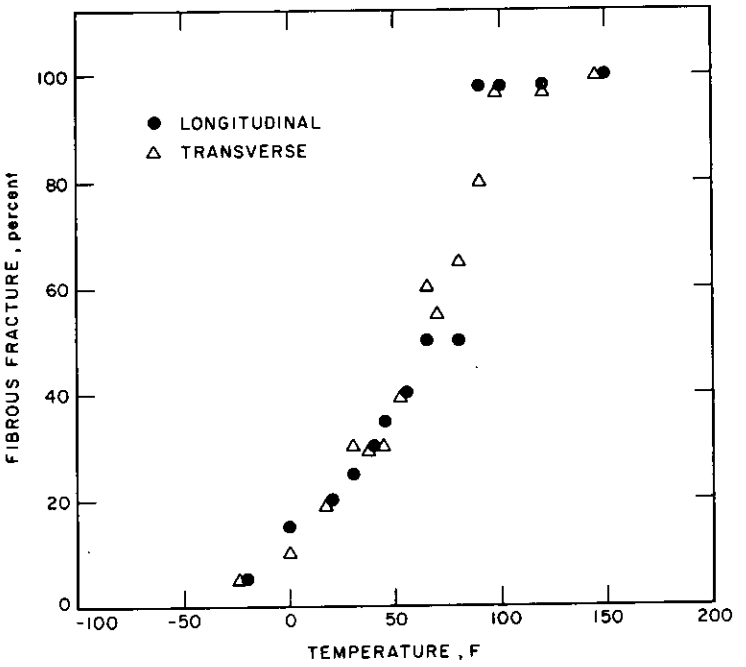

Figure C-19. Dynamic tear fibrous fracture for A588 Grade A steel.

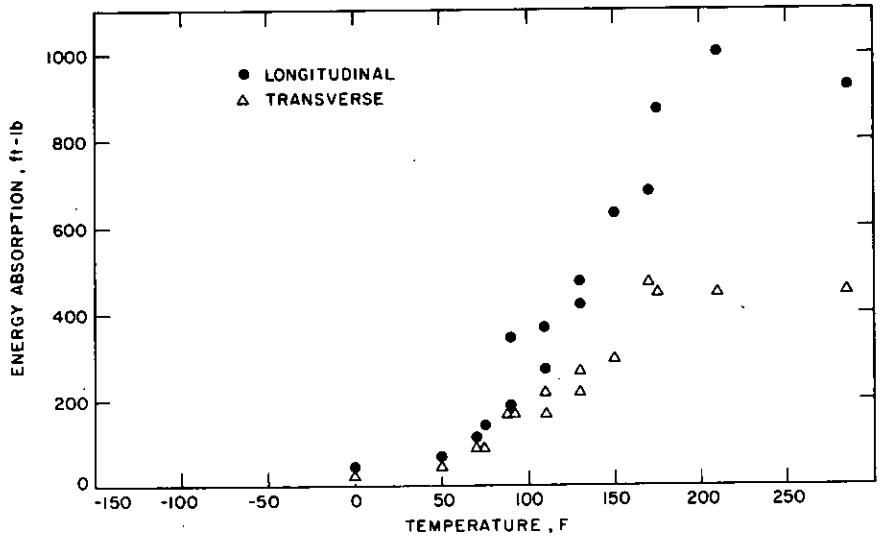

Figure C-20. Dynamic team energy absorption for A588 Grade B steel.

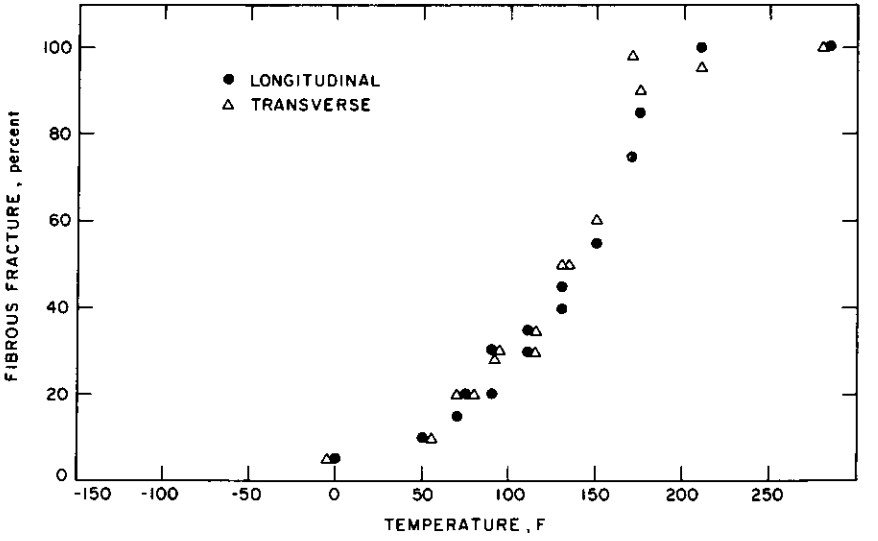

Figure C-21. Dynamic tear fibrous fracture for A588 Grade B steel.

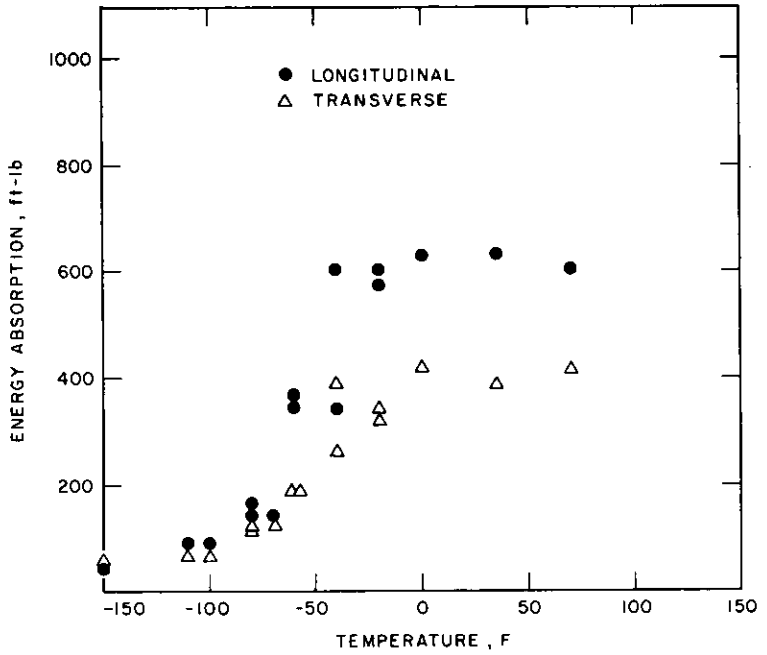

Figure C-22. Dynamic tear energy absorption for A514 Grade E steel.

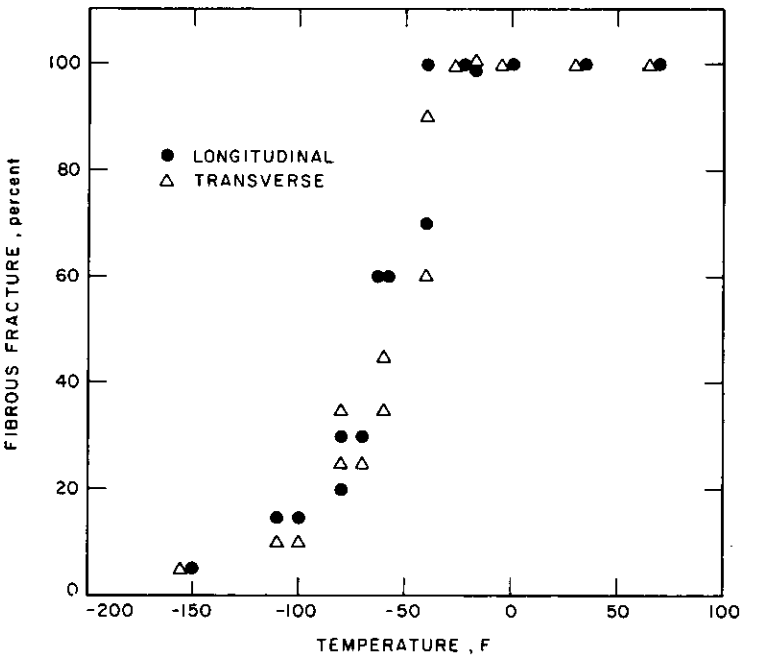

Figure C-23. Dynamic tear fibrous fracture for A514 Grade E steel.

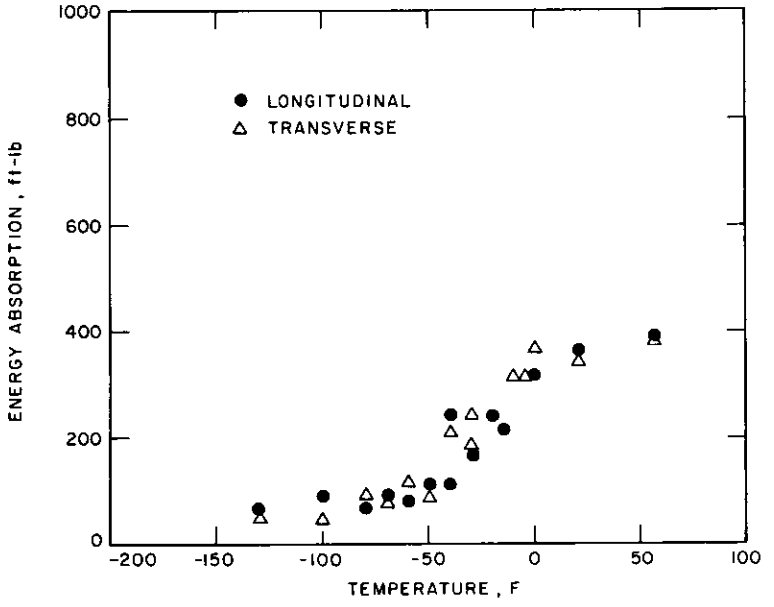

Figure C-24. Dynamic tear energy absorption for A514 Grade F steel.

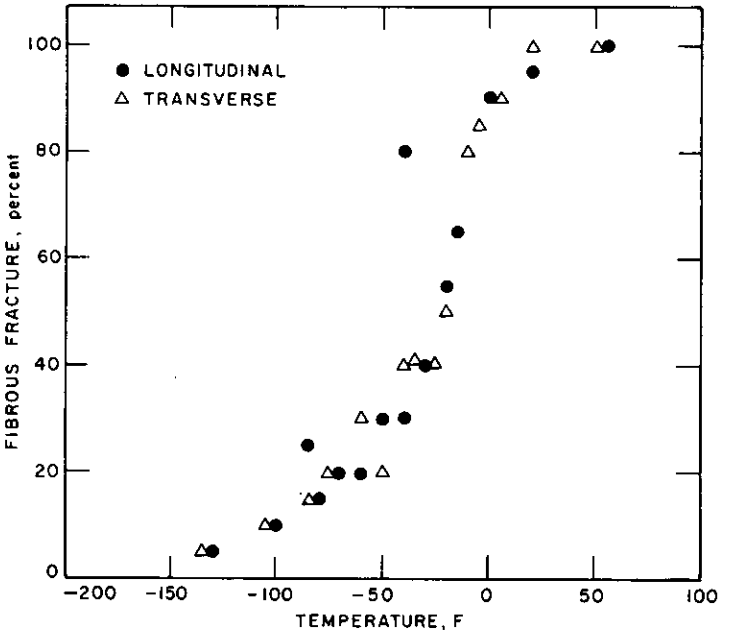

Figure C-25. Dynamic tear fibrous fracture for A514 Grade F steel.

APPENDIX D

FRACTURE (K_{Ix}) BEHAVIOR OF STEELS INVESTIGATED

The individual results of fracture toughness tests for the 1T WOL specimen are given in Table D-1, and a corresponding photograph showing typical fracture surfaces for each steel is shown in Figure D-1. Similar results for the fracture tests conducted on these same steels in cantilever bending are given in Table D-2 and Figure D-2, respectively. The results for both types of tests (Tables D-1 and D-2) are characterized in terms of both the secant intercept, X, and the clip-gage displacement, V, at the onset of maximum load, P_{max}, as well as at complete fracture, P_f, because the two events were generally not coincident. In most cases, complete (sudden) fracture occurred only after maximum load was attained and the applied load decreased due to stable crack extension.

The salient results from both types of specimen fracture tests are summarized in Table 6 using average values. These data are consistent in showing extensive resistance to fracture for each of the five steels tested. As expected, no valid K_{Ic} values were measured for any of the steels. This is apparent from the fact that the K_Q values (5-percent secant intercept values) for all tests were above the respective $K_{I,\,Lub}$ values and, further, that the values at maximum load (K_{Ix}) were all well in excess of the 1.10 K_Q limit admissible for a valid K_{Ic} test (*56*). Thus, the K_Q values occurred well in advance of the attainment of maximum load (K_{Ix}) and bear no relation to the intrinsic brittle fracture tendencies of the steels tested.

The true fracture characteristics of the steels tested are better characterized by the K_{Ix} rather than the K_Q values. All such K_{Ix} values occurred under conditions of gross plastic deformation and are synonymous with ductile rather than brittle fracture behavior. The extent of plasticity at fracture is directly evident from the lateral contraction, shear-lip development, and large amounts of stable crack extension that occurred in the fracture process (Figs. D-1 and D-2). Another measure of this plasticity can be seen in the high ratios of applied stress to the yield strength ($\sigma_{N,\,max}/\sigma_{ys}$) that occurred at maximum load for each of the steels tested (Table 6). In particular, it can be seen that this ratio was in the range 2.10 to 2.60 for each of the tests conducted on the A36, A588 Grade B steels with both specimen types. The corresponding ratios for the higher strength A514 Grade E and A514 Grade F steels were approximately 1.65 and 1.05, respectively. These latter values are somewhat lower and indicative of less plastic deformation at fracture, as might be expected, because of the higher strength.

From the preceding discussion it should be clear that LEFM concepts can not be used to quantitatively characterize the brittle fracture characteristics of the steels investigated because of both the high inherent level of fracture toughness exhibited and the limitations imposed by the 1T specimen size employed for all tests in this study. Such quantitative assessments of the true fracture behavior can only be obtained in the future with the J-integral (*38, 39*) and equivalent-energy (*40, 41*) methods of elastic-plastic fracture analysis. However, certain semiquantitative estimates of fracture behavior can be made on the basis of the results attained during this study by using the K_I-suppression effect concept discussed in Part I of this report. Moreover, the fracture tests were conducted primarily to estabilsh the basic fracture level of each steel (in whatever terms are available) for purposes of assessing degradation in this level due to SCC susceptibility. Because these objectives rely to some extent on the observed K_Q and K_{Ix} values, careful examination of these specific results is necessary.

In general, the K_Q values obtained from both types of specimens were in relatively good agreement for each of the five steels tested (Table 6). The K_Q values from the WOL specimens were generally only slightly lower than the corresponding values obtained from the cantilever beam specimens. Although this was true for the A36, A514 Grade E, and A514 Grade F steels, the K_Q values from the WOL specimens for the A588 Grade A and A588 Grade B steels (40 and 42 ksi $\sqrt{\text{in.}}$ (44 and 46 $\text{MNm}^{-3/2}$), respectively) were somewhat lower than expected on the basis of the corresponding K_Q values obtained from the cantilever beam specimens (57 and 54 ksi $\sqrt{\text{in.}}$ (63 and 59 $\text{MNm}^{-3/2}$), respectively). These lower K_Q values for the WOL specimens of the A588 Grade A and A588 Grade B steels, specifically, were apparently the result of premature yielding of the specimen arms (see Fig. D-3). Figure D-4 shows that such behavior occurred despite attempts to prevent it by using high-strength steel pins that were drilled and tapped to accommodate loading by two studs in the fracture tests. Such plastic arm bending is an inherent weak link for the WOL specimen in the testing of high-toughness steels, generally, and is the primary reason for the subsequent development and adoption of the stubbier compact tension (CT) specimen as a more rigid type of specimen for standard K_{Ic} tests (*56*). Thus, the K_Q values obtained from the cantilever beam tests are more representative of the true behavior for the steels tested, particularly the A588 Grade A and A588 Grade B steels.

In contrast to that observed for the K_Q values, the values at maximum load (K_{Ix}) were consistently higher for the WOL specimens than the corresponding values for the cantilever beam specimens for each steel (Table 6). This

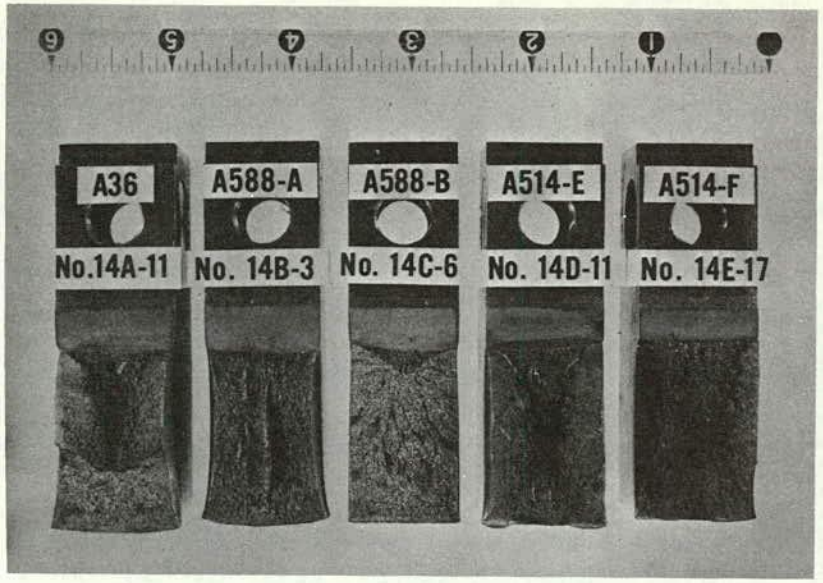

Figure D-1. Typical fracture surfaces from 1T WOL specimens tested to fracture under static loading conditions in air at 72 F.

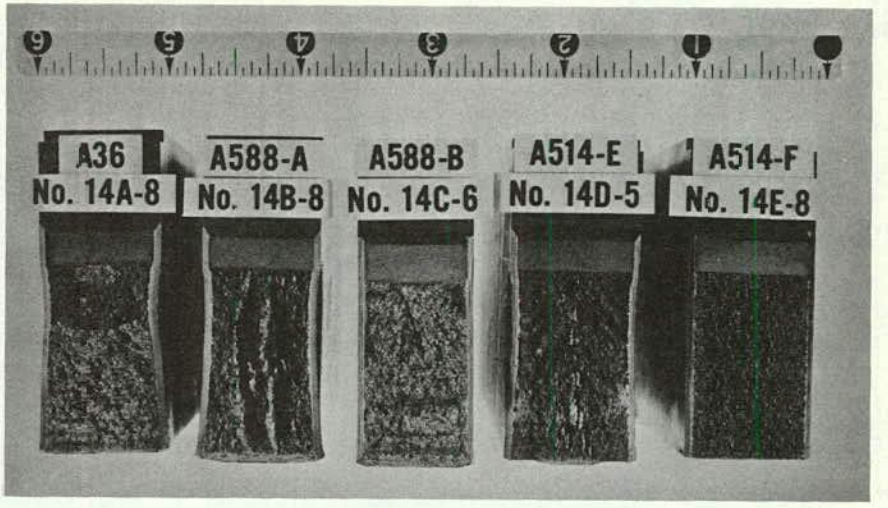

Figure D-2. Typical fracture surfaces from precracked cantilever beam specimens tested to fracture under static loading conditions in air at 72 F.

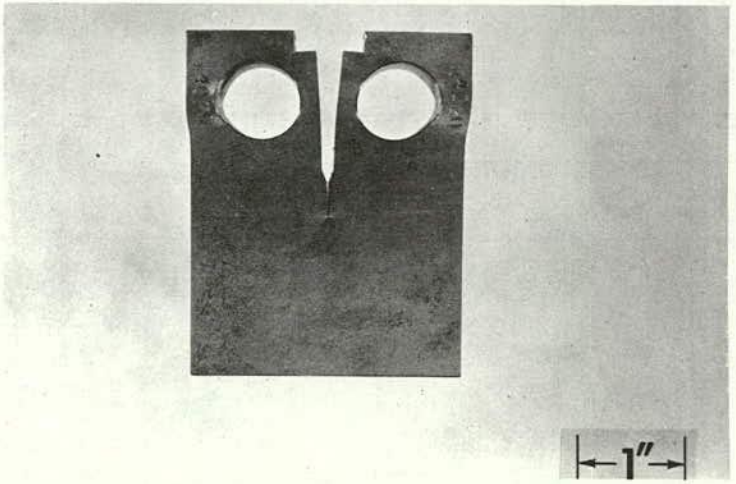

Figure D-3. Partially tested 1T WOL specimen (pin-loaded) of A588 Grade B steel showing substantial arm bending and plasticity prior to the use of high-strength steel pins and a stud loading procedure.

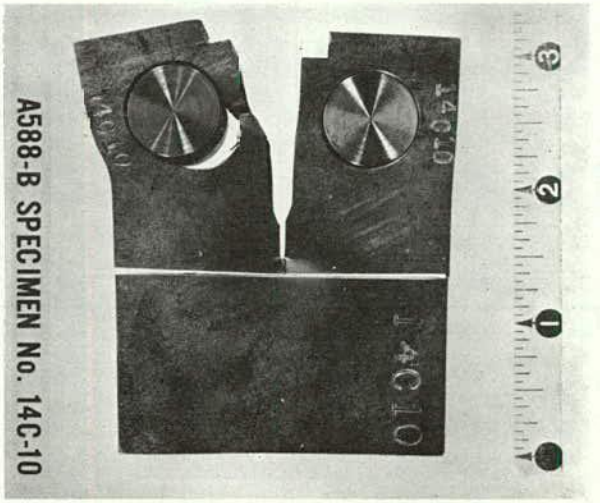

Figure D-4. 1T WOL specimen of A588 Grade B steel exhibiting gross plastic deformation of the specimen arms (thereby preventing complete fracture and necessitating a saw cut), despite the presence of high-strength steel pins made of 18Ni (180 Grade) maraging steel.

TABLE D-1

1T WOL SPECIMENS TESTED TO FRACTURE

Item No.	Steel	Specimen Code No.	Specimen Dimensions W, inches	B, inch	a, inches*	Fatigue Cracking Parameters ΔK_f, ksi $\sqrt{inch}$**	N, cycles***	$K_{I,Lub}$, ksi $\sqrt{inch}$****	Values of Parameters from Load versus COD Records: At a 5% Secant K_Q, ksi $\sqrt{inch}$**	At Maximum Load: P_{max}, pounds	$\sigma_{N,max}$, ksi+	K_{Ix}, ksi $\sqrt{inch}$**	V_x, mils++	X_{max}, percent+++	At Fracture: P_f, pounds	V_f, mils++	X_f, percent
1	A36	14A-17++++	2.559	0.999	1.101	22.0	293,000	27.6	34.6	16,100	94.3	88.2	197	84.2	16,100	210	85.2
2	A36	14A-11#	2.557	0.999	1.115	22.3	275,000	27.6	39.0	18,320	109.9	101.7	>177	>82.4	6,000	>>242	>>91.5
3	A588-A	14B-3#	2.556	0.966	1.141	27.7	187,000	34.1	41.4	17,930	115.9	105.1	>208	>83.6	< 450	>607	>95.8
4	A588-A	14B-5	2.558	0.966	1.103	22.8	295,000	34.1	39.1	19,440	118.2	110.4	>323	>89.3	<12,760##	>>323##	>>93.1##
5	A588-B	14C-6	2.556	0.925	1.109	23.9	116,000	33.8	39.8	20,590	132.3	123.3	>165	>77.2	20,590	>165	>77.2
6	A588-B	14C-10#	2.559	0.925	1.065	28.8	184,000	33.8	37.8	>21,240###	>127.2###	>121.9###	374###	88.9###	ND	ND	ND
7	A588-B	14C-20#	2.553	0.924	1.088	23.5	183,000	33.8	44.6	20,540	128.3	121.0###	505###	91.2###	20,400	529###	91.8###
8	A588-B	14C-17	2.560	0.925	1.469	43.4	245,000	33.8	44.5	11,830	141.6	102.1####	207	79.0	11,830	208	79.1
9	A514-E	14D-7#	2.554	0.988	1.086	20.3	364,000	67.8	112.4	30,120	175.2	165.1	127	57.6	~0	>656	>99.2
10	A514-E	14D-11#	2.554	0.988	1.091	21.5	649,000	67.8	101.7	30,120	176.6	166.3	>115	>53.7	~0	>643	>99.2
11	A514-F	14E-3#	2.554	0.999	1.050	20.5	627,000	81.5	90.6	22,970	125.2	120.6	87	56.9	< 3,260	>139	>96.0
12	A514-F	14E-17#	2.549	0.999	1.038	20.3	579,000	81.5	94.8	27,410	147.5	143.3	91	51.9	~0	>163	>99.9

* a is the original crack length attained by fatigue cracking ~ 0.27 to 0.37 inch beyond $a_n \cong 0.77$ inch, the machined notch tip.

** $K_I = \frac{P \cdot f(a/W)}{B\sqrt{a}}$ where f(a/W) is a function of the relative crack length; ΔK_f is the maximum ΔK_I reached during fatigue crack preparation, K_Q is the K_I value calculated from the load at a 5 percent secant on the load versus COD record, and K_{Ix} is the value calculated from the maximum load, P_{max}. All calculations were made using the length of the original fatigue crack, a.

*** N is the total number of cycles of constant amplitude zero-to-tension (R ≅ 0) sinusoidal loading required to extend a fatigue crack from a_N to the final length, a.

**** $K_{I,Lub} = \sigma_{ys}\left(\frac{B}{2.50}\right)^{1/2}$ Note that $K_{I,Gub} = 1.56\ K_{I,Lub}$.

\+ $\sigma_{N,max}$ is the nominal stress at the crack tip at maximum load ($P = P_{max}$) as calculated from the relation $\sigma_N = \frac{Mc}{I} + \frac{P}{A} = \frac{P}{B(W-a)2}[4W + 2a]$ for a WOL specimen.

++ V is the value of the COD from the load versus COD records; V_x is the value attained at maximum load and V_f is the value at gross fracture.

+++ X is the percent secant at any given point on the load versus COD record.

++++ A36 specimen No. 14A-17 exhibited an accelerated increase in COD for ~ 6 mils at a constant load, $P < P_{max}$. This appears to be the effect of a short stable crack extension and/or discontinuous yielding which may be caused by the formation of fissures (internal shear lips) near the crack front, the strain rate, and the stiffness of the test machine. The corresponding values of the various parameters at this point were P = 13,200 lb, K_I = 72 ksi $\sqrt{inch}$, V = 52 mils, and X = 51.6 percent. This phenomena, although not as pronounced, was also observed repeatedly later in the test and during the testing of other specimens.

* These specimens were totally unloaded prior to fracture, at which time the maximum lateral contraction, ΔB_{max}, was measured. This value can be used to obtain, for the 1-inch-thick plates from which these specimens were machined, an approximate measure of resistance to fracture under plane-stress conditions. This is accomplished by employing COS theory, setting $\delta \cong \Delta B_{max}$ (an empirical correlation given earlier, Reference 11) in the equation $K_R = \sqrt{\delta E \sigma_{ys}}$, where E is the modulus of elasticity of the material ($E \cong 30 \times 10^6$ psi for steel). ($K_R < K_c$, the plane-stress fracture toughness). Results for the four specimens are as follows:

1. A36 specimen No. 14A-11; ΔB_{max} = 0.131 inch, K_R = 413.9 ksi $\sqrt{inch}$, K_I = 78.6 ksi $\sqrt{inch}$, P = 14,160 lb (after P_{max}), V >> 177 mils, X >> 82.4 percent.
2. A588-A specimen No. 14B-3; ΔB_{max} = 0.089 inch, K_R = 382.9 ksi $\sqrt{inch}$, K_I = 96.8 ksi $\sqrt{inch}$, P = 16,510 lb (after P_{max}), V > 208 mils, X > 83.6 percent.
3. A588-B specimen No. 14C-10; ΔB_{max} = 0.053 inch, K_R = 297.3 ksi $\sqrt{inch}$, K_I = 127.2 ksi $\sqrt{inch}$, P = 21,240 lb (before P_{max}), V = 374 mils, X = 88.9 percent.
4. A588-B specimen No. 14C-20; $\Delta B_{max} \geq$ 0.013 inch, $K_R \stackrel{>}{=}$ 147.3 ksi $\sqrt{inch}$, K_I = 112.4 ksi $\sqrt{inch}$, P = 19,080 lb (before P_{max}), V = 180.4 mils, X = 77.1 percent.

(See footnote below regarding V and X values for the last two specimens.)

** A588-A specimen No. 14B-5 was not loaded to fracture.

*** The arms of A588-B specimens No. 14C-10 and 14C-20 deformed severely under load causing increased values of V(COD) to be recorded and therefore increased the calculated values of X, the percent secant. In addition, one arm of specimen No. 14C-10 deformed to such an extent that the net section of the specimen was not subjected to the maximum possible load and therefore was not fractured.

**** The K_{Ix} value for A588-B specimen No. 14C-17 reflects greater K_I-Suppression Effects than mating specimens due to the longer crack length, a.

\# A514-E specimens No. 14D-7 and 14D-11, and to a much greater extent A514-F specimens No. 14E-3 and 14E-17, exhibited a serrated load versus COD record consisting of discontinuous changes in slope and/or accelerated increases in COD at a constant load, $P < P_{max}$. This appears to be the effect of short, stable crack extensions and/or discontinuous yielding which may be caused by the formation of fissures (internal shear lips) near the crack front, the strain rate, and the stiffness of the test machine.

TABLE D-2

PRECRACKED CANTILEVER BEAM SPECIMENS TESTED TO FRACTURE (IN AIR)

Item No.	Steel	Specimen Code Number	Specimen Dimensions W, inches	B, inch*	a, inches**	Fatigue Cracking Parameters ΔK_f, ksi √inch***	N, cycles****	$K_{I,Lub}$, ksi √inch+	Values of Parameters from Load versus COD Records: At a 5% Secant K_Q, ksi √inch ++	At Maximum Load: P_{max}, pounds+++	$\sigma_{N,max}$, ksi++++	K_{Ix}, ksi √inch++	V_x, mils+++++	X_{max}, percent#	At Fracture: P_f, pounds+++	V_f, mils+++++	X_f, percent
1	A36	14A-6##	2.500	0.939	1.062	28.0	266,000	26.0	39.2	1058	109.8	87.9	149	92.5	< 381##	>264##	>96.5##
2	A36	14A-1###	2.500	0.941	1.074	28.3	266,000	26.0	44.4	> 971###	>102.2###	>82.0###	> 77###	>85.3###	< 969###	>260###	>95.4###
3	A36	14A-4	2.499	0.939	1.100	29.2	231,000	26.0	40.7	1065	116.7	92.7	179	92.6	1062	183	92.8
4	A588-A	14B-1	2.499	0.914	1.062	27.5	222,000	32.2	54.6	1166	124.9	100.3	98	86.7	< 879	>263	>96.0
5	A588-A	14B-8	2.496	0.913	1.043	27.0	207,000	32.2	60.4	1173	123.0	99.0	134	87.0	< 816	>263.	>96.3
6	A588-B	14C-6	2.503	0.896	1.090	29.4	143,000	32.4	56.3	1138	128.9	102.3	46	67.7	1138	46	67.7
7	A588-B	14C-2	2.500	0.896	1.112	31.1	218,000	32.4	52.9	1146	134.5	106.6	53	71.0	1146	52	71.0
8	A514-E	14D-8####	2.505	0.997	1.070	26.5	200,000	66.4	109.1	1869	182.1	146.1	29	32.0	< 218	>259	>99.1
9	A514-E	14D-5####	2.504	0.996	1.046	25.6	236,000	66.4	110.8	1904	179.9	145.5	26	23.9	< 225	>152	>98.4
10	A514-F	14E-2####	2.498	0.975	1.114	26.2	>311,000	78.3	96.0	1206	129.5	102.6	16	12.7	~ 0	>267	~100
11	A514-F	14E-8####	2.497	0.975	1.063	24.9	311,000	78.3	97.0	1316	131.7	105.7	16	14.9	~ 0	>151	~100

* Specimens were face notched to a depth, X, of 0.050 inch. $B_N = B - 2X = B - 0.100$ in inches.

** a is the original crack length attained by fatigue cracking ~ 0.24 to 0.36 inch beyond $a_n \cong 0.80$ inch, the machined notch tip.

*** ΔK_f is the maximum ΔK_I reached during the 3-point bend fatigue cracking operation and is calculated from $K = \frac{2MR}{(B\,B_N)^{1/2}\,W^{3/2}}$ where M is the calculated moment at the crack plane and R is a function of the relative crack length, a/W. (See "Stress-Intensity Factor for a Short Edge-Notched Specimen Subjected to Three-Point Loading" by H. T. Akao and A. S. Kobayashi, ASME publication 65-MET-14).

**** N is the total number of cycles of constant amplitude zero-to-tension ($R \cong 0$) sinusoidal loading required to extend a fatigue crack from a_n to the final length, a.

\+ $K_{I,Lub} = \sigma_{ys}\,(\frac{B}{2.50})^{1/2}$ Note that $K_{I,Gub} = 1.56\,K_{I,Lub}$.

++ $K_I = \frac{6M \cdot f(a/W)}{(B\,B_N)^{1/2}\,(W-a)^{3/2}}$ where M is the calculated moment at the crack plane and f(a/W) is a function of the relative crack length; K_Q is the K_I value calculated from the load at a 5 percent secant on the load versus COD record, and K_{Ix} is the value calculated from the maximum load, P_{max}. All calculations were made using the length of the original fatigue crack, a.

+++ The load was applied at a lever arm length, L, of 30.0 inches from the crack plane.

++++ $\sigma_{N,max}$ is the nominal stress at the crack tip at maximum load ($P = P_{max}$) as calculated from the relation $\sigma_N = \frac{Mc}{I} \equiv \frac{6PL}{B_N\,(W-a)^2}$ for a cantilever-beam specimen. L (30 inches) is the distance from the applied load to the crack plane (the moment arm), and B_N is the net thickness of the specimen as described above in the first footnote.

+++++ V is the value of the COD from the load versus COD record. V_x is the value attained at maximum load and V_f is the value at gross fracture of the specimen.

X is the percent secant at any given point on the load versus COD record.

A36 specimen No. 14A-8 exhibited a moderate amount of unstable crack extension ("pop in") prior to reaching maximum load. The values of the various parameters at this point were: P = 403 lb (M = 1008 ft-lb), σ_N = 41.8 ksi, K_I = 69.0 ksi $\sqrt{inch}$, V = 28 mils, and X = 36 percent.

A36 specimen No. 14A-1 reached the deflection capacity of the testing fixture thereby preventing continuation of the test. Bounds were determined for the values at fracture when the specimen was loaded a second time after modification of the testing fixture to allow greater deflection of the specimen.

A514-E specimens No. 14D-8 and 14D-5, and A514-F specimens No. 14E-2 and 14E-8 each began, at a given point, to display a serrated load versus COD record (though not as well defined as for the corresponding 1T WOL specimens) consisting of discontinuous changes in slope and accelerated increases in COD. This appears, as explained for the case of the 1T WOL specimens, to be the effect of short stable crack extensions and/or discontinuous yielding which may be caused by the formation of fissures (internal shear lips) near the crack front, the strain rate, and the stiffness of the testing fixture. For the A514-E specimens this behavior was evident both before and after maximum load, while for the A514-F specimens it could be observed only after the specimens had passed through maximum load.

was due primarily to the WOL specimens being smooth-sided and allowing full development of the shear lips on the fracture surfaces (Fig. D-1), thus requiring higher energy to attain complete fracture; the cantilever beam specimens, on the other hand, were face notched, a mechanical process which produces additional transverse constraint in the specimen at the crack tip and also prevents shear-lip formation (Fig. D-2). However, as shown by the results in Figures D-5 and D-6, it is possible to have both the presence of a fully-developed shear lip on the fracture surface of one specimen and a total absence of shear lip on another specimen in otherwise identical tests of the same steel, even when face notches are not used. The lack of macroscopic shear lip or, conversely, the development of a completely flat fracture surface is not a meaningful criterion in relation to obtaining a valid K_{Ic} (Table 6).

In general, the results for the A36 steel (Table D-2) are compeltely consistent with the results of extensive fracture tests conducted earlier on a similar A36 steel (*36, 58*). Likewise, the results for the A588 Grade A and A588 Grade B steels are in excellent agreement with each other, showing essentially no difference in basic fracture behavior. Typical high fracture resistance for the A588 Grade A steel is shown in Figure D-7. These results are consistent with results obtained earlier on a similar strength A572 steel (*37, 58*) in that they show that LEFM concepts are not

Figure D-5. Fracture surfaces of two 1T WOL specimens of A36 steel tested to fracture under identical conditions but showing different fracture topographies (presence and total absence of shear-lip development).

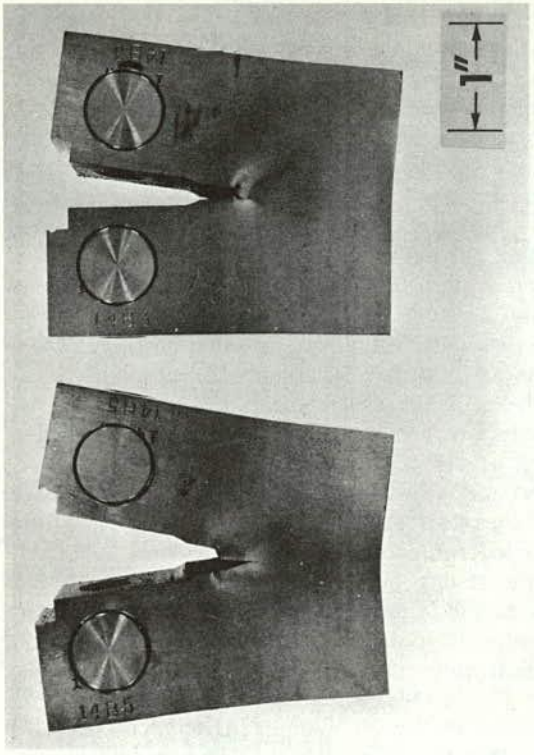

Figure D-7. Partially tested 1T WOL specimens of A588 Grade A steel exhibiting a high resistance to fracture.

applicable for analysis of plane-strain fracture behavior under static loading conditions at 72F for the 1½ in. plate thickness tested. The results also show for static fracture at 72 F that nonlinear elastic-plastic methods (J-Integral (*38, 39*), Equivalent Energy (*40, 41*), and COS (*59, 60, 61*) methods) must be used for quantitative characterization of fracture behavior for plates ranging in thickness from ½ to 1½ in.

Similar statements can also be made for the higher strength A514 steels, but to a lesser extent. In particular, the results given in Table 6 show a distinct difference in the fracture behaviors of these steels, with the A514 Grade E steel exhibiting higher fracture toughness than that of the A514 Grade F steel. However, this difference is primarily due to the untypically higher (but still acceptable) strength level for the A514 Grade F steel ($\sigma_{ys} = 126$ ksi, or 870 MN/m²; Table 3) as compared to a typical strength level for the A514 Grade E steel ($\sigma_{ys} = 108$ ksi, or 740 MN/m²; Table 3). In view of this strength differential, the observed fracture results are about what would be expected prior to testing. Furthermore, the results for the typical strength A514 Grade E steel are also in good agreement with the results from earlier fracture studies on a similar strength A517 Grade F steel (*62*). The high resistance to fracture for the A514 Grade E steel is illustrated by the partially tested WOL specimens shown in Figure D-8.

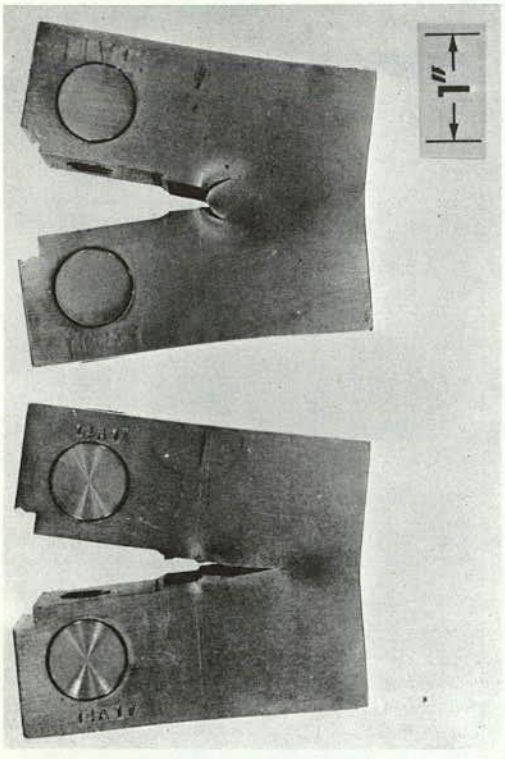

Figure D-6. Partially tested 1T WOL specimens of A36 steel showing a high resistance to fracture and contrasting behaviors concerning fracture-surface topography (presence and total absence of macroscopic shear-lip formation at the specimen surface).

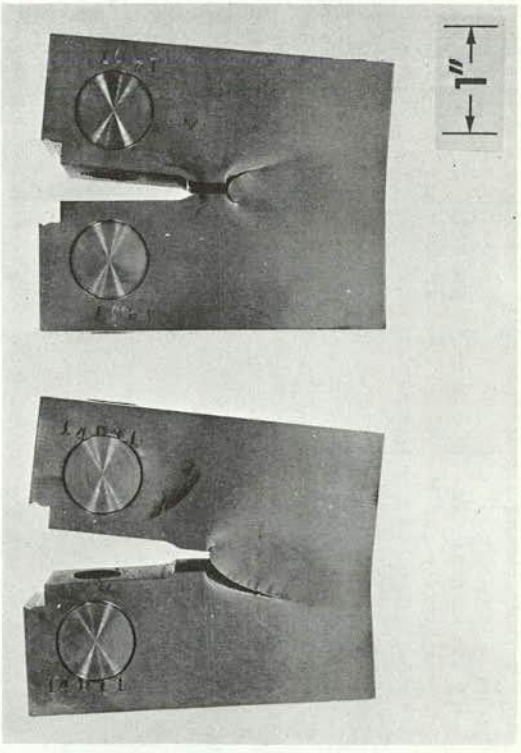

Figure D-8. Partially tested 1T WOL specimens of A514 Grade E steel exhibiting a high resistance to fracture.

APPENDIX E

FATIGUE CRACK GROWTH DATA

The following Figures E-1 through E-7 show fatigue crack growth under constant amplitude and variable amplitude load fluctuations for A36, A588 grades A and B, and A514 grades E and F steels.

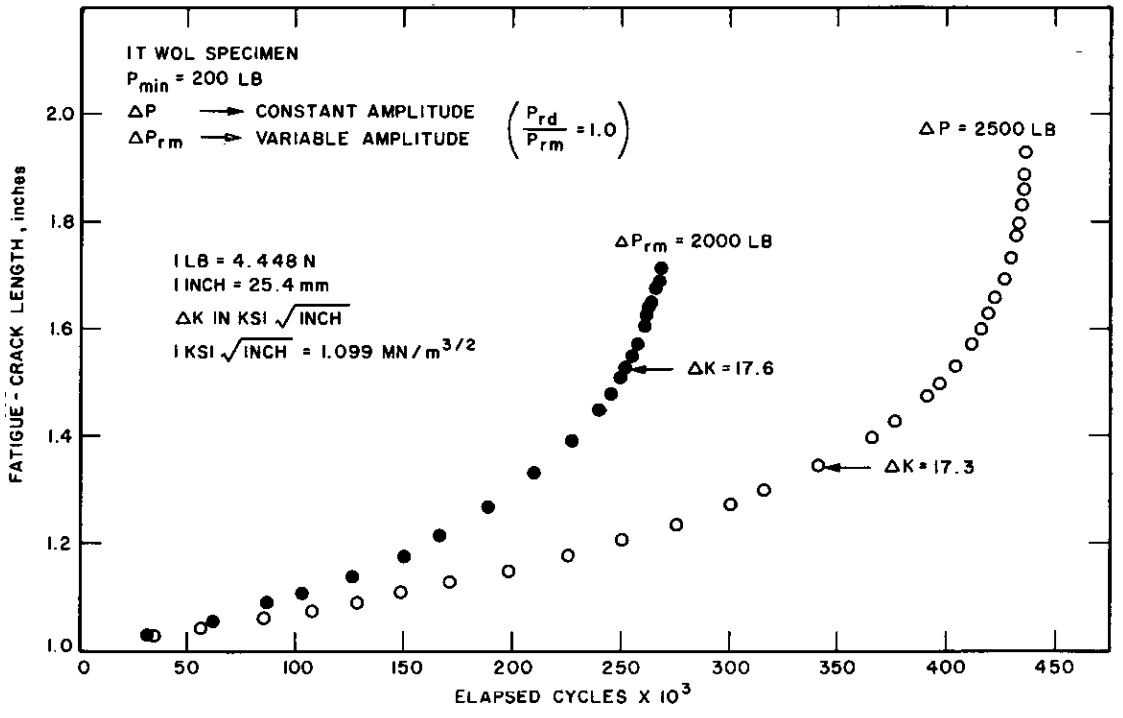

Figure E-1. Fatigue crack growth under constant amplitude and variable amplitude load fluctuations for A36 steel.

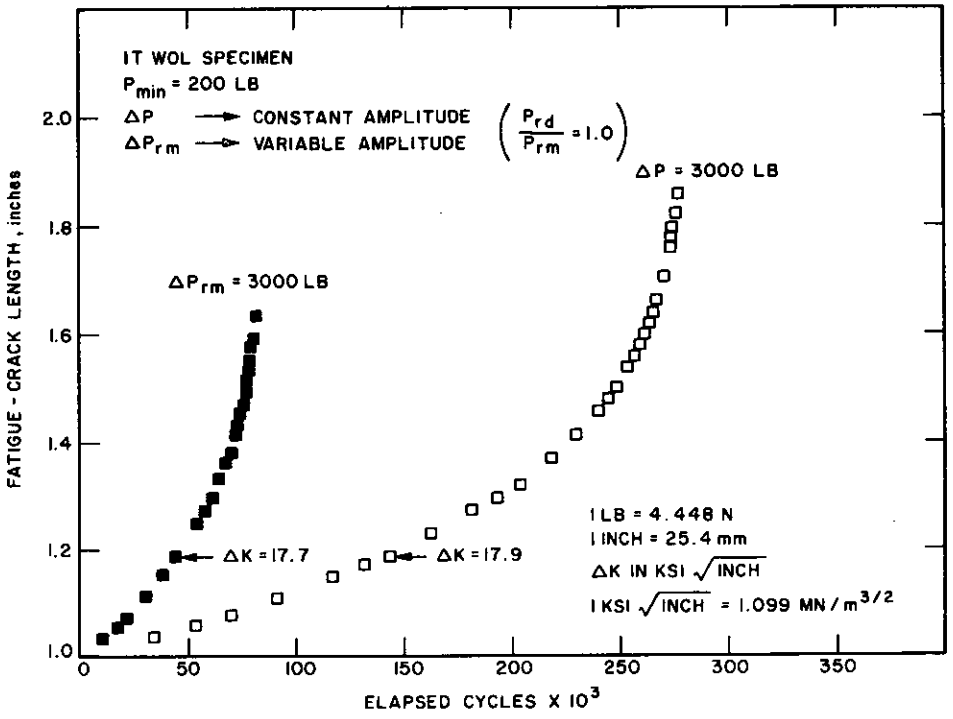

Figure E-2. Fatigue crack growth under constant amplitude and variable amplitude load fluctuations for A36 steel.

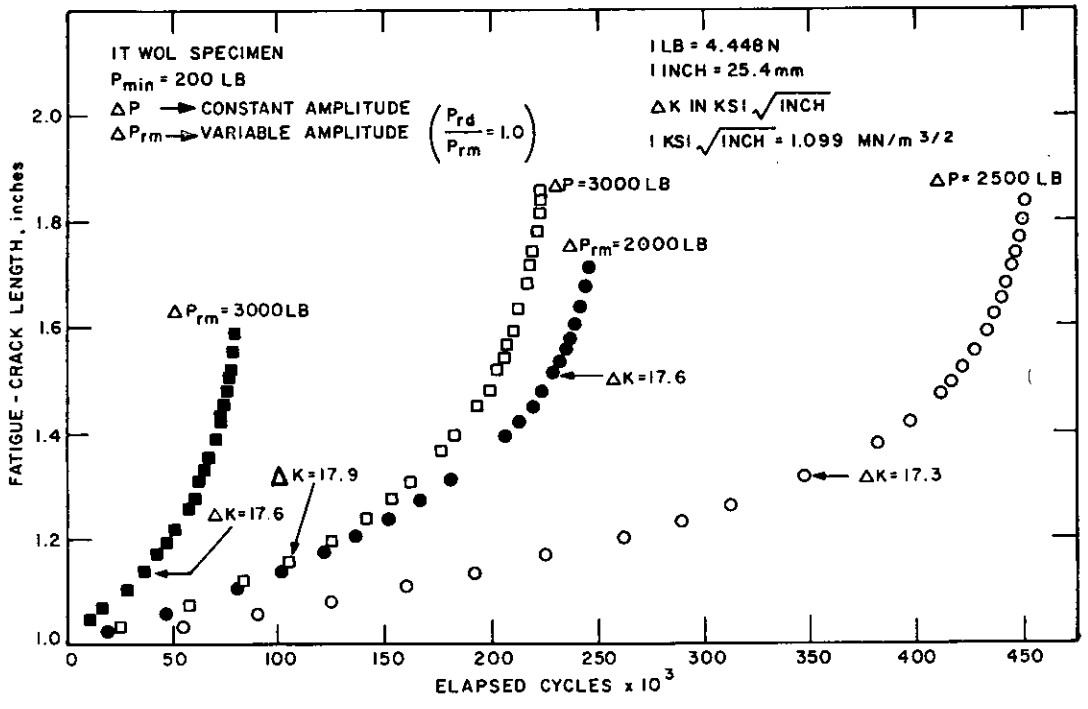

Figure E-3. Fatigue crack growth under constant amplitude and variable amplitude load fluctuations for A588 Grade A steel.

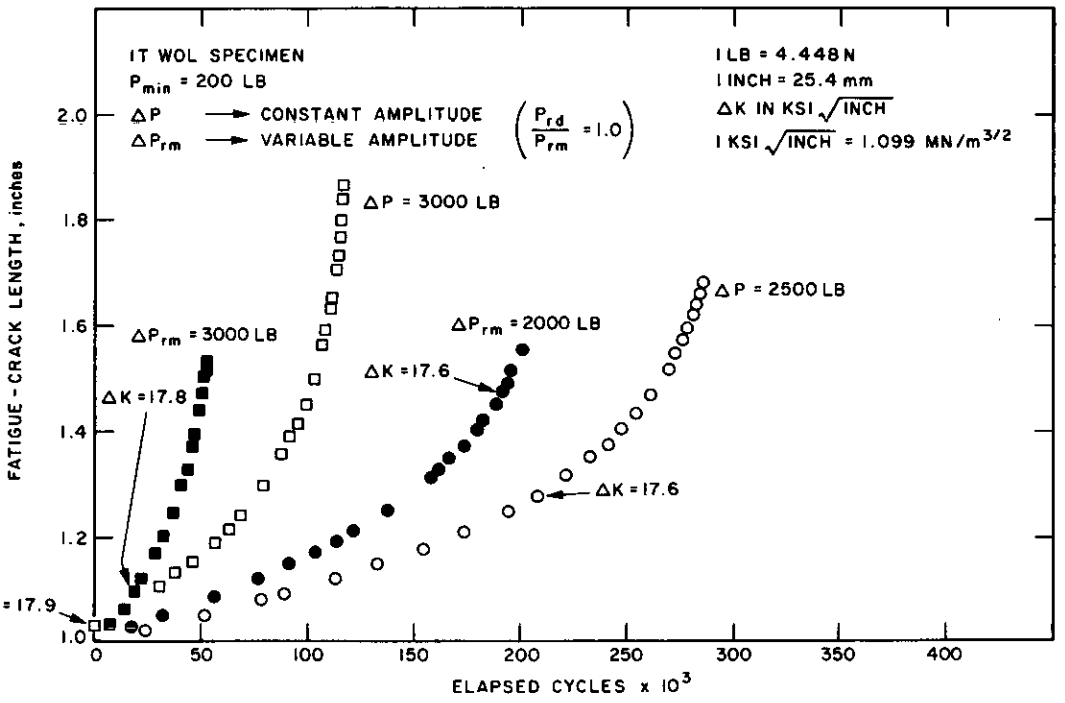

Figure E-4. Fatigue crack growth under constant amplitude and variable amplitude load fluctuations for A588 Grade B steel.

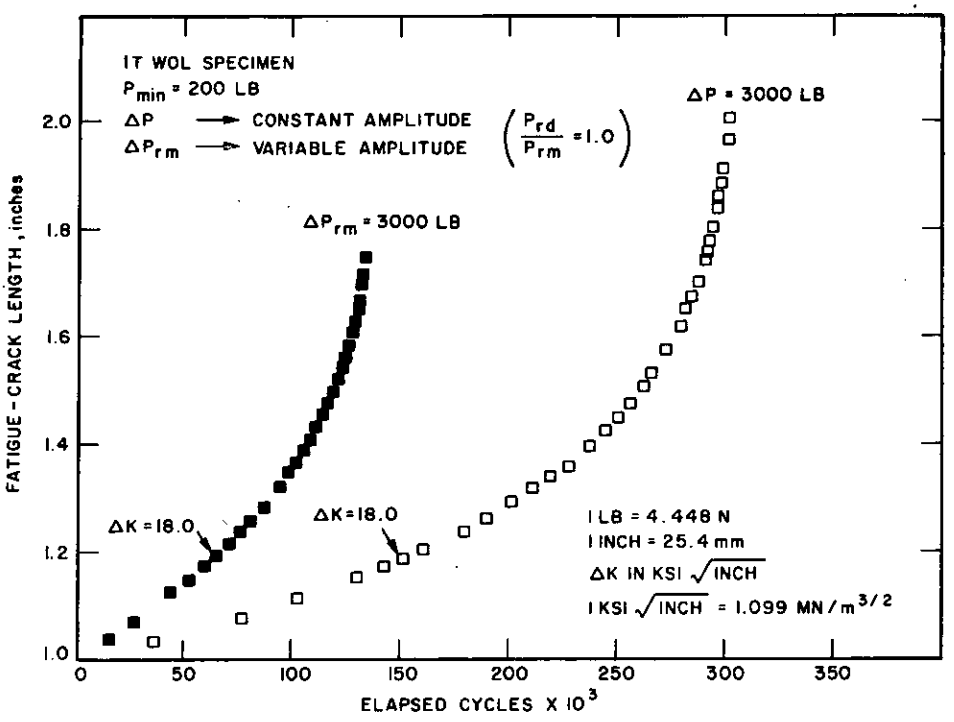

Figure E-5. Fatigue crack growth under constant amplitude and variable amplitude load fluctuations for A514 Grade E steel.

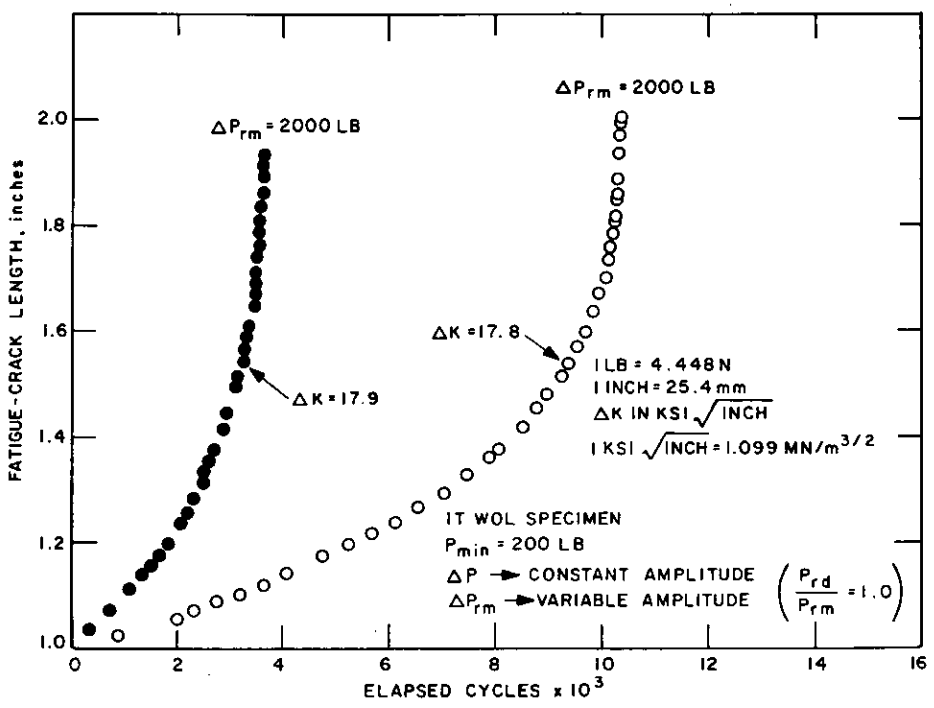

Figure E-6. Fatigue crack growth under constant amplitude and variable amplitude load fluctuations for A514 Grade E steel.

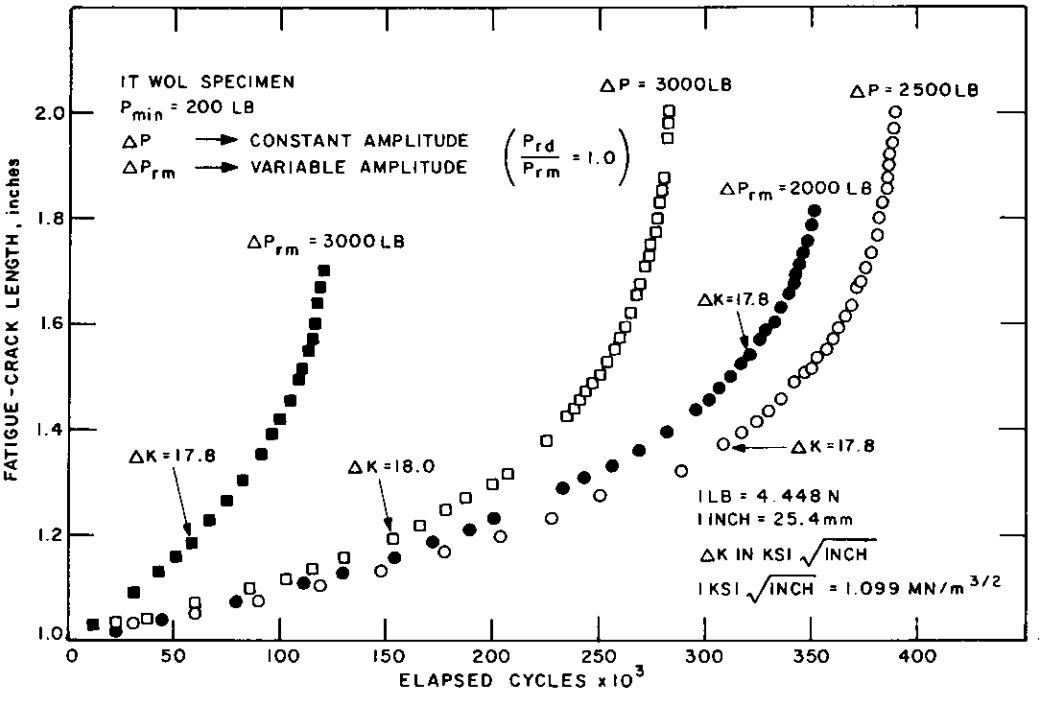

Figure E-7. Fatigue crack growth under constant amplitude and variable amplitude load fluctuations for A514 Grade F steel.

APPENDIX F

STRESS-CORROSION-CRACKING (K_{Iscc}) BEHAVIOR OF STEELS INVESTIGATED

A summary of the specimen preparation and test conditions employed in the precracked cantilever beam tests to evaluate K_{Iscc} for each of the five steels is given in Table F-1. The results of these tests are shown in Figures 19 through 23. These figures show the value of the initial stress intensity to which a specimen was loaded, K_{Ii}, plotted against log time to failure. The detailed test results are also tabulated individually for each steel and are given in Tables F-2 through F-6.

Returning to Figures 19 through 23, it is noted that Figures 19, 20, and 21 show apparent K_{Iscc} values for the A36, A588 Grade A and A588 Grade B steels of 85, 80, and 85 ksi $\sqrt{\text{in.}}$ (94, 88, and 94 MNm$^{-3/2}$), respectively. In the case of each of these three steels, the K_{Iscc} value is well above the corresponding $K_{I,\,Gub}$ value; this condition is indicative of Type III behavior (Fig. A-9 and Table A-1), the existence of severe K_I-suppression effects in the observed result, and the general inapplicability of LEFM principles for quantitative characterization of SCC behavior for each of the three steels. However, in qualitative terms, it can be seen that there is essentially no difference in the observed SCC susceptibility for the A588 Grade A and A588 Grade B steels. Furthermore, although the apparent K_{Iscc} levels for each of the three steels are about the same, a slight degradation in behavior (relative to K_{Ix}) can be seen for both the A588 Grade A and A588 Grade B steels, and essentially no degradation or a totally immune behavior for the A36 steel.

Figures 22 and 23 show that apparent K_{Iscc} values for the higher strength A514 Grade E and A514 Grade F steels were 106 and 82 ksi $\sqrt{\text{in.}}$ (117 and 90 MNm$^{-3/2}$), respectively. The result for the A514 Grade E steel exceeds the corresponding $K_{I,\,Gub}$ value (105 ksi $\sqrt{\text{in.}}$, or 116 MNm$^{-3/2}$) by a slight margin. This result for the A514 Grade E steel represents Type III SCC behavior, similar to the lower strength steels discussed earlier, and is thus subject to the same type of interpretation and restriction (but to a lesser degree). The result for the A514 Grade F steel is somewhat lower than that of the A514 Grade E steel and can be seen to marginally exceed the corresponding $K_{I,\,Lub}$ value (78 ksi $\sqrt{\text{in.}}$, or 86 MNm$^{-3/2}$). Thus, the observed results for the A514 Grade F steel represent Type II SCC behavior, with the existence of marginal to nonexistent K_I-suppression effects and a corresponding degree of applicability of LEFM concepts for quantitative characterization of SCC behavior. This somewhat lower behavior for the A514 Grade F steel (relative to A514 Grade E steel) is about what would be expected because of the abnormally high strength for this steel.

Because LEFM concepts are fully applicable (or valid) for small-scale yielding, the extent of their applicability (or inapplicability) can be measured in relation to the degree of plasticity occurring at the tip of a crack. In turn, the degree of crack-tip plasticity can be measured qualitatively (for a given specimen size) by the deviation from linearity encountered in the load-versus-displacement (P-versus-V) test record. Thus, the relative extent of plasticity encountered for each specimen in the SCC tests may be seen in perspective when the corresponding initial load level, K_{Ii}, is superimposed on a typical P-versus-V plot obtained in the measurement of K_{Ix} for a specific steel.

Such results are shown for each of the steels tested in Figures F-1 through F-5. It should be noted for the higher strength A514 Grade E and A514 Grade F steels (Figs. F-4 and F-5) that the displacement scale (V) differs from that for the lower strength A36 and A588 grades A and B steels. These results are self-evident in indicating further the high levels of net section stress, σ_{Ni} (relative to σ_{ys}) to which the individual test specimens were initially loaded in the SCC tests, as reported in Tables F-2 through F-6. Furthermore, these results also reinforce the conclusions reached concerning the general inapplicabiltiy of LEFM concepts for the quantitative characterization of both fracture (K_{Ix}) and SCC (apparent K_{Iscc}) behaviors of the steels tested.

APPENDIX G

CORROSION FATIGUE, CRACK GROWTH DATA

Figures G-1 through G-13 show the results of corrosion fatigue, crack growth tests performed on A36, A588 Grade A, A588 Grade B, A514 Grade E, and A514 Grade F steels in 3-percent solution of sodium chloride in distilled water.

TABLE F-1

SUMMARY OF DIMENSIONS AND TEST CONDITIONS EMPLOYED—PRECRACKED CANTILEVER-BEAM K_{Iscc} SPECIMEN

Item No.	Steel Type	W, inches	B, inch	B_N, inch	a_N, inch*	N, cycles**	a, inch***	Total Number of Specimens Tested	Test Duration, hours+	Total Number of Specimens Surviving the Test Period++	Number of Surviving Specimens Exhibiting Crack Extension due to SCC+++
1	A36	2.50	0.94	0.84	0.80	230,000 to 279,000	0.24	8	5800	4	0
2	A588-A	2.50	0.91	0.81	0.80	133,000 to 306,000	0.28	8	5300	3	0
3	A588-B	2.50	0.90	0.80	0.75	173,000 to 250,000	0.31	8	5200	4	0
4	A514-E	2.50	1.00	0.90	0.80	192,000 to 362,000	0.24	8	5200	4	1
5	A514-F	2.50	0.98	0.88	0.80	184,000 to 357,000	0.27	8	5300	3	0

* Initial (straight) machined-notch depth prior to fatigue precracking.

** Number of cycles used under nominal zero-to-tension loading ($R \cong 0$) to propagate a fatigue crack from the machined notch (a_N) to the average crack length (a).

*** Average fatigue-crack length.

\+ Nominal test period for specimens tested in a continuously aerated solution of 3 percent NaCl (by weight) in distilled water at room temperature.

++ Specimens not failing in the test period indicated. Certain of these exhibited subcritical crack growth.

+++ Indicated are the number of specimens for which crack extension due strictly to SCC could be ascertained ($\Delta a \geq 5$ to 10 mils)—neglecting both crack extension due to "tearing" in the initial loading process for specimens loaded to high stress levels ($K_I \geq K_{I,Gub}$) and apparent crack extension due to crevice corrosion behavior observed at all stress levels for the A514-E steel (Table F-5). Evidence of crack extension on the specimen fracture surfaces was determined by fracturing the specimens after cooling to approximately -320 F in liquid nitrogen.

TABLE F-2

SUMMARY OF K_I-STRESS CORROSION RESULTS ON A36 * STEEL

Specimen No.	W, inches	B, inch	B_N, inch	a_i, inch**	ΔK_f, ksi $\sqrt{\text{inch}}$***	N, cycles	P, pounds****	$K_{I,Lub}$, ksi $\sqrt{\text{inch}}$	K_{Ii}, ksi $\sqrt{\text{inch}}$	σ_{Ni}, ksi	$\frac{K_{Ii}}{K_{Ix}}$	Δa_f, inch+	K_{If}, ksi $\sqrt{\text{inch}}$++	Time to Failure, hours	Environment
14A-6	2.500	0.939	0.839	1.062	28.0	266,000	1058	26.0	87.9+++	109.8	1.00	—	—	—	Air
14A-1	2.500	0.941	0.841	1.074	28.3	266,000	>1030+++	26.0	>82.0++++	>108.4	1.00	—	—	—	Air
14A-4	2.499	0.939	0.839	1.100	29.2	231,000	1065	26.0	92.7+++	116.7	1.00	—	—	—	Air
14A-6	2.500	0.938	0.838	1.064	28.2	264,000	1056	26.0	88.1	110.0	0.98	I#	—	0.4	3% NaCl
14A-5	2.499	0.939	0.839	1.044	27.4	230,000	966	26.0	78.9	97.9	0.87	0.060##	84.5###	>5860.5####	3% NaCl
14A-2	2.499	0.941	0.841	1.082	28.4	246,000	844	26.0	71.7	90.0	0.79	0.010##	72.6###	>5860.5####	3% NaCl
14A-7	2.500	0.941	0.841	1.081	28.4	279,000	638	26.0	54.0	67.8	0.60	0	54.0###	>5807.0####	3% NaCl
14A-3±	2.500	0.939	0.839	1.095	29.2	279,000	316	26.0	27.3	34.3	0.30	0	27.3###	>5271.8####	3% NaCl

* σ_{ys} = 43.6 ksi, CVN energy absorption at 72 F = 28 ft-lb.

** a_i is the original crack length attained by fatigue cracking ~ 0.26 to 0.30 inch beyond $a_N \cong 0.80$ inch, the machined notch tip.

*** ΔK_f is the maximum ΔK_I reached during fatigue crack preparation as calculated from $\Delta K_f = \frac{2MR}{(B\,B_N)^{1/2}\,W^{3/2}}$ (see Reference in Table D-2).

**** Lever arm = 30.0 inches.

\+ For specimens surviving for the duration of the test, the total crack extension, Δa_f, which can be due to initial tearing on loading and/or stress corrosion cracking, was determined by fracturing the specimens after cooling to approximately -320 F in liquid nitrogen.

++ K_{If} is the K_I level of the specimen at the conclusion of the test period adjusted to reflect any crack extension, Δa_f, which may have occurred.

+++ Average K_{Ix} = 90.3 ksi $\sqrt{\text{inch}}$.

++++ Specimen No. 14A-1 reached the deflection capacity of the testing fixture.

\# Indeterminate.

Crack extension for these specimens was determined to be due solely to initial tearing on loading.

K_{If} values were also calculated considering the reduction in section due to general corrosion in addition to any crack extension, Δa_f. These values are as follows:

Specimen No.	K_{If}, ksi $\sqrt{\text{inch}}$
14A-5	87.5
14A-2	75.0
14A-7	56.0
14A-3	28.3

No failure.

± This specimen was sectioned.

NOTE: Refer to Table D-2 for definitions of above variables.

TABLE F-3

SUMMARY OF K_I-STRESS CORROSION RESULTS ON A588 GRADE A * STEEL

Specimen No.	W, inches	B, inch	B_N, inch	a_i, inch**	ΔK_f, ksi $\sqrt{\text{inch}}$***	N, cycles	P, pounds****	$K_{I,Lub}$, ksi $\sqrt{\text{inch}}$	K_{Ii}, ksi $\sqrt{\text{inch}}$	σ_{Ni}, ksi	$\frac{K_{Ii}}{K_{Ix}}$	Δa_f, inch+	K_{If}, ksi $\sqrt{\text{inch}}$++	Time to Failure, hours	Environment
14B-1	2.499	0.914	0.814	1.062	27.5	222,000	1166	32.2	100.3+++	124.9	1.00	—	—	—	Air
14B-8	2.496	0.913	0.813	1.043	27.0	207,000	1173	32.2	99.0+++	123.0	1.00	—	—	—	Air
14B-5	2.497	0.911	0.811	1.051	28.2	133,000	1095	32.2	93.1	116.2	0.92	I++++	—	1.3 - 21.0	3% NaCl
14B-2	2.497	0.911	0.811	1.080	28.1	236,000	984	32.2	86.8	108.8	0.86	I	—	22.3	3% NaCl
14B-3	2.495	0.913	0.813	1.065	27.2	301,000	963	32.2	83.0	104.3	0.82	I	—	1932.9	3% NaCl
14B-4#	2.497	0.911	0.811	1.059	28.8	223,000	873	32.2	74.9	93.7	0.74	0.002	74.9##	>5538.5###	3% NaCl
14B-6#	2.497	0.911	0.811	1.107	29.0	249,000	535	32.2	48.6	61.4	0.48	0	48.6##	>5206.7###	3% NaCl
14B-7#	2.497	0.911	0.811	1.267	36.8	306,000	268	32.2	29.7	39.3	0.29	0	29.7##	>5141.3###	3% NaCl

* σ_{ys} = 54.9 ksi, CVN energy absorption at 72 F = 69 ft-lb.

** a_i is the original crack length attained by fatigue cracking ~0.24 to 0.31 inch beyond $a_N \cong 0.80$ inch, the machined notch tip.

*** ΔK_f is the maximum ΔK_I reached during fatigue crack preparation as calculated from $\Delta K_f = \frac{2MR}{(B\,B_N)^{1/2}\,W^{3/2}}$ (see Reference in Table D-2).

**** Lever arm = 30.0 inches.

\+ For specimens surviving for the duration of the test, the total crack extension, Δa_f, which can be due to initial tearing on loading and/or stress corrosion cracking, was determined by fracturing the specimens after cooling to approximately -320 F in liquid nitrogen.

++ K_{If} is the K_I level of the specimen at the conclusion of the test period adjusted to reflect any crack extension, Δa_f, which may have occurred.

+++ Average K_{Ix} = 100.7 ksi $\sqrt{\text{inch}}$.

++++ Indeterminate.

\# These specimens were sectioned.

K_{If} values were also calculated considering the reduction in section due to general corrosion in addition to any crack extension, Δa_f. These values are as follows:

Specimen No.	K_{If}, ksi $\sqrt{\text{inch}}$
14B-4	76.3
14B-6	49.1
14B-7	30.0

No failure.

NOTE: Refer to Table D-2 for definitions of above variables.

TABLE F-4

SUMMARY OF K_I-STRESS CORROSION RESULTS ON A588 GRADE B * STEEL

Specimen No.	W, inches	B, inch	B_N, inch	a_i, inch**	ΔK_f, ksi $\sqrt{\text{inch}}$***	N, cycles	P, pounds****	$K_{I,Lub}$, ksi $\sqrt{\text{inch}}$	K_{Ii}, ksi $\sqrt{\text{inch}}$	σ_{Ni}, ksi	K_{Ii}/K_{Ix}	Δa_f, inch+	K_{If}, ksi $\sqrt{\text{inch}}$++	Time to Failure, hours	Environment
14C-6	2.503	0.896	0.796	1.090	29.4	143,000	1138	32.4	102.3	128.9	1.00	—	—	—	Air
14C-2	2.500	0.896	0.796	1.112	31.1	218,000	1146	32.4	106.6	134.5	1.00	—	—	—	Air
14C-8	2.501	0.895	0.795	1.073	29.8	173,000	1089	32.4	96.4	120.9	0.92	I++++	—	3632.7	3% NaCl
14C-3	2.501	0.895	0.795	1.216	35.8	192,000	880	32.4	92.6	120.7	0.89	I	—	4869.9	3% NaCl
14C-4	2.501	0.895	0.795	1.120	31.0	181,000	828	32.4	77.4	98.3	0.74	0	77.4#	>5209.0##	3% NaCl
14C-1	2.501	0.895	0.795	1.076	29.0	216,000	677	32.4	60.1	75.5	0.56	0	60.1#	>5135.3##	3% NaCl
14C-5	2.501	0.895	0.795	1.140	32.4	250,000	482	32.4	46.2	58.9	0.44	0	46.2#	>5207.65##	3% NaCl
14C-7	2.501	0.895	0.795	1.194	34.6	249,000	326	32.4	33.4	43.2	0.32	0	33.4#	>5207.6##	3% NaCl

* σ_{ys} = 55.6 ksi, CVN energy absorption at 72 F = 66 ft-lb.

** a_i is the original crack length obtained by fatigue cracking ~0.32 to 0.47 inch beyond $a_N \cong 0.75$ inch, the machined notch tip.

*** ΔK_f is the maximum ΔK_I reached during fatigue crack preparations calculated from $\Delta K_f \frac{2MR}{(B\,B_N)^{1/2}\,W^{3/2}}$ (see Reference in Table D-2).

**** Lever arm = 30.0 inches.

\+ For specimens surviving for the duration of the test, the total crack extension, Δa_f, was determined by fracturing the specimens after cooling to approximately -320 F in liquid nitrogen.

++ K_{If} is the K_I level of the specimen at the conclusion of the test period adjusted to reflect any crack extension, Δa_f, which may have occurred.

+++ Average K_{Ix} = 104.5 ksi $\sqrt{\text{inch}}$.

++++ Indeterminate.

\# K_{If} values were also calculated considering the reduction in section due to general corrosion in addition to any crack extension, Δa_f. These values are as follows:

Specimen No.	K_{If}, ksi $\sqrt{\text{inch}}$
14C-4	78.4
14C-1	61.2
14C-5	46.9
14C-7	34.1

No failure.

NOTE: Refer to Table D-2 for definitions of above variables.

TABLE F-5

SUMMARY OF K_I-STRESS CORROSION RESULTS ON A514 GRADE E * STEEL

Specimen No.	W, inches	B, inch	B_N, inch	a_i, inch**	ΔK_f, ksi $\sqrt{\text{inch}}$***	N, cycles	P, pounds****	$K_{I,Lub}$, ksi $\sqrt{\text{inch}}$	K_{Ii}, ksi $\sqrt{\text{inch}}$	σ_{Ni}, ksi	$\frac{K_{Ii}}{K_{Ix}}$	Δa_f, inch+	K_{If}, ksi $\sqrt{\text{inch}}$++	Time to Failure, hours	Environment
14D-8	2.505	0.997	0.897	1.070	26.5	200,000	1869	66.4	146.1+++	182.1	1.00	—	—	—	Air
14D-5	2.504	0.996	0.896	1.046	25.6	236,000	1904	66.4	145.5+++	180.0	1.00	—	—	—	Air
14D-2	2.503	0.995	0.895	1.063	26.3	256,000	1772	66.4	138.3	171.9	0.95	I++++	—	157.6	3% NaCl
14D-7	2.503	0.994	0.894	1.107	27.4	192,000	1507	66.4	123.6	155.7	0.85	I	—	1325.4	3% NaCl
14D-1#	2.503	0.994	0.894	1.052	25.9	281,000	1515	66.4	116.8	144.9	0.80	0.032	121.2##	>5273.4###	3% NaCl
14D-6#	2.503	0.994	0.894	1.039	25.4	270,000	1249	66.4	94.9	117.3	0.65	0.016	96.8###	>5206.5###	3% NaCl
14D-4#	2.503	0.994	0.894	1.051	26.0	362,000	1022	66.4	78.6	97.6	0.54	0.013	80.0##	>5188.9###	3% NaCl
14D-3#	2.503	0.994	0.894	1.071	26.7	279,000	736	66.4	58.0	72.3	0.40	0.008	58.5##	>4888.8###	3% NaCl

* σ_{ys} = 107.9, CVN energy absorption at 72 F = 68 ft-lb.

** a_i is the original crack length obtained by fatigue cracking ~ 0.24 to 0.30 inch beyond $a_N \cong 0.80$ inch, the machined notch tip.

*** ΔK_f is the maximum ΔK_I reached during fatigue crack preparation as calculated from $\Delta K_f = \frac{2MR}{(B\,B_N)^{1/2}\,W^{3/2}}$ (see Reference in Table D-2).

**** Lever arm = 30.0 inches.

\+ For specimens surviving for the duration of the test, the total crack extension, Δa_f, which can be due to initial tearing on loading and/or stress corrosion cracking, was determined by fracturing the specimens after cooling to approximately -320 F in liquid nitrogen.

++ K_{If} is the K_I level of the specimen at the conclusion of the test period adjusted to reflect any crack extension, Δa_f, which may have occurred.

+++ Average K_{Ix} = 145.8 ksi $\sqrt{\text{inch}}$.

++++ Indeterminate.

\# These specimens were sectioned.

K_{If} values were also calculated considering the reduction in section due to general corrosion in addition to any crack extension, Δa_f. These values are as follows:

Specimen No.	K_{If}, ksi $\sqrt{\text{inch}}$
14D-1	135.7
14D-6	98.4
14D-4	83.8
14D-3	65.2

No failure.

NOTE: Refer to Table D-2 for definitions of above variables.

TABLE F-6

SUMMARY OF K_I-STRESS CORROSION RESULTS ON A514 GRADE F * STEEL

Specimen No.	W, inches	B, inch	B_N, inch	a_i, inch**	ΔK_f, ksi $\sqrt{\text{inch}}$***	N, cycles	P, pounds****	$K_{I,Lub}$, ksi $\sqrt{\text{inch}}$	K_{Ii}, ksi $\sqrt{\text{inch}}$	σ_{Ni}, ksi	$\frac{K_{Ii}}{K_{Ix}}$	Δa_f, inch+	K_{If}, ksi $\sqrt{\text{inch}}$++	Time to Failure, hours	Environment
14E-2	2.498	0.975	0.875	1.114	26.2	>311,000	1206	78.3	102.6+++	129.5	1.00	—	—	—	Air
14E-8	2.497	0.975	0.875	1.063	24.9	311,000	1316	78.3	105.7+++	131.7	1.00	—	—	—	Air
14E-1	2.497	0.975	0.875	1.084	25.4	353,000	1132	78.3	93.3	116.6	0.90	I++++	—	5.0	3% NaCl
14E-6	2.497	0.975	0.875	1.063	24.9	298,000	1146	78.3	91.8	114.6	0.88	I	—	14.95	3% NaCl
14E-3	2.497	0.975	0.875	1.075	25.2	319,000	1057	78.3	86.4	107.5	0.83	I	—	871.0	3% NaCl
14E-7	2.497	0.975	0.875	1.137	27.0	227,000	853	78.3	74.7	94.9	0.72	0.002	75.0#	>5540.8##	3% NaCl
14E-5	2.497	0.975	0.875	1.121	26.4	184,000	815	78.3	70.1	88.5	0.67	0.002	70.3#	>5207.3##	3% NaCl
14E-4	2.497	0.975	0.875	1.205	29.7	357,000	637	78.3	60.6	78.5	0.58	0	60.6#	>5206.0##	3% NaCl

* σ_{ys} = 126.0, CVN Energy absorption at 72 F = 45 ft-lb.

** a_i is the original crack length obtained by fatigue cracking ~ 0.26 to 0.41 inch beyond $a_N \cong 0.80$ inch, the machined notch tip.

*** ΔK_f is the maximum ΔK_I reached during fatigue crack preparation as calculated from $\Delta K_f = \frac{2MR}{(B\,B_N)^{1/2}\,W^{3/2}}$ (see Reference in Table D-2).

**** Lever arm = 30.0 inches.

\+ For specimens surviving for the duration of the test, the total crack extension Δa_f, which can be due to the initial tearing on loading and/or stress corrosion cracking, was determined by fracturing the specimens after cooling to approximately -320 F in liquid nitrogen.

++ K_{If} is the K_I level of the specimen at the conclusion of the test period adjusted to reflect any crack extension, Δa_f, which may have occurred.

+++ Average K_{Ix} = 104.2 ksi $\sqrt{\text{inch}}$.

++++ Indeterminate.

\# K_{If} values were also calculated considering the reduction in section due to general corrosion in addition to any crack extension, Δa_f. These values are as follows:

Specimen No.	K_{If}, ksi $\sqrt{\text{inch}}$
14E-7	77.4
14E-5	72.6
14E-4	63.0

No failure.

NOTE: Refer to Table D-2 for definitions of above variables.

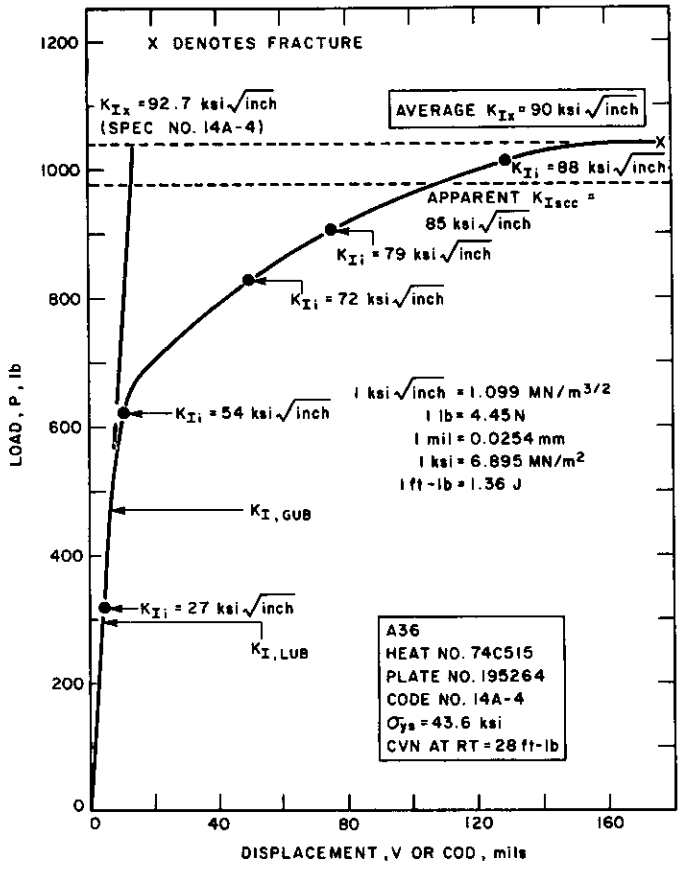

Figure F-1. Typical fracture test record (cantilever beam specimen) for A36 steel with superimposed values of the K_{Ii} levels used and the apparent K_{Iscc} result obtained in the SCC tests.

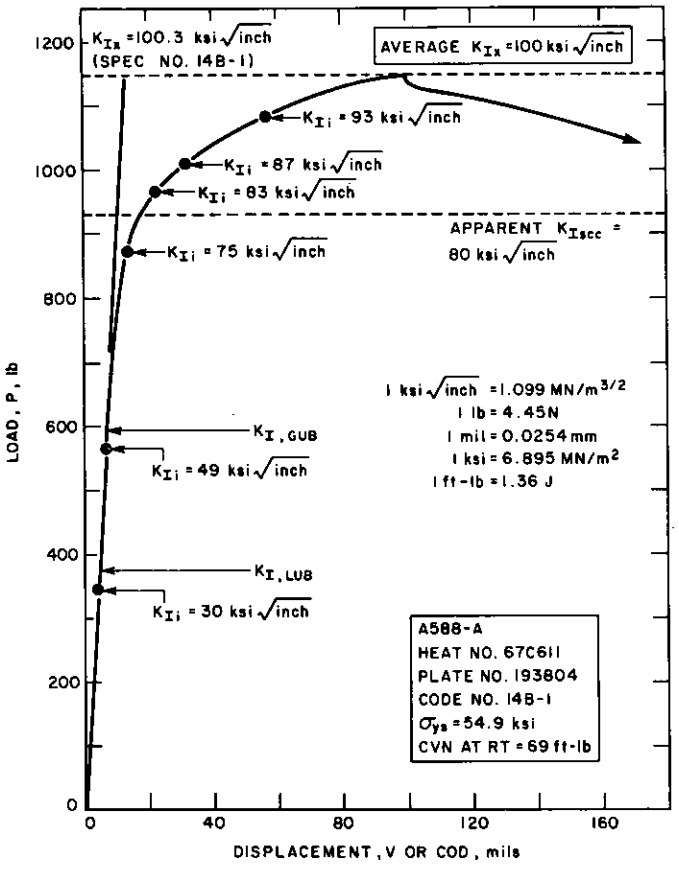

Figure F-2. Typical fracture test record (cantilever beam specimen) for A588 Grade A steel with superimposed values of the K_{Ii} levels used and the apparent K_{Iscc} result obtained in the SCC tests.

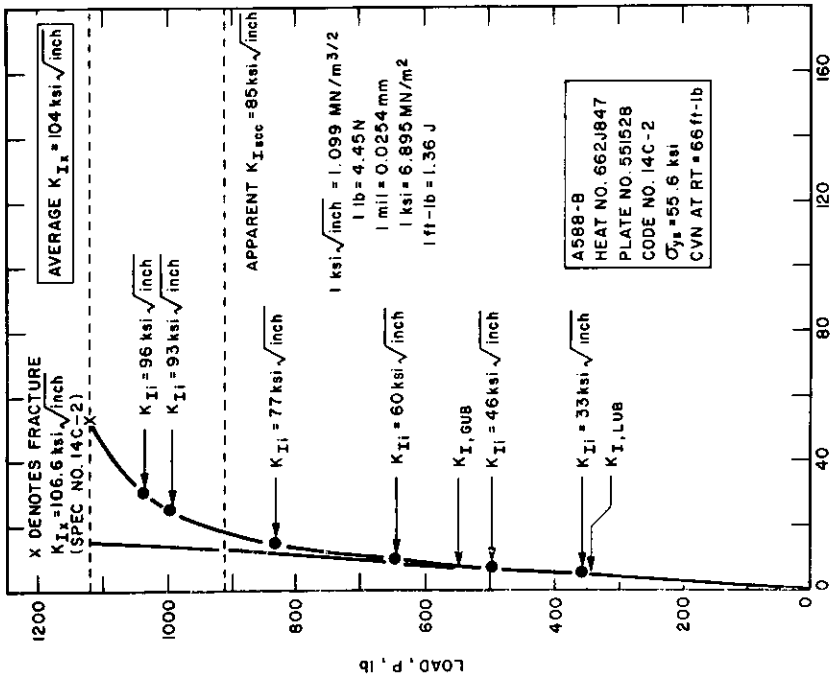

Figure F-3. Typical fracture test record (cantilever beam specimen) for A588 Grade B steel with superimposed values of the K_{Ii} levels used and the apparent K_{Iscc} result obtained in the SCC tests.

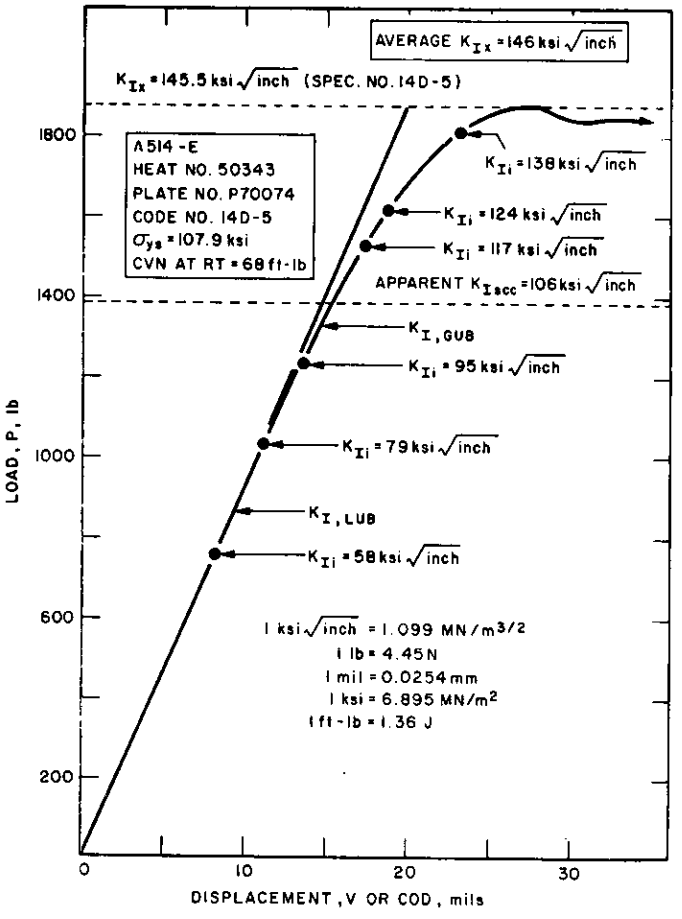

Figure F-4. Typical fracture test record (cantilever beam specimen) for A514 Grade E steel with superimposed values of the K_{Ii} levels used and the apparent K_{Iscc} result obtained in the SCC tests.

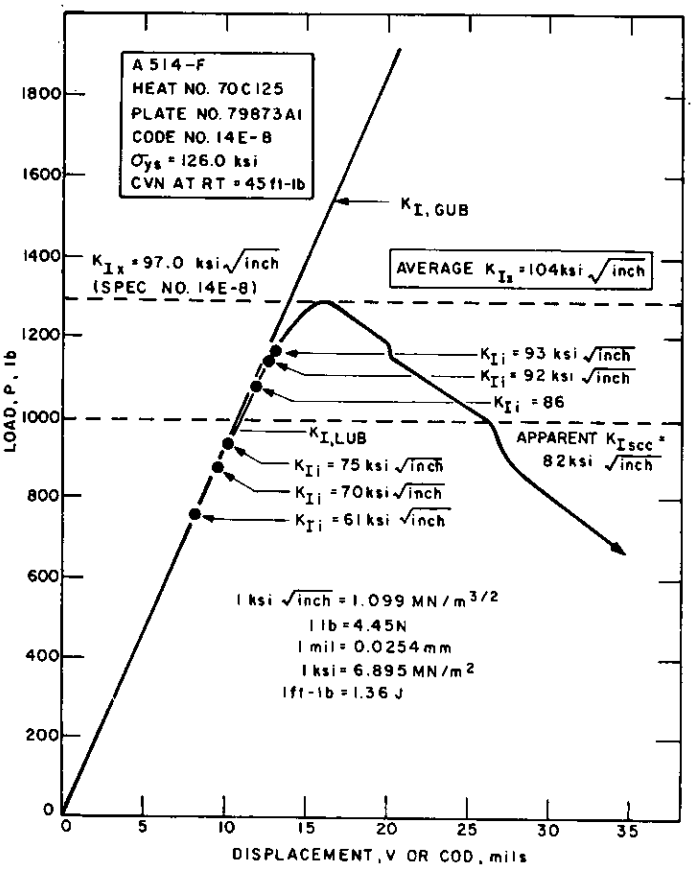

Figure F-5. Typical fracture test record (cantilever beam specimen) for A514 Grade F steel with superimposed values of the K_{Ii} levels used and the apparent K_{Iscc} result obtained in the SCC tests.

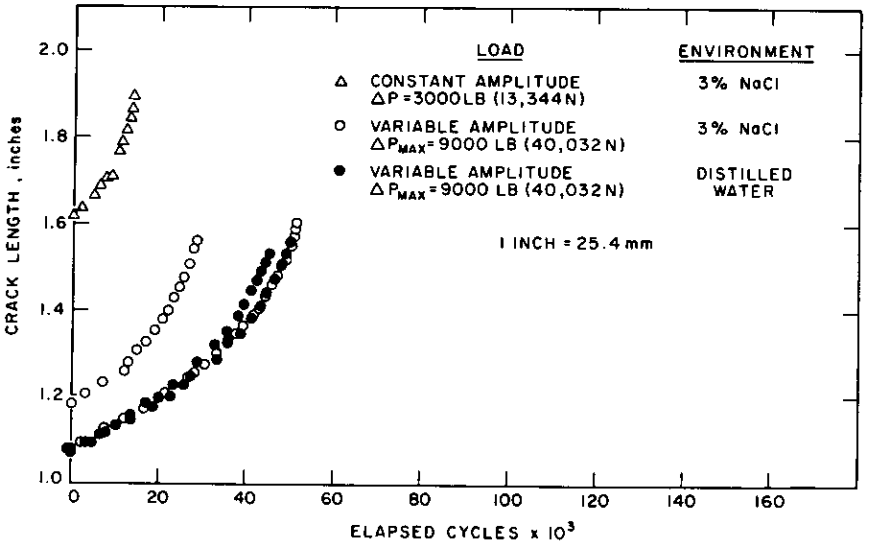

Figure G-1. Corrosion fatigue crack growth at 60 cpm for A36 steel.

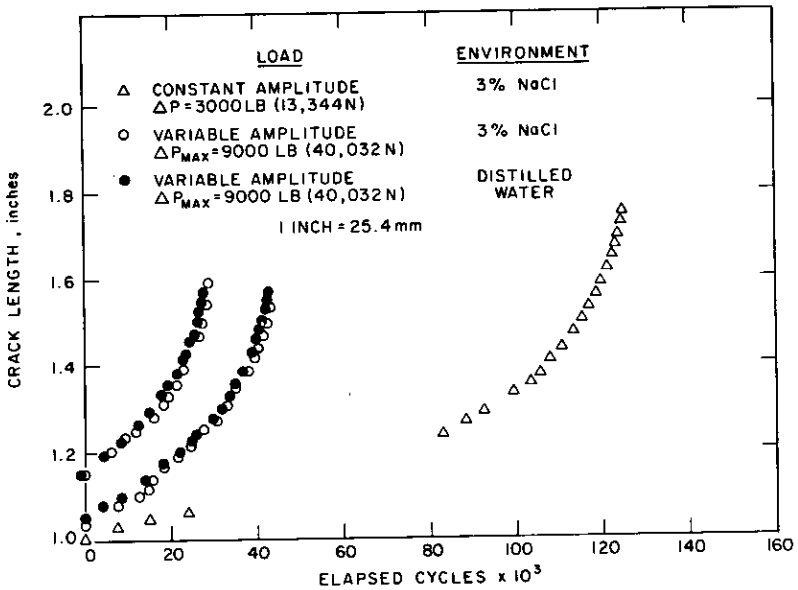

Figure G-2. Corrosion fatigue crack growth at 60 cpm for A588 Grade A steel.

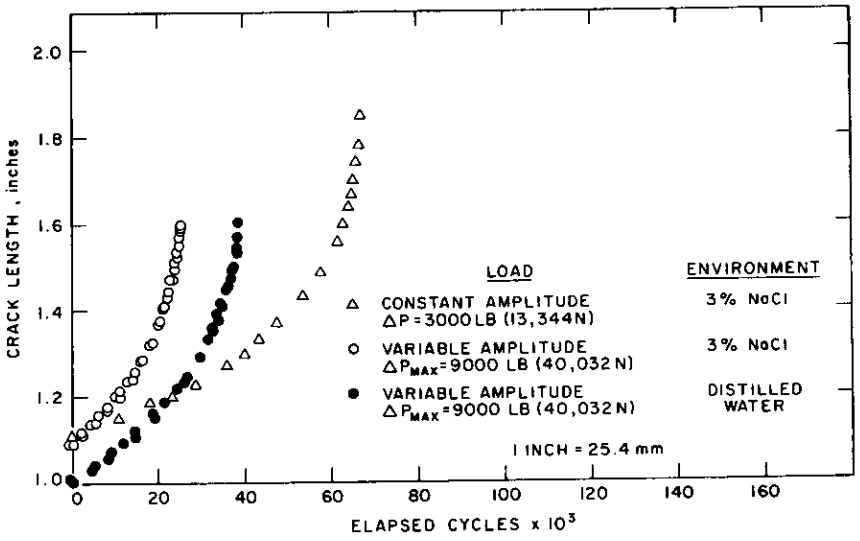

Figure G-3. Corrosion fatigue crack growth at 60 cpm for A588 Grade B steel.

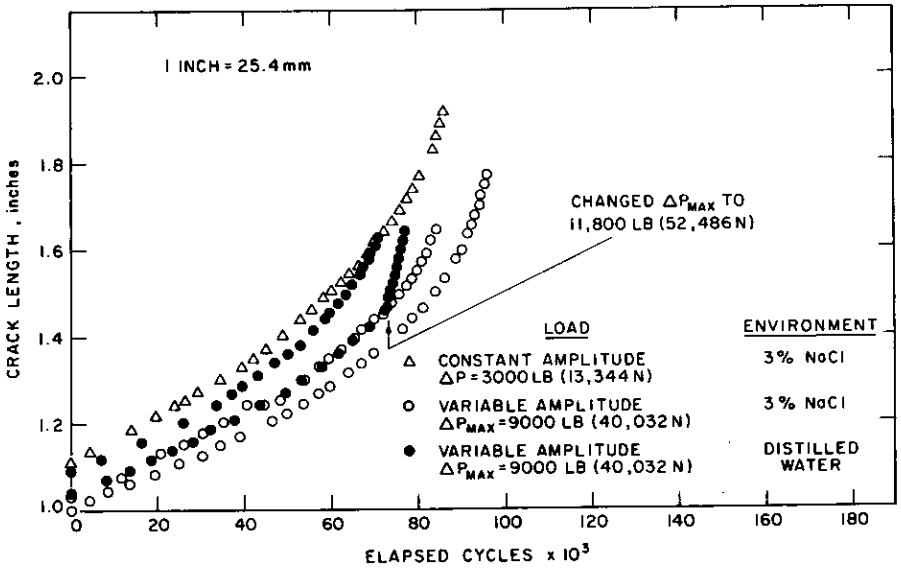

Figure G-4. Corrosion fatigue crack growth at 60 cpm for A514 Grade E steel.

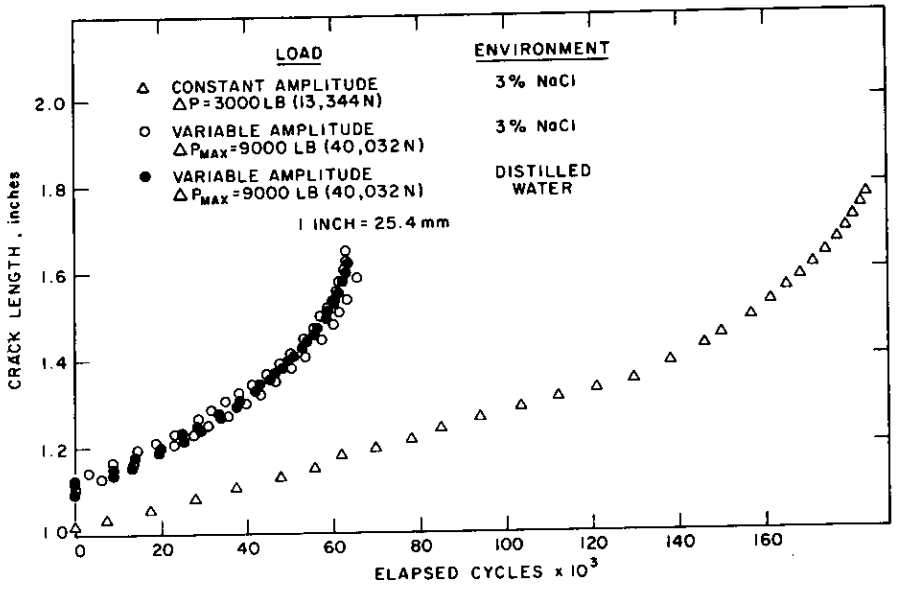

Figure G-5. Corrosion fatigue crack growth at 60 cpm for A514 Grade F steel.

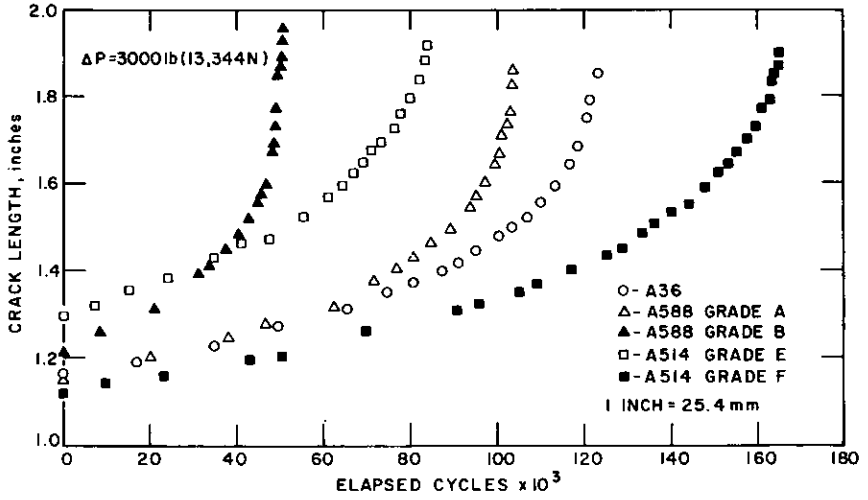

Figure G-6. Corrosion fatigue crack growth at 60 cpm under square-wave loading in 3-percent sodium chloride solution.

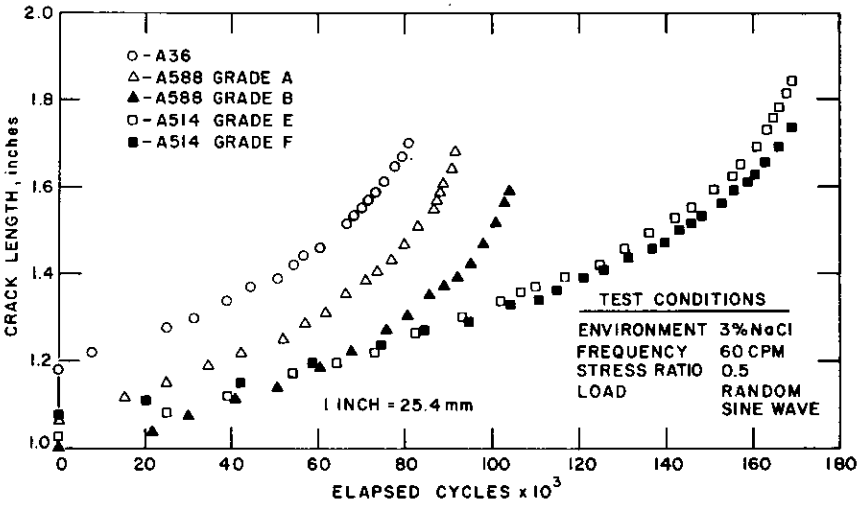

Figure G-7. Corrosion fatigue crack growth for five bridge steels.

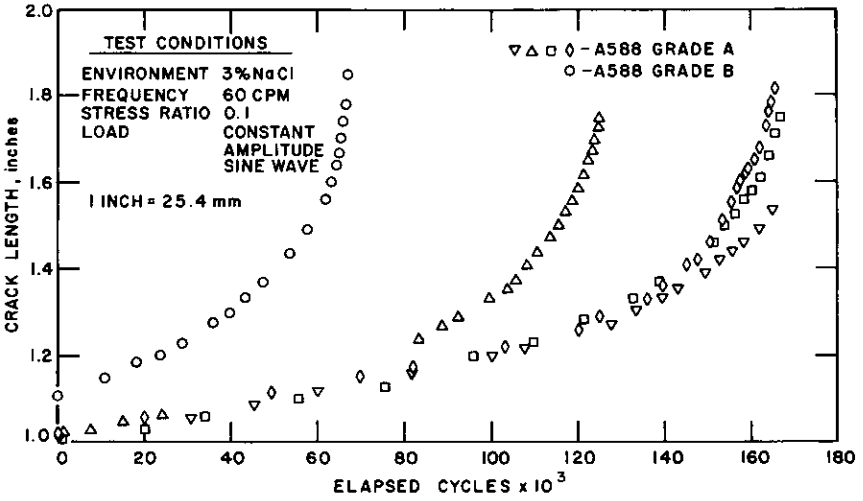

Figure G-8. Corrosion fatigue crack growth for A588 steels from various sources.

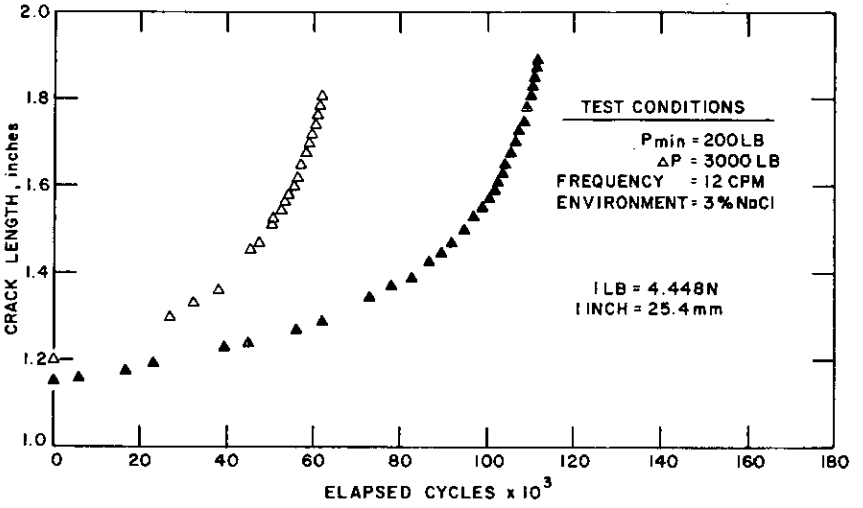

Figure G-9. Corrosion fatigue crack growth under constant amplitude load fluctuation for A36 steel.

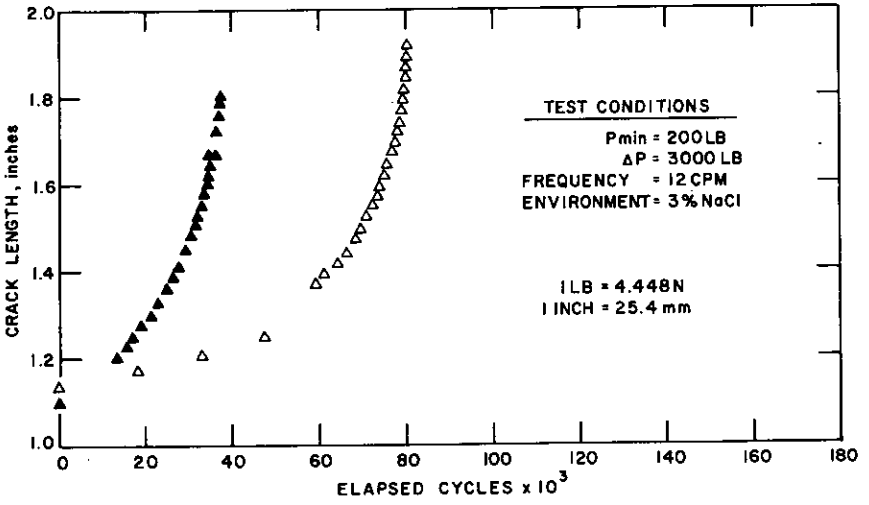

Figure G-10. Corrosion fatigue crack growth under constant amplitude load fluctuation for A588 Grade A steel.

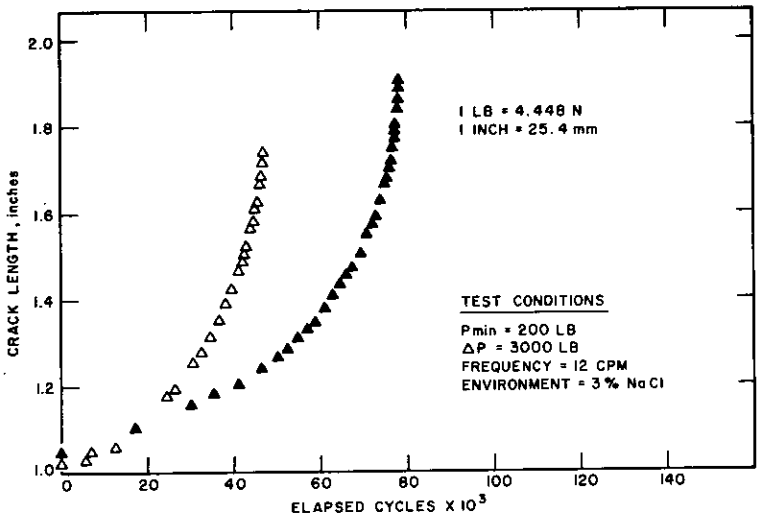

Figure G-11. Corrosion fatigue crack growth under constant amplitude load fluctuation for A588 Grade B steel.

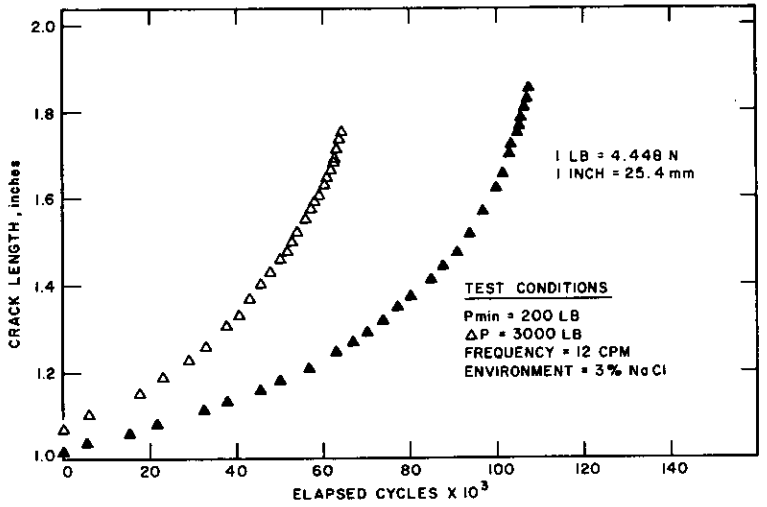

Figure G-12. Corrosion fatigue crack growth under constant amplitude load fluctuation for A514 Grade E steel.

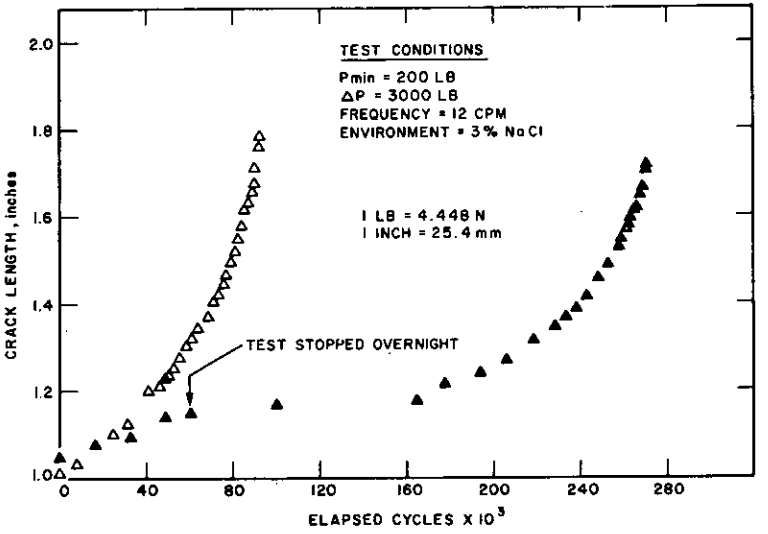

Figure G-13. Corrosion fatigue crack growth under constant amplitude load fluctuation for A514 Grade F steel.

THE TRANSPORTATION RESEARCH BOARD is an agency of the National Research Council, which serves the National Academy of Sciences and the National Academy of Engineering. The Board's purpose is to stimulate research concerning the nature and performance of transportation systems, to disseminate information that the research produces, and to encourage the application of appropriate research findings. The Board's program is carried out by more than 150 committees and task forces composed of more than 1,800 administrators, engineers, social scientists, and educators who serve without compensation. The program is supported by state transportation and highway departments, the U.S. Department of Transportation, and other organizations interested in the development of transportation.

The Transportation Research Board operates within the Commission on Sociotechnical Systems of the National Research Council. The Council was organized in 1916 at the request of President Woodrow Wilson as an agency of the National Academy of Sciences to enable the broad community of scientists and engineers to associate their efforts with those of the Academy membership. Members of the Council are appointed by the president of the Academy and are drawn from academic, industrial, and governmental organizations throughout the United States.

The National Academy of Sciences was established by a congressional act of incorporation signed by President Abraham Lincoln on March 3, 1863, to further science and its use for the general welfare by bringing together the most qualified individuals to deal with scientific and technological problems of broad significance. It is a private, honorary organization of more than 1,000 scientists elected on the basis of outstanding contributions to knowledge and is supported by private and public funds. Under the terms of its congressional charter, the Academy is called upon to act as an official—yet independent—advisor to the federal government in any matter of science and technology, although it is not a government agency and its activities are not limited to those on behalf of the government.

To share in the tasks of furthering science and engineering and of advising the federal government, the National Academy of Engineering was established on December 5, 1964, under the authority of the act of incorporation of the National Academy of Sciences. Its advisory activities are closely coordinated with those of the National Academy of Sciences, but it is independent and autonomous in its organization and election of members.

TRANSPORTATION RESEARCH BOARD
National Research Council
2101 Constitution Avenue, N.W.
Washington, D.C. 20418

ADDRESS CORRECTION REQUESTED